

# Two Ridge Solutions for the Incremental Broad Learning System on Added Nodes

Hufei Zhu

**Abstract**—The original Broad Learning System (BLS) on new added nodes and its existing efficient implementation both assume the ridge parameter  $\lambda \rightarrow 0$  in the ridge inverse to approximate the generalized inverse, and compute the generalized inverse solution for the output weights. In this paper, we propose two ridge solutions for the output weights in the BLS on added nodes, where  $\lambda \rightarrow 0$  is no longer assumed, and  $\lambda$  can be any positive real number. One of the proposed ridge solutions computes the output weights from the inverse Cholesky factor, which is updated efficiently by extending the existing inverse Cholesky factorization. The other proposed ridge solution computes the output weights from the ridge inverse, and updates the ridge inverse by extending the Greville's method that is a classical tool to compute the generalized inverse of partitioned matrices. For the proposed efficient ridge solution based on the inverse Cholesky factor, we also develop another implementation that is numerically more stable when the ridge parameter  $\lambda$  is very small.

The proposed ridge solution based on the ridge inverse and the numerically more stable implementation of the proposed efficient ridge solution require the same complexity as the original BLS and the existing efficient BLS, respectively. Moreover, the speedups of the proposed efficient ridge solution to the original BLS and the existing efficient BLS are 300% and more than 167% respectively, when the computational complexities for each update are compared, and the speedups are 199%  $\sim$  252% and 131%  $\sim$  158%, respectively, when the total training time is compared by numerical experiments. On the other hand, our numerical experiments show that both the proposed ridge solutions for BLS achieve better testing accuracies than the original BLS and the existing efficient BLS.

**Index Terms**—Big data, broad learning system (BLS), incremental learning, added nodes, random vector functional-link neural networks (RVFLNN), single layer feedforward neural networks (SLFN), efficient algorithms, partitioned matrix, inverse Cholesky factorization, generalized inverse, generalized inverse solution, ridge inverse, ridge solution, Greville's method.

## I. INTRODUCTION

Deep neural networks (DNNs), including the deep belief networks (DBN) [1], [2], the deep Boltzmann machines (DBM) [3], and the convolutional neural networks (CNN) [4], [5], have been successfully adopted in many applications [6], [7], particularly in image and speech recognition [8], [9]. However, most DNNs suffer from the time-consuming training process, since usually they possess complicated structures and need to tune a huge number of hyperparameters by back propagation of error [10], [11]. Furthermore, DNNs are treated as black boxes in most cases, which makes theoretic analysis of DNNs very difficult.

Single layer feedforward neural networks (SLFN) have been widely applied in classification and regression because

of their universal approximation capability [11]–[13]. The traditional Gradient-descent-based learning algorithms [10], [14] can be utilized to adjust the input and output weights of SLFN. However, the Gradient-descent-based algorithms are very slow in the training process, and may easily halt at local optima. Furthermore, their generalization performance is much affected by parameter settings (e.g., the setting of learning rate). Then the random vector functional-link neural network (RVFLNN) has been proposed [11] as a different train method, which generates the input weights and the biases randomly, and learns only the output weights. RVFLNN eliminates the disadvantage of slow training process, and also offers the generalization capability in function approximation [13].

For a new added node or input in the RVFLNN, the dynamic step-wise updating algorithm proposed in [15] can update the output weights easily by only computing the generalized inverse of that added node or input, which is suitable for time-varying data with moderate size. Then to process time-varying big data with high dimension, the scheme proposed in [15] was improved in [16] to propose the Broad Learning System (BLS). For BLS, several BLS variants have been proposed, which include cascade, recurrent, and broad-deep combination structures, and the proof of the universal approximation capability has been given [17].

In the original BLS algorithm [16], the output weights are the generalized inverse solution [18] computed from the generalized inverse, and the generalized inverse is updated efficiently by the Greville's method [19]. Recently in [20], we proposed an efficient implementation of the original BLS algorithm on added nodes, which computes the output weights from the inverse Cholesky factor of the Hermitian matrix in the generalized inverse, and updates the inverse Cholesky factor efficiently. With respect to the original BLS, the efficient BLS in [20] requires less than  $\frac{2}{3}$  of complexity, and achieves the same testing accuracy when the tiny differences caused by the numerical errors are neglected. Both the BLS algorithms in [16], [20] are based on the generalized inverse with the ridge regression approximation, where the ridge parameter  $\lambda \rightarrow 0$  is assumed in the ridge inverse [18] to approximate the generalized inverse.

In this paper, we will propose two ridge solutions [18] for the BLS with new added nodes, where it is no longer required to assume the ridge parameter  $\lambda \rightarrow 0$  (i.e.,  $\lambda$  can be any positive real number). In one of the proposed ridge solutions, the output weights are computed from the inverse Cholesky factor of the Hermitian matrix in the ridge inverse, and the inverse Cholesky factorization [21] is extended to update the inverse Cholesky factor efficiently. In the other proposed ridge solution, the output weights are computed

H. Zhu is with the Faculty of Intelligent Manufacturing, Wuyi University, Jiangmen 529020, Guangdong, China (e-mail: hufeizhu93@hotmail.com).

from the ridge inverse, and the Greville's method [19] for the generalized inverse is extended to update the ridge inverse. For the proposed efficient ridge solution based on the inverse Cholesky factor, we also develop another implementation that is numerically more stable when the ridge parameter  $\lambda$  is very small. In simulations, both the proposed ridge solutions usually achieve better testing accuracy than the existing generalized inverse solutions [16], [20] for BLS. Moreover, the proposed efficient ridge solution requires less complexity than the efficient generalized inverse solution in [20].

Since the training processing of big data with high dimension may exceed the capacity of a single computational node, there is a need to distribute computing tasks across multiple computational nodes, which can also be called as workers [28]. Specifically, a distributed implementation is usually necessary if data is inherently distributed or too big to store on a single worker. In distributed systems, algorithms have to be chosen and implemented to enable parallel computation. In the distributed machine learning systems, two fundamental parallelization approaches are data-parallelism and model-parallelism [28], which parallelize the data and the model, respectively, and can be applied simultaneously. Data-parallelism partitions training samples into multiple workers and then all workers apply nearly the same algorithms to different groups of training samples. On the other hand, model-parallelism partitions the model into multiple workers, of which each processes the exact copy of all training samples and operates on different parts of the model. In this paper, we will introduce the memory-saving parallel implementation of the proposed ridge solution based on the inverse Cholesky factor, and try to avoid the square-root and division operations in that implementation.

This paper is organized as follows. Section II introduces the existing generalized inverse solutions for the BLS with added nodes, and summarizes the construction model and learning procedure of BLS. Then for BLS, we propose the ridge solution by inverse Cholesky factorization in Section III, and propose the ridge solution based on the ridge inverse in Section IV. Section V compares the expected computational complexities of the presented BLS algorithms, evaluates these BLS algorithms by numerical experiments, and introduces several implementation aspects of the inverse Cholesky factorization, which include parallelization, memory saving, square-root free and division free. Finally, we make conclusion in Section VI.

## II. EXISTING GENERALIZED INVERSE SOLUTIONS FOR THE BLS WITH ADDED NODES

In RVFLNN, the expanded input matrix  $\mathbf{A} = [\mathbf{X}|\xi(\mathbf{X}\mathbf{W}_h + \beta_h)]$ , where  $\mathbf{W}_h$  and  $\beta_h$  are random,  $\mathbf{X}$  is the input data, and  $\xi$  is the activation function. The corresponding output

$$\hat{\mathbf{Y}} = \mathbf{A}\mathbf{W}, \quad (1)$$

where  $\mathbf{W}$  is the output weight matrix. For (1), the generalized inverse solution [18] is

$$\bar{\mathbf{W}} = \mathbf{A}^+ \mathbf{Y}, \quad (2)$$

where  $\mathbf{Y}$  denotes the labels and the generalized inverse

$$\mathbf{A}^+ = (\mathbf{A}^T \mathbf{A})^{-1} \mathbf{A}^T. \quad (3)$$

### A. Ridge Regression Approximation of the Generalized Inverse

In a flatted neural network, the generalized inverse solution (2) is equivalent to the least square solution

$$\underset{\bar{\mathbf{W}}}{\operatorname{argmin}} : \|\mathbf{A}\bar{\mathbf{W}} - \mathbf{Y}\|_2 \quad (4)$$

of the linear equation (1), which is a very convenient approach to obtain the output weights [15], [16]. Although the least square solution (4) is aimed to minimize training errors, usually it can not achieve the minimum generalization errors, especially for ill-conditioned problems. To improve the generalization performance, instead of the least square solution (4), we can use the regularized least-square solution

$$\underset{\mathbf{W}}{\operatorname{argmin}} : \|\mathbf{A}\mathbf{W} - \mathbf{Y}\|_2^2 + \lambda \|\mathbf{W}\|_2^2, \quad (5)$$

where  $\|\bullet\|_2^2$  denotes the  $l_2$  norm, and  $\lambda > 0$  is the constraint on the sum of the squared weights  $\mathbf{W}$ . The solution (5) is equivalent to the ridge solution [18]

$$\mathbf{W} = \mathbf{A}^\dagger \mathbf{Y}, \quad (6)$$

where the ridge inverse

$$\mathbf{A}^\dagger = (\mathbf{A}^T \mathbf{A} + \lambda \mathbf{I})^{-1} \mathbf{A}^T. \quad (7)$$

In (7), the ridge parameter  $\lambda$  can be any positive real number. When  $\lambda \rightarrow 0$ , the ridge solution (6) degenerates into the generalized inverse solution (2), and the ridge inverse degenerates into the generalized inverse [16, equation (3)], i.e.,

$$\lim_{\lambda \rightarrow 0} \mathbf{A}^\dagger = \lim_{\lambda \rightarrow 0} (\mathbf{A}^T \mathbf{A} + \lambda \mathbf{I})^{-1} \mathbf{A}^T = \mathbf{A}^+. \quad (8)$$

In [16], the ridge regression approximation of the generalized inverse, i.e., (8), is applied to compute the generalized inverse.

### B. Broad Learning Model on Added Nodes

In the BLS, the input data  $\mathbf{X}$  is mapped to form the feature nodes, and then the feature nodes are enhanced as the enhancement nodes. At last, the connections of all the feature and enhancement nodes are fed into the output.

The BLS projects the input data  $\mathbf{X}$  to obtain the  $i$ -th group of mapped features  $\ddot{\mathbf{Z}}_i$  by

$$\ddot{\mathbf{Z}}_i = \phi(\mathbf{X}\mathbf{W}_{e_i} + \beta_{e_i}), \quad (9)$$

where the weights  $\mathbf{W}_{e_i}$  and the biases  $\beta_{e_i}$  are generated randomly and then fine-tuned slightly with the linear inverse problem [16]. All the  $n$  groups of features nodes can be concatenated into

$$\ddot{\mathbf{Z}}^n \equiv [\ddot{\mathbf{Z}}_1 \quad \cdots \quad \ddot{\mathbf{Z}}_n], \quad (10)$$

which are enhanced to obtain the  $j$ -th group of enhancement nodes  $\ddot{\mathbf{H}}_j$  by

$$\ddot{\mathbf{H}}_j = \xi(\ddot{\mathbf{Z}}^n \mathbf{W}_{h_j} + \beta_{h_j}), \quad (11)$$

where  $\mathbf{W}_{h_j}$  and  $\beta_{h_j}$  are random. Then all the  $m$  groups of enhancement nodes can also be concatenated into

$$\ddot{\mathbf{H}}^m \equiv [\ddot{\mathbf{H}}_1, \dots, \ddot{\mathbf{H}}_m]. \quad (12)$$

All the feature and enhancement nodes can be denoted as the expanded input matrix  $\ddot{\mathbf{A}}_n^m = [\ddot{\mathbf{Z}}^n | \ddot{\mathbf{H}}^m]$ , where the subscript  $n$  and the superscript  $m$  of  $\ddot{\mathbf{A}}_n^m$  represent  $n$  groups of feature nodes and  $m$  groups of enhancement nodes, respectively. Finally, the connections of all the feature and enhancement nodes are fed into the output by

$$\hat{\mathbf{Y}} = [\ddot{\mathbf{Z}}^n | \ddot{\mathbf{H}}^m] \ddot{\mathbf{W}}_n^m = \ddot{\mathbf{A}}_n^m \ddot{\mathbf{W}}_n^m, \quad (13)$$

where the desired connection weights  $\ddot{\mathbf{W}}_n^m$  are computed by (2) from  $(\ddot{\mathbf{A}}_n^m)^+$ , the pseudoinverse with the ridge regression.

It can be seen that all the  $n$  groups of feature nodes are enhanced by (11) synchronously, to obtain the  $j$ -th group of enhancement nodes  $\ddot{\mathbf{H}}_j$ . In [16], a different construction is also proposed, which connects each group of feature nodes to a group of enhancement nodes. That construction with  $n$  groups of feature and enhancement nodes can be denoted as

$$\hat{\mathbf{Y}} = [\ddot{\mathbf{Z}}_1, \xi(\ddot{\mathbf{Z}}_1 \mathbf{W}_{h_1} + \beta_{h_1}) | \dots | \ddot{\mathbf{Z}}_n, \xi(\ddot{\mathbf{Z}}_n \mathbf{W}_{h_n} + \beta_{h_n})] \ddot{\mathbf{W}}_n^m.$$

### C. Incremental Learning for the Original BLS (i.e., Orig.)

In this subsection, we introduce the incremental learning algorithm for the original BLS [16], which is abbreviated as **Orig.** in this paper. When the model cannot reach the desired accuracy, additional nodes can be inserted to achieve a better performance, and the incremental learning algorithm for the original BLS can remodel the system in an incremental way without retraining the whole network. In BLS, the inserted nodes can be some enhancement nodes, or some feature nodes with the corresponding enhancement nodes.

When some enhancement nodes are inserted, the inserted nodes can be represented as the  $(m+1)$ -th group of enhancement nodes, i.e.,  $\ddot{\mathbf{H}}_{m+1}$  defined by (11). Accordingly, the expanded input matrix  $\ddot{\mathbf{A}}_n^m$  is updated into

$$\ddot{\mathbf{A}}_n^{m+1} = [\ddot{\mathbf{A}}_n^m | \ddot{\mathbf{H}}_{m+1}]. \quad (14)$$

Moreover, when some feature nodes and the corresponding enhancement nodes are inserted, the added feature nodes can be denoted as the  $(n+1)$ -th group of feature nodes, i.e.,  $\ddot{\mathbf{Z}}_{n+1}$  defined by (9), and then  $\ddot{\mathbf{Z}}_{n+1}$  is substituted into (11) to get the added enhancement nodes in the  $j$ -th group (corresponding to  $\ddot{\mathbf{Z}}_{n+1}$ ), i.e.,  $\ddot{\mathbf{H}}_{j,ex} = \xi(\ddot{\mathbf{Z}}_{n+1} \mathbf{W}_{ex_j} + \beta_{ex_j})$ . The  $m$  groups of added enhancement nodes is concatenated into  $\ddot{\mathbf{H}}_{ex_m} = [\ddot{\mathbf{H}}_{1,ex}, \ddot{\mathbf{H}}_{2,ex}, \dots, \ddot{\mathbf{H}}_{m,ex}]$  by (12). Then  $\ddot{\mathbf{Z}}_{n+1}$  and  $\ddot{\mathbf{H}}_{ex_m}$  are applied to update the expanded input matrix  $\ddot{\mathbf{A}}_n^m$  into [16]

$$\ddot{\mathbf{A}}_{n+1}^m = [\ddot{\mathbf{A}}_n^m | \ddot{\mathbf{Z}}_{n+1} | \ddot{\mathbf{H}}_{ex_m}]. \quad (15)$$

Assume  $l$  training samples and  $k$  nodes in the expanded input matrix  $\ddot{\mathbf{A}}_n^m$ . Then  $\ddot{\mathbf{A}}_n^m \in \mathbb{R}^{l \times k}$  can be written as

$$\mathbf{A}_k = \ddot{\mathbf{A}}_n^m = [\ddot{\mathbf{Z}}^n | \ddot{\mathbf{H}}^m], \quad (16)$$

---

### Algorithm 1 : The Broad Learning Algorithm: Computation of Output Weights and Increment of Feature Nodes and Enhancement Nodes

---

**Input:** Training samples  $\mathbf{X}$  and labels  $\mathbf{Y}$

**Output:** Output weights  $\mathbf{W}$

```

1: for  $i = 1 : n$  do
2:   Fine-tune random  $\mathbf{W}_{e_i}$  and  $\beta_{e_i}$ ;
3:   Compute  $\ddot{\mathbf{Z}}_i = \phi(\mathbf{X} \mathbf{W}_{e_i} + \beta_{e_i})$ ;
4: end for
5: Concatenate the feature nodes into  $\ddot{\mathbf{Z}}^n \equiv [\ddot{\mathbf{Z}}_1 \dots \ddot{\mathbf{Z}}_n]$ ;
6: for  $j = 1 : m$  do
7:   Random  $\mathbf{W}_{h_j}$  and  $\beta_{h_j}$ ;
8:   Compute  $\ddot{\mathbf{H}}_j = \xi(\ddot{\mathbf{Z}}^n \mathbf{W}_{h_j} + \beta_{h_j})$ ;
9: end for
10: Set the enhancement nodes group  $\ddot{\mathbf{H}}^m \equiv [\ddot{\mathbf{H}}_1, \dots, \ddot{\mathbf{H}}_m]$ ;
11: Set  $\ddot{\mathbf{A}}_n^m = [\ddot{\mathbf{Z}}^n | \ddot{\mathbf{H}}^m]$ ;
12: Compute the intermediate result and  $\ddot{\mathbf{W}}_n^m$ ;
13: while The target training error is not reached do
14:   if only enhancement nodes are added then
15:     Random  $\mathbf{W}_{h_{m+1}}$  and  $\beta_{h_{m+1}}$ ;
16:     Compute  $\ddot{\mathbf{H}}_{m+1} = \xi(\ddot{\mathbf{Z}}^n \mathbf{W}_{h_{m+1}} + \beta_{h_{m+1}})$ ;
17:     Set  $\ddot{\mathbf{A}}_n^{m+1} = [\ddot{\mathbf{A}}_n^m | \ddot{\mathbf{H}}_{m+1}]$ ;
18:     Update the intermediate result, and update  $\ddot{\mathbf{W}}_n^m$ 
       into  $\ddot{\mathbf{W}}_n^{m+1}$ ;
19:      $m = m + 1$ ;
20:   else [feature nodes are added]
21:     Fine-tune random  $\mathbf{W}_{e_{n+1}}$  and  $\beta_{e_{n+1}}$ ;
22:     Compute  $\ddot{\mathbf{Z}}_{n+1} = \phi(\mathbf{X} \mathbf{W}_{e_{n+1}} + \beta_{e_{n+1}})$ ;
23:     Set  $\ddot{\mathbf{Z}}^{n+1} = [\ddot{\mathbf{Z}}^n | \ddot{\mathbf{Z}}_{n+1}]$ ;
24:     for  $j = 1 : m$  do
25:       Random  $\mathbf{W}_{ex_j}$  and  $\beta_{ex_j}$ ;
26:       Compute  $\ddot{\mathbf{H}}_{j,ex} = \xi(\ddot{\mathbf{Z}}_{n+1} \mathbf{W}_{ex_j} + \beta_{ex_j})$ ;
27:     end for
28:     Set  $\ddot{\mathbf{H}}_{ex_m} = [\ddot{\mathbf{H}}_{1,ex}, \dots, \ddot{\mathbf{H}}_{m,ex}]$ ;
29:     Set  $\ddot{\mathbf{A}}_{n+1}^m = [\ddot{\mathbf{A}}_n^m | \ddot{\mathbf{Z}}_{n+1} | \ddot{\mathbf{H}}_{ex_m}]$ ;
30:     Update the intermediate result, and update  $\ddot{\mathbf{W}}_n^m$ 
       into  $\ddot{\mathbf{W}}_{n+1}^m$ ;
31:      $n = n + 1$ ;
32:   end if
33: end while
34:  $\mathbf{W} = \ddot{\mathbf{W}}_n^m$ ;

```

---

where the subscript  $k$  in  $\mathbf{A}_k$  denotes the number of columns. We can also write both  $\ddot{\mathbf{A}}_n^{m+1}$  and  $\ddot{\mathbf{A}}_{n+1}^m$  as  $\mathbf{A}_{k+q}$  with  $k+q$  columns, to unify (14) and (15) into

$$\mathbf{A}_{k+q} = [\mathbf{A}_k | \mathbf{H}], \quad (17)$$

where  $\mathbf{H}$  with  $q$  columns is defined by

$$\mathbf{H} = \ddot{\mathbf{H}}_{m+1} \quad (18)$$

for (14), or by

$$\mathbf{H} = [\ddot{\mathbf{Z}}_{n+1} | \ddot{\mathbf{H}}_{ex_m}] \quad (19)$$

for (15).

The incremental learning algorithm for BLS in [16] applies the Greville's method [19] to compute the generalized inverse of the column-partitioned matrix  $\mathbf{A}_{k+q} = [\mathbf{A}_k | \mathbf{H}]$ , by

$$\mathbf{A}_{k+q}^+ = [\mathbf{A}_k | \mathbf{H}]^+ = \begin{bmatrix} \mathbf{A}_k^+ - \bar{\mathbf{D}}\bar{\mathbf{B}}^T \\ \bar{\mathbf{B}}^T \end{bmatrix} \quad (20)$$

where the newly added sub-matrix <sup>1</sup>

$$\bar{\mathbf{B}}^T = \begin{cases} \bar{\mathbf{C}}^+ = (\bar{\mathbf{C}}^T \bar{\mathbf{C}})^{-1} \bar{\mathbf{C}}^T & \text{if } \bar{\mathbf{C}} \neq \mathbf{0} \\ (\mathbf{I} + \bar{\mathbf{D}}^T \bar{\mathbf{D}})^{-1} \bar{\mathbf{D}}^T \mathbf{A}_k^+ & \text{if } \bar{\mathbf{C}} = \mathbf{0}, \end{cases} \quad (21a)$$

$$\bar{\mathbf{C}} = \mathbf{H} - \mathbf{A}_k \bar{\mathbf{D}}, \quad (22)$$

and

$$\bar{\mathbf{D}} = \mathbf{A}_k^+ \mathbf{H}. \quad (23)$$

After the generalized inverse  $\mathbf{A}_k^+$  is updated into  $\mathbf{A}_{k+q}^+$  by (20), the sub-matrix  $\bar{\mathbf{B}}^T$  in  $\mathbf{A}_{k+q}^+$  is utilized to update the generalized inverse solution  $\bar{\mathbf{W}}_k$  into  $\bar{\mathbf{W}}_{k+q}$  by

$$\bar{\mathbf{W}}_{k+q} = \begin{bmatrix} \bar{\mathbf{W}}_k - \bar{\mathbf{D}}\bar{\mathbf{B}}^T \mathbf{Y} \\ \bar{\mathbf{B}}^T \mathbf{Y} \end{bmatrix}, \quad (24)$$

which forms the output weights.

---

**Algorithm 2 : The Existing Generalized Inverse Solution for BLS (i.e., Orig.): Initialization and Update of Generalized Inverse and Output Weights**

---

```

.....
12: Compute  $(\ddot{\mathbf{A}}_n^m)^+ = \lim_{\lambda \rightarrow 0} ((\ddot{\mathbf{A}}_n^m)^T \ddot{\mathbf{A}}_n^m + \lambda \mathbf{I})^{-1} (\ddot{\mathbf{A}}_n^m)^T$ 
    and  $\ddot{\mathbf{W}}_n^m = (\ddot{\mathbf{A}}_n^m)^+ \mathbf{Y}$ ;
.....
18: Compute  $(\ddot{\mathbf{A}}_n^{m+1})^+$  and  $\ddot{\mathbf{W}}_n^{m+1}$  by
     $\psi_1((\ddot{\mathbf{A}}_n^m)^+, \ddot{\mathbf{A}}_n^m, \ddot{\mathbf{H}}_{m+1}, \ddot{\mathbf{W}}_n^m, \mathbf{Y})$ ;
.....
30: Compute  $(\ddot{\mathbf{A}}_{n+1}^m)^+$  and  $\ddot{\mathbf{W}}_{n+1}^m$  by
     $\psi_1((\ddot{\mathbf{A}}_n^m)^+, \ddot{\mathbf{A}}_n^m, [\ddot{\mathbf{Z}}_{n+1} | \ddot{\mathbf{H}}_{exm}], \ddot{\mathbf{W}}_n^m, \mathbf{Y})$ ;
.....

```

---



---

**Algorithm 3** The Algorithm to Update  $\mathbf{A}_k^+$  and  $\bar{\mathbf{W}}_k$  for **Orig.**

---

```

function  $\psi_1(\mathbf{A}_k^+, \mathbf{A}_k, \mathbf{H}, \bar{\mathbf{W}}_k, \mathbf{Y})$ 
     $\bar{\mathbf{D}} = \mathbf{A}_k^+ \mathbf{H}$ 
     $\bar{\mathbf{C}} = \mathbf{H} - \mathbf{A}_k \bar{\mathbf{D}}$ 
     $\bar{\mathbf{B}}^T = \lim_{\lambda \rightarrow 0} (\bar{\mathbf{C}}^T \bar{\mathbf{C}} + \lambda \mathbf{I})^{-1} \bar{\mathbf{C}}^T$ 
     $\mathbf{A}_{k+q}^+ = \begin{bmatrix} \mathbf{A}_k^+ - \bar{\mathbf{D}}\bar{\mathbf{B}}^T \\ \bar{\mathbf{B}}^T \end{bmatrix}$ 
     $\bar{\mathbf{W}}_{k+q} = \begin{bmatrix} \bar{\mathbf{W}}_k - \bar{\mathbf{D}}\bar{\mathbf{B}}^T \mathbf{Y} \\ \bar{\mathbf{B}}^T \mathbf{Y} \end{bmatrix}$ 
    return  $\mathbf{A}_{k+q}^+, \bar{\mathbf{W}}_{k+q}$ 
end function

```

---

<sup>1</sup>In [16], the generalized inverse (8) is utilized to compute  $\bar{\mathbf{C}}^+$  in (21a), where  $\lim_{\lambda \rightarrow 0} (\bar{\mathbf{C}}^T \bar{\mathbf{C}} + \lambda \mathbf{I})^{-1} \bar{\mathbf{C}}^T$  is written as  $(\bar{\mathbf{C}}^T \bar{\mathbf{C}})^{-1} \bar{\mathbf{C}}^T$  for simplicity.

*D. The Existing Efficient Generalized Inverse Solution for BLS by Inverse Cholesky Factorization (i.e., Exg-E)*

The existing efficient BLS proposed in [20] accelerates the original BLS [16] for added nodes, which is abbreviated as **Exg-E** in this paper. It computes the output weights  $\bar{\mathbf{W}}$  from the inverse Cholesky factor of the Hermitian matrix

$$\bar{\mathbf{R}}_k = \lim_{\lambda \rightarrow 0} (\mathbf{A}_k^T \mathbf{A}_k + \lambda \mathbf{I}) \quad (25)$$

in the pseudoinverse (8), and updates the inverse Cholesky factor efficiently. Write the inverse Cholesky factor of  $\bar{\mathbf{R}}_k$  as

$$\bar{\mathbf{F}}_k \bar{\mathbf{F}}_k^T = \bar{\mathbf{R}}_k^{-1} = \lim_{\lambda \rightarrow 0} (\mathbf{A}_k^T \mathbf{A}_k + \lambda \mathbf{I})^{-1}. \quad (26)$$

Then we can substitute (26) into (8) to denote  $\mathbf{A}_k^+$  as

$$\mathbf{A}_k^+ = \bar{\mathbf{F}}_k \bar{\mathbf{F}}_k^T \mathbf{A}_k^T, \quad (27)$$

which is substituted into (2) to compute  $\bar{\mathbf{W}}_k$  by

$$\bar{\mathbf{W}}_k = \bar{\mathbf{F}}_k \bar{\mathbf{F}}_k^T \mathbf{A}_k^T \mathbf{Y}. \quad (28)$$

In [20],  $\bar{\mathbf{C}}$  is computed by

$$\bar{\mathbf{C}} = \mathbf{H} - \mathbf{A}_k \bar{\mathbf{F}}_k \bar{\mathbf{F}}_k^T \mathbf{A}_k^T \mathbf{H}. \quad (29)$$

Let us substitute (27) into (23) to obtain

$$\bar{\mathbf{D}} = \bar{\mathbf{F}}_k \bar{\mathbf{F}}_k^T \mathbf{A}_k^T \mathbf{H}, \quad (30)$$

and then we can write (29) as (22) with  $\bar{\mathbf{D}}$  defined by (30). Finally,  $\bar{\mathbf{C}}$  is applied to update  $\bar{\mathbf{F}}_k$  into  $\bar{\mathbf{F}}_{k+q}$  by

$$\bar{\mathbf{F}}_{k+q} = \begin{bmatrix} \bar{\mathbf{F}}_k & \bar{\mathbf{T}} \\ \mathbf{0} & \bar{\mathbf{G}} \end{bmatrix} \quad (31)$$

with <sup>2</sup>

$$\begin{cases} \bar{\mathbf{G}} \bar{\mathbf{G}}^T = \lim_{\lambda \rightarrow 0} (\bar{\mathbf{C}}^T \bar{\mathbf{C}} + \lambda \mathbf{I})^{-1} \\ \bar{\mathbf{T}} = -\bar{\mathbf{D}} \bar{\mathbf{G}}, \end{cases} \quad (32a)$$

$$\bar{\mathbf{T}} = -\bar{\mathbf{D}} \bar{\mathbf{G}}, \quad (32b)$$

while  $\bar{\mathbf{T}}$  and  $\bar{\mathbf{G}}$  in (31) are applied to update  $\bar{\mathbf{W}}_k$  into

$$\bar{\mathbf{W}}_{k+q} = \begin{bmatrix} \bar{\mathbf{W}}_k + \bar{\mathbf{T}} \bar{\mathbf{G}}^T (\mathbf{H}^T \mathbf{Y} - \mathbf{H}^T \mathbf{A}_k \bar{\mathbf{W}}_k) \\ \bar{\mathbf{G}} \bar{\mathbf{G}}^T (\mathbf{H}^T \mathbf{Y} - \mathbf{H}^T \mathbf{A}_k \bar{\mathbf{W}}_k) \end{bmatrix}. \quad (33)$$

*E. Construction Model and Learning Procedure of BLS*

Both the existing BLS algorithms for the increment of nodes follow the same construction model and learning procedure, which is summarized in **Algorithm 1**. Different methods are utilized by the existing BLS algorithms to implement several steps in **Algorithm 1**, i.e., the step to compute the intermediate result and  $\bar{\mathbf{W}}_n^m$  in row 12, the step to update the intermediate result and  $\bar{\mathbf{W}}_n^{m+1}$  in row 18, and the step to update the intermediate result and  $\bar{\mathbf{W}}_{n+1}^m$  in row 30.

**Algorithms 2** and **4** describe the implementations of the steps in rows 12, 18 and 30 of **Algorithm 1**, for the original BLS in [16] (i.e., **Orig.**) and the existing efficient BLS in [20] (i.e., **Exg-E**), respectively. The functions  $\psi_1(\bullet)$  and  $\psi_2(\bullet)$  utilized in **Algorithms 2** and **4** are defined by **Algorithms 3** and **5**, respectively. Notice that **Algorithm 2** includes (8) and

<sup>2</sup>In (32a),  $\bar{\mathbf{G}}$  denotes the upper-triangular inverse Cholesky factor of  $\lim_{\lambda \rightarrow 0} (\bar{\mathbf{C}}^T \bar{\mathbf{C}} + \lambda \mathbf{I})$ .

---

**Algorithm 4 : The Existing Efficient Generalized Inverse Solution for BLS (i.e., Exg-E): Initialization and Update of Inverse Cholesky Factor and Output Weights**


---

- .....
- 12: Compute the upper-triangular  $\ddot{\mathbf{F}}_n^m$  satisfying  
 $\ddot{\mathbf{F}}_n^m (\ddot{\mathbf{F}}_n^m)^T = \lim_{\lambda \rightarrow 0} ((\ddot{\mathbf{A}}_n^m)^T \ddot{\mathbf{A}}_n^m + \lambda \mathbf{I})^{-1}$ ,  
 and compute  $\ddot{\mathbf{W}}_n^m = \ddot{\mathbf{F}}_n^m (\ddot{\mathbf{F}}_n^m)^T (\ddot{\mathbf{A}}_n^m)^T \mathbf{Y}$ ;  
 .....
- 18: Compute  $\ddot{\mathbf{F}}_n^{m+1}$  and  $\ddot{\mathbf{W}}_n^{m+1}$  by  
 $\psi_2(\ddot{\mathbf{F}}_n^m, \ddot{\mathbf{A}}_n^m, \ddot{\mathbf{H}}_{m+1}, \ddot{\mathbf{W}}_n^m, \mathbf{Y})$ ;  
 .....
- 30: Compute  $\ddot{\mathbf{F}}_{n+1}^m$  and  $\ddot{\mathbf{W}}_{n+1}^m$  by  
 $\psi_2(\ddot{\mathbf{F}}_n^m, \ddot{\mathbf{A}}_n^m, [\ddot{\mathbf{Z}}_{n+1} | \ddot{\mathbf{H}}_{exm}], \ddot{\mathbf{W}}_n^m, \mathbf{Y})$ ;  
 .....
- 

---

**Algorithm 5 The Algorithm to Update  $\bar{\mathbf{F}}_k$  and  $\bar{\mathbf{W}}_k$  for Exg-E**


---

```

function  $\psi_2(\bar{\mathbf{F}}_k, \mathbf{A}_k, \mathbf{H}, \bar{\mathbf{W}}_k, \mathbf{Y})$ 
   $\bar{\mathbf{D}} = \bar{\mathbf{F}}_k \bar{\mathbf{F}}_k^T \mathbf{A}_k^T \mathbf{H}$ 
   $\bar{\mathbf{C}} = \mathbf{H} - \mathbf{A}_k \bar{\mathbf{D}}$ 
  Compute  $\bar{\mathbf{G}}$  satisfying  $\bar{\mathbf{G}} \bar{\mathbf{G}}^T = \lim_{\lambda \rightarrow 0} (\bar{\mathbf{C}}^T \bar{\mathbf{C}} + \lambda \mathbf{I})^{-1}$ 
   $\bar{\mathbf{T}} = -\bar{\mathbf{D}} \bar{\mathbf{G}}$ 
   $\bar{\mathbf{F}}_{k+q} = \begin{bmatrix} \bar{\mathbf{F}}_k & \bar{\mathbf{T}} \\ \mathbf{0} & \bar{\mathbf{G}} \end{bmatrix}$ 
   $\bar{\mathbf{W}}_{k+q} = \begin{bmatrix} \bar{\mathbf{W}}_k + \bar{\mathbf{T}} \bar{\mathbf{G}}^T (\mathbf{H}^T \mathbf{Y} - \mathbf{H}^T \mathbf{A}_k \bar{\mathbf{W}}_k) \\ \bar{\mathbf{G}} \bar{\mathbf{G}}^T (\mathbf{H}^T \mathbf{Y} - \mathbf{H}^T \mathbf{A}_k \bar{\mathbf{W}}_k) \end{bmatrix}$ 
  return  $\bar{\mathbf{F}}_{k+q}, \bar{\mathbf{W}}_{k+q}$ 
end function

```

---

(2), **Algorithm 3** includes (20)-(24), **Algorithm 4** includes (26) and (28), and **Algorithm 5** includes (22) and (30)-(33).

### III. PROPOSED RIDGE SOLUTION FOR BLS BY INVERSE CHOLESKY FACTORIZATION OF A PARTITIONED MATRIX

The original BLS algorithm in [16] is based on the Greville's method [19], which can only compute the generalized inverse of a partitioned matrix. As shown in (8), the ridge inverse can be viewed as an approximate generalized inverse [16], [18]. However, the ridge inverse is not the generalized inverse [18], e.g., the ridge inverse  $\mathbf{A}^\dagger$  does not obey  $\mathbf{A} \mathbf{A}^\dagger \mathbf{A} = \mathbf{A}$ , while the generalized inverse  $\mathbf{A}^+$  obeys [19]  $\mathbf{A} \mathbf{A}^+ \mathbf{A} = \mathbf{A}$ . So the Greville's method for the generalized inverse [19], [22] is usually inapplicable to the ridge inverse, but it can be applied to the ridge regression (8) in the original BLS, since the ridge parameter  $\lambda$  is set to a very small positive real number [16], e.g.,  $10^{-8}$ , and then  $\lambda \rightarrow 0$  can be assumed to assure that the ridge regression (8) is equal to the generalized inverse.

The BLS algorithm proposed in [20] is only an efficient implementation of the original BLS on added nodes, which is based on the inverse Cholesky factor of the Hermitian matrix in the ridge regression (8). Thus the efficient BLS in [20] also assumes the ridge parameter  $\lambda \rightarrow 0$ , as the original BLS.

For the incremental BLS on added nodes, we will propose an efficient ridge solution based on the inverse Cholesky factor [21] and its numerically more stable implementation,

which are abbreviated as **Chol-1** and **Chol-2**, respectively. It is no longer required to assume the ridge parameter  $\lambda \rightarrow 0$  in the proposed efficient ridge solution, which computes the output weights from the inverse Cholesky factor of the Hermitian matrix  $\mathbf{A}^T \mathbf{A} + \lambda \mathbf{I}$  in the ridge inverse (7), and updates the inverse Cholesky factor efficiently by extending the inverse Cholesky factorization in [21].

#### A. Efficient Inverse Cholesky Factorization of a Hermitian Matrix Partitioned into $2 \times 2$ Blocks for Proposed Chol-1

In this subsection, we extend the efficient inverse Cholesky factorization proposed in [21], to develop an efficient inverse Cholesky factorization for a Hermitian matrix partitioned into  $2 \times 2$  blocks, which will be utilized in what follows.

In [21], the inverse Cholesky factor of a Hermitian matrix  $\mathbf{R}_k \in \mathbb{R}^{k \times k}$  is the upper-triangular  $\mathbf{F}_k$  that satisfies

$$\mathbf{F}_k \mathbf{F}_k^T = \mathbf{R}_k^{-1} = (\mathbf{A}_k^T \mathbf{A}_k + \lambda \mathbf{I})^{-1}, \quad (34)$$

where  $\mathbf{R}_k$  is defined by <sup>3</sup>

$$\mathbf{R}_k = \mathbf{A}_k^T \mathbf{A}_k + \lambda \mathbf{I}. \quad (35)$$

From (88), we can deduce

$$\mathbf{F}_k^{-T} \mathbf{F}_k^{-1} = \mathbf{R}_k, \quad (36)$$

which shows that the lower-triangular  $\mathbf{F}_k^{-T}$  is the conventional Cholesky factor [23, Theorem 4.2.5] of  $\mathbf{R}_k$ .

The efficient inverse Cholesky factorization [21] partitions a Hermitian matrix  $\mathbf{R}_{k+1}$  into

$$\mathbf{R}_{k+1} = \begin{bmatrix} \mathbf{R}_k & \mathbf{p} \\ \mathbf{p}^T & u \end{bmatrix}, \quad (37)$$

and updates the inverse Cholesky factor of  $\mathbf{R}_k$  into that of  $\mathbf{R}_{k+1}$  by

$$\mathbf{F}_{k+1} = \begin{bmatrix} \mathbf{F}_k & \mathbf{t} \\ \mathbf{0} & g \end{bmatrix} \quad (38)$$

where

$$\begin{cases} g = 1/\sqrt{u - \mathbf{p}^T \mathbf{F}_k \mathbf{F}_k^T \mathbf{p}} \\ \mathbf{t} = -g \mathbf{F}_k \mathbf{F}_k^T \mathbf{p}. \end{cases} \quad (39a) \quad (39b)$$

In (92)-(94),  $u$  and  $g$  are scalars, while  $\mathbf{p}$  and  $\mathbf{t}$  are column vectors of length  $k$ .

In the more general case, we can partition a Hermitian matrix  $\mathbf{R}_{k+q} = \mathbf{A}_{k+q}^T \mathbf{A}_{k+q} + \lambda \mathbf{I} = [\mathbf{A}_k | \mathbf{H}]^T [\mathbf{A}_k | \mathbf{H}] + \lambda \mathbf{I}$  into a  $2 \times 2$  block Hermitian matrix, i.e.,

$$\mathbf{R}_{k+q} = \begin{bmatrix} \mathbf{R}_k & \mathbf{P} \\ \mathbf{P}^T & \mathbf{U} \end{bmatrix} = \begin{bmatrix} \mathbf{R}_k & \mathbf{A}_k^T \mathbf{H} \\ \mathbf{H}^T \mathbf{A}_k & \mathbf{H}^T \mathbf{H} + \lambda \mathbf{I} \end{bmatrix}, \quad (40)$$

where  $\mathbf{U} = \mathbf{H}^T \mathbf{H} + \lambda \mathbf{I} \in \mathbb{R}^{q \times q}$  and  $\mathbf{P} = \mathbf{A}_k^T \mathbf{H} \in \mathbb{R}^{k \times q}$ . We can apply (94) and (38) to update the inverse Cholesky factor of  $\mathbf{R}_k$  into that of  $\mathbf{R}_{k+q}$  through  $q$  iterations, to obtain

$$\mathbf{F}_{k+q} = \begin{bmatrix} \mathbf{F}_k & \mathbf{T} \\ \mathbf{0} & \mathbf{G} \end{bmatrix} \quad (41)$$

<sup>3</sup>Notice that the ridge parameter  $\lambda$  can be any positive real number for  $\mathbf{R}_k$  defined in (89), while  $\lambda \rightarrow 0$  needs to be assumed for  $\bar{\mathbf{R}}_k$  defined in (25).

where  $\mathbf{T} \in \mathbb{R}^{k \times q}$  and  $\mathbf{G} \in \mathbb{R}^{q \times q}$ . However, we prefer to update  $\mathbf{F}_k$  into  $\mathbf{F}_{k+q}$  through only 1 iteration, by computing

$$\begin{cases} \mathbf{G}\mathbf{G}^T = (\mathbf{H}^T\mathbf{H} + \lambda\mathbf{I} - \mathbf{H}^T\mathbf{A}_k\mathbf{F}_k\mathbf{F}_k^T\mathbf{A}_k^T\mathbf{H})^{-1} & (42a) \\ \mathbf{T} = -\mathbf{F}_k\mathbf{F}_k^T\mathbf{A}_k^T\mathbf{H}\mathbf{G}, & (42b) \end{cases}$$

which can be regarded as an extension of (94), and will be deduced in Appendix A.

Now we can update the inverse Cholesky factor of  $\mathbf{R}_k$  into that of  $\mathbf{R}_{k+q}$  by the above-described block inverse Cholesky factorization, i.e., we can update  $\mathbf{F}_k$  into  $\mathbf{F}_{k+q}$  by (99) and (98), and compute the initial  $\mathbf{F}_k$  by (88). In (99a), the upper-triangular inverse Cholesky factor  $\mathbf{G}$  can be computed by the inverse Cholesky factorization [21] or by inverting and transposing the lower-triangular Cholesky factor<sup>4</sup>.

### B. Utilizing the Inverse Cholesky Factor to Compute the Ridge Inverse and the Ridge Solution for Proposed Chol-1

In this subsection, we will utilize the inverse Cholesky factor to compute the ridge inverse and the ridge solution.

We can compute the ridge inverse  $\mathbf{A}_k^\dagger$  from  $\mathbf{F}_k$  by

$$\mathbf{A}_k^\dagger = \mathbf{F}_k\mathbf{F}_k^T\mathbf{A}_k^T, \quad (43)$$

which is deduced by substituting (88) into (7). Then to update  $\mathbf{A}_k^\dagger$  into  $\mathbf{A}_{k+q}^\dagger$ , let us substitute (17) and (98) into (43) to write

$$\begin{aligned} \mathbf{A}_{k+q}^\dagger &= \begin{bmatrix} \mathbf{F}_k & \mathbf{T} \\ \mathbf{0} & \mathbf{G} \end{bmatrix} \begin{bmatrix} \mathbf{F}_k & \mathbf{T} \\ \mathbf{0} & \mathbf{G} \end{bmatrix}^T \begin{bmatrix} \mathbf{A}_k & \mathbf{H} \end{bmatrix}^T \\ &= \begin{bmatrix} \mathbf{F}_k\mathbf{F}_k^T\mathbf{A}_k^T + \mathbf{T}\mathbf{T}^T\mathbf{A}_k^T + \mathbf{T}\mathbf{G}^T\mathbf{H}^T \\ \mathbf{G}\mathbf{T}^T\mathbf{A}_k^T + \mathbf{G}\mathbf{G}^T\mathbf{H}^T \end{bmatrix}, \end{aligned}$$

into which we substitute (43) and (32b) to obtain

$$\begin{aligned} \mathbf{A}_{k+q}^\dagger &= \begin{bmatrix} \mathbf{A}_k^\dagger + \mathbf{T}(-\mathbf{F}_k\mathbf{F}_k^T\mathbf{A}_k^T\mathbf{H}\mathbf{G})^T\mathbf{A}_k^T + \mathbf{T}\mathbf{G}^T\mathbf{H}^T \\ \mathbf{G}(-\mathbf{F}_k\mathbf{F}_k^T\mathbf{A}_k^T\mathbf{H}\mathbf{G})^T\mathbf{A}_k^T + \mathbf{G}\mathbf{G}^T\mathbf{H}^T \end{bmatrix} \\ &= \begin{bmatrix} \mathbf{A}_k^\dagger + \mathbf{T}\mathbf{G}^T(\mathbf{H}^T - \mathbf{H}^T\mathbf{A}_k\mathbf{F}_k\mathbf{F}_k^T\mathbf{A}_k^T) \\ \mathbf{G}\mathbf{G}^T(\mathbf{H}^T - \mathbf{H}^T\mathbf{A}_k\mathbf{F}_k\mathbf{F}_k^T\mathbf{A}_k^T) \end{bmatrix} \quad (44) \end{aligned}$$

$$= \begin{bmatrix} \mathbf{A}_k^\dagger + \mathbf{T}\mathbf{G}^T(\mathbf{H}^T - \mathbf{H}^T\mathbf{A}_k\mathbf{A}_k^\dagger) \\ \mathbf{G}\mathbf{G}^T(\mathbf{H}^T - \mathbf{H}^T\mathbf{A}_k\mathbf{A}_k^\dagger) \end{bmatrix}. \quad (45)$$

Notice that the sub-matrices  $\mathbf{G}$  and  $\mathbf{T}$  in  $\mathbf{F}_{k+q}$  are utilized to update  $\mathbf{A}_k^\dagger$  into  $\mathbf{A}_{k+q}^\dagger$  by (45).

We can also use  $\mathbf{F}_k$  to compute the ridge solution  $\mathbf{W}_k$  by

$$\mathbf{W}_k = \mathbf{F}_k\mathbf{F}_k^T\mathbf{A}_k^T\mathbf{Y}, \quad (46)$$

which is deduced by substituting (43) into (6). To update  $\mathbf{W}_k$  into  $\mathbf{W}_{k+q}$ , substitute (45) into (6) (i.e.,  $\mathbf{W} = \mathbf{A}^\dagger\mathbf{Y}$ ) to write

$$\begin{aligned} \mathbf{W}_{k+q} &= \begin{bmatrix} \mathbf{A}_k^\dagger\mathbf{Y} + \mathbf{T}\mathbf{G}^T(\mathbf{H}^T\mathbf{Y} - \mathbf{H}^T\mathbf{A}_k\mathbf{A}_k^\dagger\mathbf{Y}) \\ \mathbf{G}\mathbf{G}^T(\mathbf{H}^T\mathbf{Y} - \mathbf{H}^T\mathbf{A}_k\mathbf{A}_k^\dagger\mathbf{Y}) \end{bmatrix} \\ &= \begin{bmatrix} \mathbf{W}_k + \mathbf{T}\mathbf{G}^T(\mathbf{H}^T\mathbf{Y} - \mathbf{H}^T\mathbf{A}_k\mathbf{W}_k) \\ \mathbf{G}\mathbf{G}^T(\mathbf{H}^T\mathbf{Y} - \mathbf{H}^T\mathbf{A}_k\mathbf{W}_k) \end{bmatrix}. \quad (47) \end{aligned}$$

When the ridge solution is computed by (46) or (47), the ridge inverse  $\mathbf{A}_k^\dagger$  or  $\mathbf{A}_{k+q}^\dagger$  is not required. Accordingly, there is

<sup>4</sup>Similarly,  $\mathbf{F}_k$  can be obtained by inverting and transposing the Cholesky factor  $\mathbf{F}_k^{-T}$ , as shown in (90).

actually no need to compute the ridge inverse from the inverse Cholesky factor by (43) or (45).

### C. A Numerically More Stable Implementation to Update the Inverse Cholesky Factor and the Ridge Solution (i.e., Chol-2)

Let us define

$$\mathbf{D} = \mathbf{F}_k\mathbf{F}_k^T\mathbf{A}_k^T\mathbf{H} \quad (48)$$

and

$$\mathbf{C} = \mathbf{H} - \mathbf{A}_k\mathbf{D} = \mathbf{H} - \mathbf{A}_k\mathbf{F}_k\mathbf{F}_k^T\mathbf{A}_k^T\mathbf{H}, \quad (49)$$

which are similar to (30) and (22), respectively. Then we can apply (49) to write (99a) as

$$\begin{aligned} \mathbf{G}\mathbf{G}^T &= (\mathbf{H}^T(\mathbf{H} - \mathbf{A}_k\mathbf{F}_k\mathbf{F}_k^T\mathbf{A}_k^T\mathbf{H}) + \lambda\mathbf{I})^{-1} \\ &= (\mathbf{H}^T\mathbf{C} + \lambda\mathbf{I})^{-1}. \end{aligned} \quad (50)$$

To write (50) in another form, let us substitute  $\mathbf{H} = \mathbf{C} + \mathbf{A}_k\mathbf{D}$  (deduced from (49)) into  $\mathbf{H}^T\mathbf{C}$  (in (50)) to obtain

$$\mathbf{H}^T\mathbf{C} = \mathbf{C}^T\mathbf{C} + \mathbf{D}^T\mathbf{A}_k^T\mathbf{C}, \quad (51)$$

where  $\mathbf{D}^T\mathbf{A}_k^T\mathbf{C}$  satisfies

$$\mathbf{D}^T\mathbf{A}_k^T\mathbf{C} = \lambda\mathbf{D}^T\mathbf{D}, \quad (52)$$

as will be verified in Appendix B. Then we substitute (52) into (51) to obtain

$$\mathbf{H}^T\mathbf{C} = \mathbf{C}^T\mathbf{C} + \lambda\mathbf{D}^T\mathbf{D}, \quad (53)$$

which is substituted into (50) to rewrite it as

$$\mathbf{G}\mathbf{G}^T = (\mathbf{C}^T\mathbf{C} + \lambda\mathbf{D}^T\mathbf{D} + \lambda\mathbf{I})^{-1}. \quad (54)$$

It can easily be seen that

$$\begin{aligned} \mathbf{x}^T(\mathbf{C}^T\mathbf{C} + \lambda\mathbf{D}^T\mathbf{D} + \lambda\mathbf{I})\mathbf{x} &= \\ &= (\mathbf{C}\mathbf{x})^T(\mathbf{C}\mathbf{x}) + \lambda(\mathbf{D}\mathbf{x})^T(\mathbf{D}\mathbf{x}) + \lambda\mathbf{x}^T\mathbf{x} > 0 \end{aligned} \quad (55)$$

is satisfied for any vector  $\mathbf{x} \neq \mathbf{0}$ . Thus  $\mathbf{C}^T\mathbf{C} + \lambda\mathbf{D}^T\mathbf{D} + \lambda\mathbf{I}$  in (54) is positive definite, which partly explains the fact that (54) is numerically more stable than (50) in the simulations when the ridge parameter  $\lambda$  is very small.

$\mathbf{D}$  computed by (48) can be utilized to simplify (99b) into

$$\mathbf{T} = -\mathbf{D}\mathbf{G}. \quad (56)$$

Moreover, we utilize (46) and (49) in turn to obtain

$$\begin{aligned} \mathbf{H}^T\mathbf{Y} - \mathbf{H}^T\mathbf{A}_k\mathbf{W}_k &= \mathbf{H}^T\mathbf{Y} - \mathbf{H}^T\mathbf{A}_k\mathbf{F}_k\mathbf{F}_k^T\mathbf{A}_k^T\mathbf{Y} \\ &= (\mathbf{H}^T - \mathbf{H}^T\mathbf{A}_k\mathbf{F}_k\mathbf{F}_k^T\mathbf{A}_k^T)\mathbf{Y} \\ &= \mathbf{C}^T\mathbf{Y}, \end{aligned} \quad (57)$$

which is substituted into (47) to write it as

$$\mathbf{W}_{k+q} = \begin{bmatrix} \mathbf{W}_k + \mathbf{T}\mathbf{G}^T\mathbf{C}^T\mathbf{Y} \\ \mathbf{G}\mathbf{G}^T\mathbf{C}^T\mathbf{Y} \end{bmatrix}. \quad (58)$$

### D. Construction Model and Learning Procedure of Proposed Chol-1 and Chol-2

The proposed efficient ridge solution (i.e., **Chol-1**) and its numerically more stable implementation (i.e., **Chol-2**) follow the construction model and learning procedure summarized in

**Algorithm 1**, and utilize **Algorithm 6** to implement the steps in rows 12, 18 and 30 of **Algorithm 1** (which compute the output weights). The functions  $\psi_3(\bullet)$  and  $\psi'_3(\bullet)$  in **Algorithm 6** are defined by **Algorithms 7** and **8**, respectively. When the ridge parameter  $\lambda$  is very small, we can choose  $\psi'_3(\bullet)$  for **Chol-2** instead of  $\psi_3(\bullet)$  for **Chol-1** in **Algorithm 6**, to obtain the numerically more stable implementation. Notice that **Algorithm 6** includes (88) and (46), **Algorithm 7** includes (98), (99) and (47), and **Algorithm 8** includes (48), (49), (54), (56), (98) and (58).

---

**Algorithm 6 : The Proposed Efficient Ridge Solution for BLS / its Numerically More Stable Implementation (i.e., Chol-1 / Chol-2): Initialization and Update of Inverse Cholesky Factor and Output Weights**

---

- .....
- 12: Compute the upper-triangular  $\tilde{\mathbf{F}}_n^m$  satisfying  $\tilde{\mathbf{F}}_n^m(\tilde{\mathbf{F}}_n^m)^T = \left( (\tilde{\mathbf{A}}_n^m)^T \tilde{\mathbf{A}}_n^m + \lambda \mathbf{I} \right)^{-1}$ , and compute  $\tilde{\mathbf{W}}_n^m = \tilde{\mathbf{F}}_n^m(\tilde{\mathbf{F}}_n^m)^T(\tilde{\mathbf{A}}_n^m)^T \mathbf{Y}$ ;
- .....
- 18: Compute  $\tilde{\mathbf{F}}_n^{m+1}$  and  $\tilde{\mathbf{W}}_n^{m+1}$  by  $\psi_3(\tilde{\mathbf{F}}_n^m, \tilde{\mathbf{A}}_n^m, \tilde{\mathbf{H}}_{m+1}, \tilde{\mathbf{W}}_n^m, \mathbf{Y})$  or  $\psi'_3(\dots)$ ;
- .....
- 30: Compute  $\tilde{\mathbf{F}}_{n+1}^m$  and  $\tilde{\mathbf{W}}_{n+1}^m$  by  $\psi_3(\tilde{\mathbf{F}}_n^m, \tilde{\mathbf{A}}_n^m, [\tilde{\mathbf{Z}}_{n+1} | \tilde{\mathbf{H}}_{exm}], \tilde{\mathbf{W}}_n^m, \mathbf{Y})$  or  $\psi'_3(\dots)$ ;
- .....
- 

---

**Algorithm 7 The Algorithm to Update  $\mathbf{F}_k$  and  $\mathbf{W}_k$  for Chol-1**

---

**function**  $\psi_3(\mathbf{F}_k, \mathbf{A}_k, \mathbf{H}, \mathbf{W}_k, \mathbf{Y})$   
 Compute  $\mathbf{G}$  by  $\mathbf{G}\mathbf{G}^T = \begin{pmatrix} \mathbf{H}^T \mathbf{H} + \lambda \mathbf{I} & -\mathbf{H}^T \mathbf{A}_k \mathbf{F}_k \mathbf{F}_k^T \mathbf{A}_k^T \mathbf{H} \\ \mathbf{H}^T \mathbf{A}_k \mathbf{F}_k \mathbf{F}_k^T \mathbf{A}_k^T \mathbf{H} & \end{pmatrix}^{-1}$   
 $\mathbf{T} = -\mathbf{F}_k \mathbf{F}_k^T \mathbf{A}_k^T \mathbf{H} \mathbf{G}$   
 $\mathbf{F}_{k+q} = \begin{bmatrix} \mathbf{F}_k & \mathbf{T} \\ \mathbf{0} & \mathbf{G} \end{bmatrix}$   
 $\mathbf{W}_{k+q} = \begin{bmatrix} \mathbf{W}_k + \mathbf{T} \mathbf{G}^T (\mathbf{H}^T \mathbf{Y} - \mathbf{H}^T \mathbf{A}_k \mathbf{W}_k) \\ \mathbf{G} \mathbf{G}^T (\mathbf{H}^T \mathbf{Y} - \mathbf{H}^T \mathbf{A}_k \mathbf{W}_k) \end{bmatrix}$   
**return**  $\mathbf{F}_{k+q}, \mathbf{W}_{k+q}$   
**end function**

---



---

**Algorithm 8 The Numerically More Stable Implementation to Update  $\mathbf{F}_k$  and  $\mathbf{W}_k$  for Chol-2**

---

**function**  $\psi'_3(\mathbf{F}_k, \mathbf{A}_k, \mathbf{H}, \mathbf{W}_k, \mathbf{Y})$   
 $\mathbf{D} = \mathbf{F}_k \mathbf{F}_k^T \mathbf{A}_k^T \mathbf{H}$   
 $\mathbf{C} = \mathbf{H} - \mathbf{A}_k \mathbf{D}$   
 Compute  $\mathbf{G}$  by  $\mathbf{G}\mathbf{G}^T = (\mathbf{C}^T \mathbf{C} + \lambda \mathbf{D}^T \mathbf{D} + \lambda \mathbf{I})^{-1}$   
 $\mathbf{T} = -\mathbf{D} \mathbf{G}$   
 $\mathbf{F}_{k+q} = \begin{bmatrix} \mathbf{F}_k & \mathbf{T} \\ \mathbf{0} & \mathbf{G} \end{bmatrix}$   
 $\mathbf{W}_{k+q} = \begin{bmatrix} \mathbf{W}_k + \mathbf{T} \mathbf{G}^T \mathbf{C}^T \mathbf{Y} \\ \mathbf{G} \mathbf{G}^T \mathbf{C}^T \mathbf{Y} \end{bmatrix}$   
**return**  $\mathbf{F}_{k+q}, \mathbf{W}_{k+q}$   
**end function**

---

TABLE I: Comparison of Flops between the Existing and Proposed Efficient BLS Algorithms by Inverse Cholesky Factorization

Existing Alg. 5 (for Exg-E)		Proposed Alg. 7 (for Chol-1)	
Eqn.	Flops	Eqn.	Flops
(30)	$2qkl + 2qk^2$	$\mathbf{A}_k^T \mathbf{H}$	$2qkl$
(22)	$2qkl$		
(32a)	$q^2l + \frac{2}{3}q^3$	(99a)	$q^2l + qk^2 + q^2k + \frac{2}{3}q^3$
(32b)	$q^2k$	(99b)	$qk^2 + q^2k$
(33)	$2cql + 4cqk + 2cq^2$	(47)	$2cql + 4cqk + 2cq^2$
Sum	$(4qk + q^2 + 2cq)l + 2qk^2 + (q^2 + 4cq)k + \frac{2}{3}q^3 + 2cq^2 \approx (4qk + q^2)l$	Sum	$(2qk + q^2 + 2cq)l + 2qk^2 + (2q^2 + 4cq)k + \frac{2}{3}q^3 + 2cq^2 \approx (2qk + q^2)l$

*E. Comparison of Existing and Proposed Efficient BLS Algorithms by Inverse Cholesky Factorization*

As we write (47) as (58), we utilize (28) and (29) in turn to obtain  $\mathbf{H}^T \mathbf{Y} - \mathbf{H}^T \mathbf{A}_k \bar{\mathbf{W}}_k = \mathbf{H}^T \mathbf{Y} - \mathbf{H}^T \mathbf{A}_k \bar{\mathbf{F}}_k \bar{\mathbf{F}}_k^T \mathbf{A}_k^T \mathbf{Y} = \bar{\mathbf{C}} \mathbf{Y}$ , which is substituted into (33) to write it as

$$\bar{\mathbf{W}}_{k+q} = \begin{bmatrix} \bar{\mathbf{W}}_k + \bar{\mathbf{T}} \bar{\mathbf{G}}^T \bar{\mathbf{C}} \mathbf{Y} \\ \bar{\mathbf{G}} \bar{\mathbf{G}}^T \bar{\mathbf{C}} \mathbf{Y} \end{bmatrix}. \quad (59)$$

Then we can compare **Algorithm 8** to **Algorithm 5** with (33) replaced by (59), to conclude that the only difference between the existing and proposed efficient BLS algorithms lies between (54) and (32a).

Compared to (32a), (54) only adds the entry  $\lambda \mathbf{D}^T \mathbf{D}$ . Then (54) is equal to (32a) when  $\lambda \rightarrow 0$ , while usually (54) is different from (32a) when  $\lambda \rightarrow 0$  is not satisfied. Accordingly, (32a) can be regarded as the special case of (54) with  $\lambda \rightarrow 0$ , while (54) can be regarded as an extension of (32a).

IV. PROPOSED RIDGE SOLUTION FOR BLS BY UPDATING THE RIDGE INVERSE

The BLS algorithm proposed in the last section utilizes the sub-matrices in the inverse Cholesky factor  $\mathbf{F}_{k+q}$  to update the output weights, and updates the inverse Cholesky factor efficiently. In this section, we will utilize a sub-matrix in the ridge inverse  $\mathbf{A}_{k+q}^\dagger$  to update the output weights, and we will also propose an algorithm to update the ridge inverse. The proposed algorithm to update the ridge inverse, which actually computes the ridge inverse of a partitioned matrix, can be regarded as an extension of the well-known Greville's method [19] that can only compute the generalized inverse of a partitioned matrix. Specifically, we will show that the proposed algorithm to update the ridge inverse is equivalent to the Greville's Method when the ridge parameter  $\lambda \rightarrow 0$ , i.e., it includes the Greville's method as a special case.

*A. The Algorithm to Update the Ridge Inverse and Solution without Using the Inverse Cholesky Factor (i.e., R-Inv)*

The ridge inverse and solution are updated in (45) and (47), respectively, by utilizing the sub-matrices in the inverse Cholesky factor  $\mathbf{F}_{k+q}$ , i.e.,  $\mathbf{G}$  and  $\mathbf{T}$  in (98). To avoid using any sub-matrix in  $\mathbf{F}_{k+q}$ , we will propose the ridge solution

by updating the ridge inverse in this subsection, which is abbreviated as **R-Inv**.

To update the ridge inverse, substitute (49) and (56) into (44) to get

$$\mathbf{A}_{k+q}^\dagger = \begin{bmatrix} \mathbf{A}_k^\dagger - \mathbf{D}\mathbf{G}\mathbf{G}^T\mathbf{C}^T \\ \mathbf{G}\mathbf{G}^T\mathbf{C}^T \end{bmatrix}. \quad (60)$$

Then we write (60) as

$$\mathbf{A}_{k+q}^\dagger = [\mathbf{A}_k | \mathbf{H}]^\dagger = \begin{bmatrix} \mathbf{A}_k^\dagger - \mathbf{D}\mathbf{B}^T \\ \mathbf{B}^T \end{bmatrix}, \quad (61)$$

where  $\mathbf{D}$  has been defined by (48), and

$$\mathbf{B}^T = \mathbf{G}\mathbf{G}^T\mathbf{C}^T. \quad (62)$$

To update the ridge solution, substitute (62) into (58) to get

$$\mathbf{W}_{k+q} = \begin{bmatrix} \mathbf{W}_k - \mathbf{D}\mathbf{B}^T\mathbf{Y} \\ \mathbf{B}^T\mathbf{Y} \end{bmatrix}. \quad (63)$$

In (48) and (62), the sub-matrices in  $\mathbf{F}_{k+q}$  are still utilized, e.g.,  $\mathbf{F}_k$  and  $\mathbf{G}$ . So we substitute (43) into (48) to obtain

$$\mathbf{D} = \mathbf{A}_k^\dagger \mathbf{H}, \quad (64)$$

and substitute (54) into (62) to obtain

$$\mathbf{B}^T = (\mathbf{C}^T\mathbf{C} + \lambda\mathbf{D}^T\mathbf{D} + \lambda\mathbf{I})^{-1}\mathbf{C}^T. \quad (65)$$

We can also compute  $\mathbf{B}^T$  by

$$\mathbf{B}^T = (\mathbf{H}^T\mathbf{C} + \lambda\mathbf{I})^{-1}\mathbf{C}^T, \quad (66)$$

which is obtained by substituting (50) into (62). However, usually (65) is numerically more stable than (66) in the simulations when the ridge parameter  $\lambda$  is small. This may be explained by the fact that the theoretical positive definite  $\mathbf{H}^T\mathbf{C} + \lambda\mathbf{I}$  in (66) may no longer be positive definite due to numerical errors when  $\lambda$  is small, while  $\mathbf{C}^T\mathbf{C} + \lambda\mathbf{D}^T\mathbf{D} + \lambda\mathbf{I}$  always results in a positive definite matrix, as shown in (55).

### B. Construction Model and Learning Procedure of R-Inv

In the proposed ridge solution for BLS based on the ridge inverse, the construction model and learning procedure in **Algorithm 1** are followed, and **Algorithm 9** is utilized to implement the steps in rows 12, 18 and 30 of **Algorithm 1** (which compute the output weights). The function  $\psi_4(\bullet)$  in **Algorithm 9** is defined by **Algorithm 10**. Notice that **Algorithm 9** includes (7) and (6), while **Algorithm 10** includes (64), (49), (65), (61) and (63).

### C. Comparison of the Proposed Algorithm to Update the Ridge Inverse and the Greville's Method to Update the Generalized Inverse

By comparing **Algorithm 3** including (20)-(24) with **Algorithm 10** including (64), (49), (65), (61) and (63), it can be seen that the only difference lies between (21) and (65).

Appendix C shows that (65) is equal to (21) when  $\lambda \rightarrow 0$ . Moreover, (65) is utilized in **Algorithm 10** to update the ridge inverse, while (21) is utilized in **Algorithm 3** to update the generalized inverse by extending the Greville's method. Then

---

### Algorithm 9 : The Proposed Ridge Solution for BLS by Updating the Ridge Inverse (i.e., R-Inv): Initialization and Update of Ridge Inverse and Output Weights

---

```

.....
12: Compute  $(\ddot{\mathbf{A}}_n^m)^\dagger = ((\ddot{\mathbf{A}}_n^m)^T \ddot{\mathbf{A}}_n^m + \lambda\mathbf{I})^{-1} (\ddot{\mathbf{A}}_n^m)^T$ 
    and  $\ddot{\mathbf{W}}_n^m = (\ddot{\mathbf{A}}_n^m)^\dagger \mathbf{Y}$ ;
.....
18: Compute  $(\ddot{\mathbf{A}}_n^{m+1})^\dagger$  and  $\ddot{\mathbf{W}}_n^{m+1}$  by
     $\psi_4((\ddot{\mathbf{A}}_n^m)^\dagger, \ddot{\mathbf{A}}_n^m, \ddot{\mathbf{H}}_{m+1}, \ddot{\mathbf{W}}_n^m, \mathbf{Y})$ ;
.....
30: Compute  $(\ddot{\mathbf{A}}_{n+1}^m)^\dagger$  and  $\ddot{\mathbf{W}}_{n+1}^m$  by
     $\psi_4((\ddot{\mathbf{A}}_n^m)^\dagger, \ddot{\mathbf{A}}_n^m, [\ddot{\mathbf{Z}}_{n+1} | \ddot{\mathbf{H}}_{exm}], \ddot{\mathbf{W}}_n^m, \mathbf{Y})$ ;
.....

```

---



---

### Algorithm 10 The Algorithm to Update $\mathbf{A}_k^\dagger$ and $\mathbf{W}_k$ for R-Inv

---

```

function  $\psi_4(\mathbf{A}_k^\dagger, \mathbf{A}_k, \mathbf{H}, \mathbf{W}_k, \mathbf{Y})$ 
     $\mathbf{D} = \mathbf{A}_k^\dagger \mathbf{H}$ 
     $\mathbf{C} = \mathbf{H} - \mathbf{A}_k \mathbf{D}$ 
     $\mathbf{B}^T = (\mathbf{C}^T\mathbf{C} + \lambda\mathbf{D}^T\mathbf{D} + \lambda\mathbf{I})^{-1}\mathbf{C}^T$ 
     $\mathbf{A}_{k+q}^\dagger = \begin{bmatrix} \mathbf{A}_k^\dagger - \mathbf{D}\mathbf{B}^T \\ \mathbf{B}^T \end{bmatrix}$ 
     $\mathbf{W}_{k+q} = \begin{bmatrix} \mathbf{W}_k - \mathbf{D}\mathbf{B}^T\mathbf{Y} \\ \mathbf{B}^T\mathbf{Y} \end{bmatrix}$ 
    return  $\mathbf{A}_{k+q}^\dagger, \mathbf{W}_{k+q}$ 
end function

```

---

it can be concluded that when  $\lambda \rightarrow 0$ , the proposed algorithm to update the ridge inverse is equivalent to the Greville's method utilized in [16] to update the generalized inverse. Accordingly, the Greville's method to update the generalized inverse can be regarded as the special case with  $\lambda \rightarrow 0$  of the proposed algorithm to update the ridge inverse.

When  $\lambda \rightarrow 0$  is not satisfied, usually  $\lambda\mathbf{D}^T\mathbf{D} \neq \mathbf{0}$  and then it can easily be seen that (65) is different from (21a) in the case with  $\bar{\mathbf{C}} \neq \mathbf{0}$ . So usually the proposed algorithm to update the ridge inverse is different from the Greville's method when  $\lambda \rightarrow 0$  is not satisfied. Accordingly, the proposed algorithm, which actually computes the ridge inverse of a partitioned matrix  $[\mathbf{A}_k | \mathbf{H}]$ , can be regarded as an extension of the Greville's method that computes the generalized inverse of a partitioned matrix [19]. In other words, the proposed algorithm expands the application range of the Greville's method from the generalized inverse to the ridge inverse.

### V. COMPLEXITY COMPARISON, NUMERICAL EXPERIMENTS, AND IMPLEMENTATION ASPECTS

In this section, we compare the expected flops (floating-point operations) of the presented BLS algorithms. Then to evaluate the accuracy and training time of the presented BLS algorithms, we perform classification experiments on the Modified National Institute of Standards and Technology (MNIST) dataset [24] and the New York University object recognition benchmark (NORB) dataset [25]. Our simulations are carried out on MATLAB software platform under a Microsoft Windows Server with 128 GB of RAM. The tansig function is



TABLE II: Snapshot Results of Testing Accuracy on MNIST Dataset with the Ridge Parameter  $\lambda = 10^{-8}, 10^{-7}, 10^{-6}$ 

Number of Feature Nodes				60	60	70	80	90	100	110	120	130	140	150	160	
				60	↓	↓	↓	↓	↓	↓	↓	↓	↓	↓	↓	
Number of Enhancement Nodes				3000	3000	5000	7000	9000	11000	13000	15000	17000	19000	21000	23000	
					↓	↓	↓	↓	↓	↓	↓	↓	↓	↓	↓	
					5000	7000	9000	11000	13000	15000	17000	19000	21000	23000	25000	
Testing Accuracy (%) for $\lambda = 10^{-8}$	Gen. Inv. Sol.	Orig.	Mean Std	98.30 0.060	98.62 0.058	98.76 0.059	98.85 0.054	<b>98.88</b> <b>0.052</b>	98.88 0.059	98.86 0.065	98.81 0.071	98.73 0.072	98.59 0.076	98.39 0.098	98.10 0.135	
		Exg-E	Mean Std	98.30 0.060	98.62 0.058	98.76 0.059	98.85 0.053	<b>98.89</b> <b>0.054</b>	98.88 0.053	98.86 0.056	98.82 0.063	98.73 0.069	98.61 0.085	98.42 0.101	98.16 0.148	
	Ridge Solutions	Chol-1	Mean Std	98.30 0.060	98.62 0.057	98.76 0.061	98.85 0.048	98.90 0.050	NA NA	NA NA	NA NA	NA NA	NA NA	NA NA	NA NA	
		Chol-2	Mean Std	98.30 0.060	98.62 0.057	98.76 0.060	98.85 0.047	98.89 0.052	98.90 0.059	98.92 0.050	98.93 0.050	98.93 0.057	98.92 0.055	98.91 0.055	98.89 0.059	
		R-Inv	Mean Std	98.30 0.060	98.62 0.057	98.76 0.059	98.85 0.047	98.89 0.048	98.90 0.054	98.92 0.053	98.92 0.058	98.91 0.061	98.89 0.071	98.88 0.075	98.86 0.073	
		D-Rdg	Mean Std	98.30 0.060	98.62 0.057	98.76 0.060	98.85 0.047	98.90 0.047	98.91 0.049	98.93 0.052	98.94 0.043	98.95 0.043	98.95 0.045	98.95 0.040	98.95 0.039	
	Testing Accuracy (%) for $\lambda = 10^{-7}$	Gen. Inv. Sol.	Orig.	Mean Std	98.30 0.072	98.58 0.067	98.72 0.042	98.79 0.050	98.81 0.067	98.77 0.094	98.69 0.142	98.52 0.209	98.27 0.311	97.91 0.425	97.38 0.588	96.69 0.764
			Exg-E	Mean Std	98.30 0.072	98.58 0.066	98.72 0.042	98.80 0.051	98.82 0.068	98.78 0.092	98.68 0.143	98.53 0.215	98.27 0.305	97.90 0.422	97.40 0.579	96.73 0.763
Ridge Solutions		Chol-1	Mean Std	98.30 0.072	98.57 0.062	98.72 0.051	98.81 0.053	98.86 0.053	98.90 0.050	98.93 0.044	<b>98.95</b> <b>0.046</b>	NA NA	NA NA	NA NA	NA NA	
		Chol-2	Mean Std	98.30 0.072	98.57 0.062	98.72 0.050	98.81 0.054	98.87 0.055	98.90 0.049	98.93 0.051	98.95 0.047	98.96 0.049	98.95 0.056	<b>98.96</b> <b>0.046</b>	98.96 0.046	
		R-Inv	Mean Std	98.30 0.072	98.57 0.062	98.71 0.050	98.81 0.052	98.87 0.053	98.90 0.050	98.93 0.050	98.94 0.051	<b>98.95</b> <b>0.039</b>	98.95 0.049	98.95 0.044	98.95 0.041	
		D-Rdg	Mean Std	98.30 0.072	98.57 0.062	98.72 0.051	98.81 0.053	98.86 0.053	98.90 0.049	98.93 0.045	98.95 0.047	98.96 0.041	98.97 0.044	98.97 0.040	98.98 0.044	
Testing Accuracy (%) for $\lambda = 10^{-6}$		Gen. Inv. Sol.	Orig.	Mean Std	98.22 0.071	98.50 0.060	98.65 0.055	98.70 0.069	98.65 0.090	98.50 0.149	98.22 0.260	97.79 0.421	97.15 0.659	96.32 0.940	95.19 1.240	93.82 1.602
			Exg-E	Mean Std	98.22 0.071	98.50 0.060	98.65 0.055	98.69 0.067	98.65 0.093	98.50 0.148	98.22 0.266	97.79 0.420	97.16 0.653	96.33 0.929	95.21 1.260	93.82 1.599
	Ridge Solutions	Chol-1	Mean Std	98.22 0.071	98.48 0.061	98.64 0.060	98.73 0.053	98.79 0.050	98.83 0.052	98.86 0.041	98.88 0.045	98.91 0.041	98.93 0.041	98.94 0.037	<b>98.96</b> <b>0.042</b>	
		Chol-2	Mean Std	98.22 0.071	98.48 0.060	98.64 0.060	98.73 0.053	98.79 0.049	98.83 0.052	98.86 0.043	98.88 0.044	98.91 0.037	98.92 0.040	98.94 0.034	<b>98.95</b> <b>0.034</b>	
		R-Inv	Mean Std	98.22 0.071	98.48 0.060	98.64 0.060	98.73 0.052	98.79 0.049	98.83 0.049	98.86 0.039	98.89 0.046	98.91 0.040	98.92 0.043	98.94 0.038	<b>98.95</b> <b>0.041</b>	
		D-Rdg	Mean Std	98.22 0.071	98.48 0.061	98.64 0.060	98.73 0.053	98.79 0.050	98.83 0.052	98.86 0.041	98.88 0.045	98.91 0.041	98.93 0.041	98.94 0.038	98.96 0.042	

adopted for the enhancement nodes, where the weights  $\mathbf{W}_{h_j}$  and the biases  $\beta_{h_j}$  ( $j = 1, 2, \dots, m$ ) are drawn from the standard uniform distributions on the interval  $[-1, 1]$ .

#### A. Complexity Comparison

When counting the flops, we utilize the well-known fact that  $lq(2k-1) \approx 2lkq$  flops are required to multiply a  $l \times k$  matrix by a  $k \times q$  matrix, and  $lk = O(lkq)$  flops are required to sum two  $l \times k$  matrices. Moreover, notice that for a  $k \times k$  Hermitian matrix,  $k^3$  flops are required to compute the inverse by the inv function in Matlab [20], while  $\frac{2}{3}k^3$  flops are required to compute the inverse Cholesky factorization [21].

The original BLS [16] requires  $(6qk+3q^2+2cq)l+2cqk+q^3$  flops [20] in each update for **Algorithm 3**, where  $c$  denotes the number of output nodes. As mentioned in Subsection C of Section IV, the only difference between the proposed BLS based on the ridge inverse and the original BLS lies between

(65) and (21). Compared to <sup>5</sup>(21a), (65) requires the extra  $q^2k$  flops to compute  $\lambda \mathbf{D}^T \mathbf{D}$ . Then the proposed BLS based on the ridge inverse requires  $(6qk+3q^2+2cq)l+2cqk+q^3+q^2k$  flops in each update for **Algorithm 10**.

Table I compares the flops of **Algorithms 5** and **7**, which update the intermediate results and the output weights for the existing efficient BLS (i.e., **Exg-E**) and the proposed efficient BLS (i.e., **Chol-1**), respectively. We list the flops for each equation, and give the corresponding total flops. To calculate the flops, notice that  $\mathbf{F}_k^T \mathbf{A}_k^T \mathbf{H}$  computed in (99a) is utilized in (99b). Moreover, both  $\mathbf{F}_k$  and  $\mathbf{G}$  are triangular, and only about half entries need to be computed for the Hermitian matrices. It can be seen that (33) and (47) have the same form and require the same flops, while the flops for (33) claimed in [20] need to be revised, to include the flops of  $2cql$ ,  $2cqk$ ,  $cq^2$ ,  $cq^2$  and

<sup>5</sup>When comparing flops, we only consider the usual case where  $\bar{\mathbf{C}} \neq \mathbf{0}$ .

TABLE III: Snapshot Results of Testing Accuracy on MNIST Dataset with the Ridge Parameter  $\lambda = 10^{-5}, 10^{-4}, 10^{-3}, 10^{-2}, 10^{-1}$ 

Number of Feature Nodes				60	60 ↓ 70	70 ↓ 80	80 ↓ 90	90 ↓ 100	100 ↓ 110	110 ↓ 120	120 ↓ 130	130 ↓ 140	140 ↓ 150	150 ↓ 160	160 ↓ 170
Number of Enhancement Nodes				3000 ↓ 5000	3000 ↓ 5000	5000 ↓ 7000	7000 ↓ 9000	9000 ↓ 11000	11000 ↓ 13000	13000 ↓ 15000	15000 ↓ 17000	17000 ↓ 19000	19000 ↓ 21000	21000 ↓ 23000	23000 ↓ 25000
Testing Accuracy (%) for $\lambda = 10^{-5}$	Gen. Sol.	Orig.	Mean	97.98	98.27	98.43	98.47	98.38	98.17	97.78	97.20	96.34	95.18	93.70	91.88
			Std	0.094	0.079	0.082	0.094	0.138	0.225	0.396	0.645	0.943	1.336	1.807	2.270
	Gen. Inv. Sol.	Exg-E	Mean	97.98	98.27	98.43	98.47	98.38	98.17	97.78	97.20	96.34	95.17	93.70	91.88
			Std	0.094	0.079	0.082	0.094	0.137	0.221	0.393	0.649	0.949	1.341	1.814	2.274
	Ridge Solutions	Chol-2	Mean	97.98	98.24	98.38	98.47	98.56	98.63	98.67	98.71	98.74	98.77	98.79	98.81
			Std	0.094	0.075	0.075	0.060	0.061	0.054	0.056	0.055	0.054	0.045	0.052	0.040
		R-Inv	Mean	97.98	98.24	98.38	98.48	98.56	98.63	98.66	98.71	98.74	98.77	98.79	98.81
			Std	0.094	0.075	0.076	0.060	0.062	0.054	0.052	0.055	0.055	0.046	0.051	0.043
		Chol-1 & D-Rdg	Mean	97.98	98.24	98.38	98.47	98.56	98.63	98.66	98.71	98.74	98.77	98.79	98.81
			Std	0.094	0.075	0.075	0.060	0.061	0.055	0.055	0.055	0.054	0.046	0.052	0.041
Testing Accuracy (%) for $\lambda = 10^{-4}$	Gen. Sol.	Orig.	Mean	97.47	97.84	98.01	98.06	97.93	97.66	97.17	96.42	95.35	93.95	92.21	90.12
			Std	0.105	0.101	0.074	0.099	0.135	0.221	0.383	0.646	0.981	1.389	1.843	2.301
	Gen. Inv. Sol.	Exg-E	Mean	97.47	97.84	98.01	98.06	97.93	97.66	97.17	96.42	95.35	93.95	92.22	90.12
			Std	0.105	0.101	0.074	0.099	0.135	0.221	0.384	0.646	0.981	1.392	1.839	2.301
	Ridge Sol.	R-Inv	Mean	97.47	97.80	97.98	98.10	98.19	98.25	98.32	98.36	98.40	98.44	98.48	98.50
			Std	0.105	0.092	0.073	0.078	0.075	0.069	0.062	0.061	0.056	0.061	0.053	0.046
		Chol-1, Chol-2 & D-Rdg	Mean	97.47	97.80	97.98	98.10	98.19	98.25	98.32	98.36	98.40	98.45	98.48	98.50
			Std	0.105	0.092	0.073	0.078	0.075	0.069	0.062	0.061	0.056	0.060	0.053	0.046
Testing Accuracy (%) for $\lambda = 10^{-3}$	Gen. Sol.	Orig.	Mean	96.65	97.13	97.35	97.40	97.24	96.84	96.18	95.16	93.77	92.07	90.06	87.78
			Std	0.186	0.128	0.127	0.163	0.272	0.504	0.885	1.442	2.096	2.797	3.539	4.184
	Gen. Inv. Sol.	Exg-E	Mean	96.65	97.13	97.35	97.40	97.24	96.84	96.18	95.16	93.77	92.07	90.06	87.78
			Std	0.186	0.128	0.127	0.163	0.272	0.504	0.885	1.442	2.096	2.797	3.539	4.184
	Rdg. Sol.	Chol-1, Chol-2, R-Inv & D-Rdg	Mean	96.65	97.06	97.30	97.48	97.62	97.71	97.78	97.85	97.90	97.96	98.00	98.04
			Std	0.186	0.136	0.125	0.105	0.082	0.082	0.070	0.070	0.063	0.060	0.059	0.059
Testing Accuracy (%) for $\lambda = 10^{-2}$	Gen.	Orig. & Exg-E	Mean	95.44	96.03	96.29	96.32	96.05	95.51	94.61	93.29	91.64	89.58	87.24	84.66
			Std	0.263	0.168	0.170	0.231	0.397	0.684	1.119	1.717	2.371	3.094	3.788	4.328
	Rdg.	Chol-1, Chol-2, R-Inv & D-Rdg	Mean	95.44	95.98	96.28	96.50	96.65	96.79	96.89	96.98	97.07	97.13	97.19	97.23
			Std	0.263	0.152	0.127	0.120	0.117	0.105	0.095	0.083	0.077	0.084	0.086	0.076
Testing Accuracy (%) for $\lambda = 10^{-1}$	Gen.	Orig. & Exg-E	Mean	93.64	94.45	94.82	94.89	94.63	94.03	93.05	91.64	89.91	87.83	85.50	83.02
			Std	0.370	0.252	0.179	0.266	0.492	0.888	1.419	2.126	2.804	3.504	4.122	4.667
	Rdg.	Chol-1, Chol-2, R-Inv & D-Rdg	Mean	93.64	94.41	94.82	95.11	95.32	95.48	95.63	95.73	95.83	95.92	95.99	96.07
			Std	0.370	0.236	0.151	0.122	0.116	0.118	0.114	0.097	0.100	0.101	0.087	0.096

$2cqk$  to compute  $\mathbf{H}^T \times \mathbf{Y}$ ,  $(\mathbf{H}^T \mathbf{A}_k) \times \bar{\mathbf{W}}_k$ ,  $\bar{\mathbf{G}}^T \times (\cdots)$ ,  $\bar{\mathbf{G}} \times \bar{\mathbf{G}}^T (\cdots)$  and  $\bar{\mathbf{T}} \times \bar{\mathbf{G}}^T (\cdots)$ , respectively.

To compare the dominant flops, we assume

$$\begin{cases} q = 0(l) \\ c = 0(q), \end{cases} \quad (67a)$$

$$(67b)$$

as in [20], since usually the new added hidden nodes are much less than the training samples, and we focus on the situation where the new added hidden nodes are much more than the output nodes. Then the original BLS [16], the existing efficient BLS [20] and the proposed efficient BLS require the dominant flops of  $(6qk + 3q^2)l$ ,  $(4qk + q^2)l$  and  $(2qk + q^2)l$ , respectively, for **Algorithms 3, 5** and **7**. Thus in each update, compared to the proposed efficient BLS, the original BLS requires

$$\frac{(6qk + 3q^2)l}{(2qk + q^2)l} = 3 \quad (68)$$

times of flops, while the existing efficient BLS, which spends

the extra  $2qkl$  flops to get  $\bar{\mathbf{C}} = \mathbf{H} - \mathbf{A}_k \bar{\mathbf{D}}$  by (22), requires

$$\frac{(4qk + q^2)l}{(2qk + q^2)l} = 2 - \frac{1}{1 + 2(k/q)} > \frac{5}{3} \approx 1.67 \quad (69)$$

times <sup>6</sup> of flops. Moreover, it can be seen that **Algorithms 8** and **5** require the same dominant flops <sup>7</sup> in each update, and so do the numerically more stable implementation of the proposed efficient BLS and the existing efficient BLS.

To compute the initial  $\mathbf{A}_k^\dagger$  and  $\bar{\mathbf{W}}_k$  by (7) and (6), respectively, the proposed BLS based on the ridge inverse requires the flops of  $k^2l + k^3$ ,  $2k^2l$  and  $2klc$  to compute  $(\mathbf{A}_k^T \times \mathbf{A}_k + \lambda \mathbf{I})^{-1}$ ,  $(\cdots)^{-1} \times \mathbf{A}_k^T$  and  $\mathbf{A}_k^\dagger \times \mathbf{Y}$ , respectively,

<sup>6</sup>Here we only consider the usual case with  $k > q$ , i.e., the existing nodes are more than the nodes inserted in an update.

<sup>7</sup>**Algorithm 8** requires extra  $q^2k = 0(qkl)$  flops to compute  $\lambda \mathbf{D}^T \mathbf{D}$  in (54), compared to **Algorithm 5** with (33) replaced by (59), while only the  $2cqk = 0(qkl)$  flops to compute  $(\mathbf{H}^T \mathbf{A}_k) \times \bar{\mathbf{W}}_k$  in (33) is saved in (59).

TABLE IV: Snapshot Results of Testing Accuracy on NORB Dataset with the Ridge Parameter  $\lambda = 10^{-8}, 10^{-7}, 10^{-6}, 10^{-5}$ 

Number of Enhancement Nodes				2000	2000	3500	3500	5000	5000	6500	6500	8000	8000	9500	9500	11000	11000	12500	12500
				2000	↓	↓	↓	↓	↓	↓	↓	↓	↓	↓	↓	↓	↓	↓	↓
					3500	5000	6500	8000	9500	11000	12500	14000							
Testing Accuracy (%) for $\lambda = 10^{-8}$																			
	Gen. Inv. Sol.	Orig.	Mean	88.55	88.20	87.88	87.70	87.44	86.91	86.35	85.24	83.53							
			Std	0.570	0.500	0.563	0.595	0.599	0.545	0.650	0.733	0.827							
	Exg-E	Mean	88.55	88.20	87.88	87.70	87.43	86.92	86.33	85.28	83.61								
		Std	0.570	0.500	0.565	0.594	0.597	0.545	0.634	0.691	0.764								
	Chol-1	Mean	88.55	88.21	87.90	87.73	87.50	87.08	86.78	86.39	85.84								
		Std	0.570	0.497	0.563	0.607	0.584	0.495	0.509	0.523	0.547								
	Chol-2	Mean	88.55	88.21	87.90	87.72	87.51	87.09	86.78	86.39	85.84								
		Std	0.570	0.497	0.563	0.608	0.584	0.495	0.512	0.524	0.545								
	R-Inv	Mean	88.55	88.21	87.90	87.72	87.50	87.08	86.76	86.33	85.68								
		Std	0.570	0.497	0.560	0.612	0.587	0.490	0.538	0.572	0.579								
	D-Rdg	Mean	88.55	88.21	87.90	87.73	87.50	87.08	86.78	86.39	85.84								
		Std	0.570	0.498	0.563	0.607	0.584	0.495	0.510	0.523	0.544								
Testing Accuracy (%) for $\lambda = 10^{-7}$																			
	Gen. Inv. Sol.	Orig.	Mean	88.62	88.22	87.86	87.56	87.14	86.59	85.84	84.67	82.66							
			Std	0.568	0.632	0.628	0.606	0.582	0.653	0.635	0.753	0.966							
	Exg-E	Mean	88.62	88.22	87.86	87.55	87.14	86.60	85.84	84.69	82.69								
		Std	0.568	0.632	0.627	0.608	0.581	0.652	0.631	0.737	0.943								
	Chol-1	Mean	88.62	88.24	87.88	87.64	87.32	87.05	86.83	86.67	86.67								
		Std	0.568	0.628	0.619	0.603	0.614	0.670	0.580	0.577	0.648								
	Chol-2	Mean	88.62	88.24	87.88	87.64	87.32	87.05	86.83	86.67	86.67								
		Std	0.568	0.627	0.619	0.602	0.614	0.671	0.580	0.578	0.649								
	R-Inv	Mean	88.62	88.24	87.88	87.64	87.32	87.05	86.83	86.66	86.63								
		Std	0.568	0.627	0.618	0.603	0.613	0.666	0.571	0.571	0.664								
	D-Rdg	Mean	88.62	88.24	87.88	87.64	87.32	87.05	86.83	86.66	86.67								
		Std	0.568	0.627	0.619	0.602	0.614	0.671	0.580	0.578	0.649								
Testing Accuracy (%) for $\lambda = 10^{-6}$																			
	Gen. Inv. Sol.	Orig.	Mean	88.57	88.41	88.19	87.82	87.42	86.73	85.35	83.08	79.74							
			Std	0.660	0.555	0.549	0.537	0.611	0.720	1.125	1.765	2.496							
	Exg-E	Mean	88.57	88.41	88.19	87.82	87.42	86.72	85.36	83.09	79.74								
		Std	0.660	0.555	0.548	0.536	0.608	0.723	1.123	1.776	2.499								
	Chol-1	Mean	88.57	88.49	88.36	88.18	88.14	88.18	88.21	88.31	88.43								
		Std	0.660	0.549	0.539	0.494	0.530	0.515	0.496	0.475	0.482								
	Chol-2	Mean	88.57	88.49	88.36	88.18	88.14	88.18	88.21	88.31	88.43								
		Std	0.660	0.549	0.539	0.494	0.530	0.515	0.496	0.474	0.482								
	R-Inv	Mean	88.57	88.49	88.36	88.18	88.14	88.18	88.21	88.30	88.41								
		Std	0.660	0.549	0.538	0.494	0.531	0.515	0.498	0.473	0.492								
	D-Rdg	Mean	88.57	88.49	88.36	88.18	88.14	88.18	88.21	88.31	88.43								
		Std	0.660	0.549	0.539	0.494	0.530	0.515	0.496	0.475	0.482								
Testing Accuracy (%) for $\lambda = 10^{-5}$																			
	Gen. Inv. Sol.	Orig.	Mean	88.84	88.73	88.49	87.83	86.48	84.16	80.75	76.34	71.49							
			Std	0.637	0.567	0.621	0.773	1.112	1.831	2.746	3.509	4.041							
	Exg-E	Mean	88.84	88.73	88.49	87.83	86.48	84.16	80.75	76.33	71.49								
		Std	0.637	0.567	0.621	0.773	1.112	1.830	2.745	3.507	4.041								
	Chol-1	Mean	88.84	88.98	89.10	89.10	89.14	89.22	89.29	89.38	89.46								
		Std	0.637	0.542	0.536	0.528	0.486	0.399	0.424	0.385	0.373								
	Chol-2	Mean	88.84	88.98	89.10	89.10	89.14	89.22	89.29	89.38	89.46								
		Std	0.637	0.543	0.536	0.528	0.486	0.399	0.424	0.385	0.373								
	R-Inv	Mean	88.84	88.98	89.10	89.10	89.14	89.22	89.29	89.38	89.46								
		Std	0.637	0.543	0.537	0.528	0.485	0.401	0.426	0.385	0.373								
	D-Rdg	Mean	88.84	88.98	89.10	89.10	89.13	89.22	89.29	89.38	89.46								
		Std	0.637	0.543	0.536	0.528	0.486	0.399	0.424	0.385	0.373								

and the corresponding total flops are <sup>8</sup>

$$3k^2l + k^3 + 2klc \approx 3k^2l + k^3. \quad (70)$$

As a comparison, to compute the initial  $\mathbf{F}_k$  and  $\mathbf{W}_k$  by (88) and (46), respectively, the proposed efficient BLS based on the inverse Cholesky factor requires the flops of  $k^2l + \frac{2}{3}k^3$ ,  $2klc$  and  $2k^2c$  to compute the inverse Cholesky factorization

<sup>8</sup>In (70) and the following (71), we assume  $c = 0(k)$ , which holds in most cases since  $c = 0(q)$  (i.e., (67b)) and usually  $q \leq k$ .

$\mathbf{F}_k \mathbf{F}_k^T = (\mathbf{A}_k^T \times \mathbf{A}_k + \lambda \mathbf{I})^{-1}$ ,  $\mathbf{A}_k^T \times \mathbf{Y}$  and  $\mathbf{F}_k \times (\mathbf{F}_k^T \times \mathbf{A}_k^T \mathbf{Y})$ , respectively, and the corresponding total flops are

$$k^2l + \frac{2}{3}k^3 + 2klc + 2k^2c \approx k^2l + \frac{2}{3}k^3. \quad (71)$$

From (70) and (71), we can conclude that with respect to the proposed efficient BLS based on the inverse Cholesky factor,

the proposed BLS based on the ridge inverse requires

$$\frac{3k^2l + k^3}{k^2l + \frac{2}{3}k^3} = 3 - \frac{3}{2 + 3(l/k)} > \frac{12}{5} \quad (72)$$

times<sup>9</sup> of flops. Moreover, it can be seen that the flops of (70) and (71) are also required by the original BLS [16] and the existing efficient BLS [20], respectively, to compute the initial intermediate result and output weights.

### B. Numerical Experiments on MNIST and NORB Datasets

The MNIST dataset consists of 70000 handwritten digital images partitioned into training and test sets of 60000 and 10000 images, respectively. As the simulations for Table IV in [16], we set the initial network as  $10 \times 6$  feature nodes and 3000 enhancement nodes. Then in each update, we add 10 feature nodes, 750 enhancement nodes only corresponding to the added feature nodes, and 1250 additional enhancement nodes, till we reach 170 feature nodes and 25000 enhancement nodes after 11 updates<sup>10</sup>.

On the other hand, the NORB dataset [25] consists of 48600 images with  $2 \times 32 \times 32$  pixels each. The images belong to five distinct categories: (1) animals; (2) humans; (3) airplanes; (4) trucks; and (5) cars. Of these images, half are selected into the training set, and the other half form the test set. We set the initial network as  $100 \times 10$  feature nodes, as the simulations for Table VII in [16]. Starting from the initial network of 2000 enhancement nodes, we add 1500 enhancement nodes in each update, till we reach 14000 enhancement nodes after 8 updates.

For each update, the testing accuracies of the presented BLS algorithms on the MNIST and NORB datasets are shown in Tables II, III and Tables IV, V, respectively, where we list the mean and standard deviation of 100 simulations. Moreover, Table VI lists the training time of the presented BLS algorithms on the MNIST dataset, which is the average value of 500 simulations. In Tables II-VI and the rest of this section, **D-Rdg** denotes the direct ridge inverse and solution (by (7) and (6)), while the abbreviations **Orig.**, **Exg-E**, **Chol-1**, **Chol-2** and **R-Inv** have been defined in the previous sections.

When the ridge parameter  $\lambda \leq 10^{-6}$  in Table II and  $\lambda \leq 10^{-5}$  in Table IV, the generalized inverse solutions **Orig.** and **Exg-E** sometimes achieve different testing accuracies due to numerical errors, and so do the ridge solutions **Chol-1**, **Chol-2**, **R-Inv** and **D-Rdg**. Then Tables II and IV lists the results for each BLS algorithm. Moreover, the ridge parameter satisfies  $10^{-5} \leq \lambda \leq 10^{-1}$  and  $10^{-4} \leq \lambda \leq 10^{-1}$  in Tables III and V, respectively. Our simulations for Table III show that **Chol-1**, **Chol-2** and **R-Inv** always achieve the same testing accuracy<sup>11</sup> as **D-Rdg** when  $\lambda$  is not less than  $10^{-5}$ ,  $10^{-4}$  and  $10^{-3}$ , respectively, and **Orig.** always achieve the same testing accuracy as **Exg-E** when  $\lambda \geq 10^{-2}$ . On the other hand, our simulations for Table V show that **Chol-1** and **Chol-2** always achieve the same testing accuracy as **D-Rdg** when  $\lambda \geq 10^{-4}$ ,

and when  $\lambda \geq 10^{-2}$ , both the generalized inverse solutions achieve the same testing accuracy, and so do all the ridge solutions. Then when multiple different BLS algorithms get the same testing accuracy, the testing accuracy is listed only once in Tables III and V for simplicity.

When the ridge parameter  $\lambda$  is too small, our simulations on the MNIST dataset show that accumulation of numerical errors may make  $\mathbf{H}^T \mathbf{H} + \lambda \mathbf{I} - \mathbf{H}^T \mathbf{A}_k \mathbf{F}_k \mathbf{F}_k^T \mathbf{A}_k^T \mathbf{H}$  in (99a) no longer positive definite, resulting in the unavailable inverse Cholesky factor **G**. Accordingly, Table II shows that the testing accuracy is not available (i.e., NA) for **Chol-1** from the 5<sup>th</sup> and 8<sup>th</sup> update when  $\lambda$  is  $10^{-8}$  and  $10^{-7}$ , respectively.

Table VI lists the training time of **Orig.**, **Exg-E**, **Chol-1**, **Chol-2** and **R-Inv**, and shows the speedups in training time of the proposed efficient ridge solution (i.e., **Chol-1**) to the original BLS [16] (i.e., **Orig.**) and the existing efficient BLS [20] (i.e., **Exg-E**), respectively. The speedup in Table VI is the ratio between the training time of the existing BLS and that of the proposed efficient ridge solution. As observed from Table IV, the proposed ridge solution based on the ridge inverse (i.e., **R-Inv**) and the numerically more stable implementation of the proposed efficient ridge solution (i.e., **Chol-2**) require nearly the same training time as the original BLS (i.e., **Orig.**) and the existing efficient BLS (i.e., **Exg-E**), respectively, while the speedups in total training time of the proposed efficient ridge solution (i.e., **Chol-1**) to the original BLS and the existing efficient BLS are  $1.99 \sim 2.52$  and  $1.31 \sim 1.58$ , respectively. It can be seen that the above comparisons of training time are consistent with the theoretical calculation of flops in the last subsection.

### C. Analysis of the Maximum Testing Accuracies Achieved under Different Ridge Parameters

Based on the testing accuracies in Tables II-V, we show the maximum testing accuracies achieved under different ridge parameters on MNIST and NORB datasets in Fig. 1. On the NORB dataset, both the generalized inverse solutions achieve the same maximum testing accuracies, and so do all the ridge solutions. Then for simplicity, Fig. 1.b only shows the maximum testing accuracies for the generalized inverse solutions and those for the ridge solutions.

From Tables II, III and Fig. 1.a, it can be seen that on the MNIST dataset, the existing generalized inverse solutions **Orig.** and **Exg-E** achieve the maximum testing accuracy of  $98.88\% \sim 98.89\%$  when  $\lambda = 10^{-8}$ , while the proposed ridge solutions **Chol-1**, **Chol-2** and **R-Inv** achieve the maximum testing accuracy of  $98.95\% \sim 98.96\%$  when  $\lambda = 10^{-7}, 10^{-6}$ . On the other hand, it can be seen from Tables IV, V and Fig. 1.b that on the NORB dataset, the existing generalized inverse solutions (i.e., **Orig.** and **Exg-E**) and the proposed ridge solutions (i.e., **Chol-1**, **Chol-2** and **R-Inv**) achieve the maximum testing accuracies of  $89.51\%$  and  $90.38\%$ , respectively, when  $\lambda = 10^{-3}$ . Accordingly, it can be concluded that the proposed ridge solutions achieve better testing accuracies than the existing generalized inverse solutions.

<sup>9</sup>Here we consider the usual case with  $l > k$ .

<sup>10</sup>Notice that only 4 updates are included in Table IV of [16].

<sup>11</sup>A sufficiently big  $\lambda$  can assure the positive definiteness of  $\mathbf{H}^T \mathbf{H} + \lambda \mathbf{I} - \mathbf{H}^T \mathbf{A}_k \mathbf{F}_k \mathbf{F}_k^T \mathbf{A}_k^T \mathbf{H}$  in (99a) and  $\mathbf{C}^T \mathbf{C} + \lambda \mathbf{D}^T \mathbf{D} + \lambda \mathbf{I}$  in (54) and (65), which can reduce the numerical errors caused by the corresponding inverse Cholesky factorization or inverse.

TABLE V: Snapshot Results of Testing Accuracy on NORB Dataset with the Ridge Parameter  $\lambda = 10^{-4}, 10^{-3}, 10^{-2}, 10^{-1}$ 

Number of Enhancement Nodes				2000	2000 ↓ 3500	3500 ↓ 5000	5000 ↓ 6500	6500 ↓ 8000	8000 ↓ 9500	9500 ↓ 11000	11000 ↓ 12500	12500 ↓ 14000
Testing Accuracy (%) for $\lambda = 10^{-4}$	Gen. Inv. Sol.	Orig.	Mean	89.42	89.35	88.83	87.79	85.87	82.98	79.19	74.89	70.44
			Std	0.419	0.473	0.847	1.280	2.192	3.425	4.554	5.382	5.853
		Exg-E	Mean	89.42	89.35	88.83	87.79	85.87	82.98	79.19	74.89	70.44
			Std	0.419	0.473	0.847	1.280	2.192	3.425	4.553	5.381	5.853
	Ridge Sol.	R-Inv	Mean	89.42	89.76	89.81	89.89	89.96	90.03	90.06	90.07	90.10
			Std	0.419	0.408	0.464	0.403	0.341	0.297	0.327	0.340	0.323
		Chol-1, Chol-2 & D-Rdg	Mean	89.42	89.76	89.81	89.89	89.96	90.03	90.06	90.07	90.10
			Std	0.419	0.408	0.464	0.403	0.341	0.298	0.327	0.340	0.323
Testing Accuracy (%) for $\lambda = 10^{-3}$	Gen. Inv. Sol.	Orig.	Mean	89.49	<b>89.51</b>	89.46	88.84	87.76	86.00	83.62	80.79	77.66
			Std	0.380	0.433	0.562	1.013	1.901	3.146	4.545	5.928	7.168
		Exg-E	Mean	89.49	<b>89.51</b>	89.46	88.84	87.76	86.00	83.62	80.79	77.66
			Std	0.380	0.433	0.562	1.013	1.901	3.146	4.545	5.928	7.168
	Ridge Sol.	R-Inv	Mean	89.49	89.89	90.13	90.25	90.32	90.33	90.33	90.34	<b>90.38</b>
			Std	0.380	0.314	0.288	0.289	0.292	0.290	0.268	0.254	0.238
		Chol-1, Chol-2 & D-Rdg	Mean	89.49	89.89	90.13	90.25	90.32	90.33	90.33	90.34	<b>90.38</b>
			Std	0.380	0.314	0.288	0.289	0.292	0.290	0.268	0.254	0.238
Testing Accuracy (%) for $\lambda = 10^{-2}$	Gen.	Orig. & Exg-E	Mean	88.87	89.22	89.42	89.49	89.37	89.03	88.39	87.52	86.39
			Std	0.413	0.363	0.340	0.431	0.723	1.279	2.153	3.180	4.322
	Rdg.	Chol-1, Chol-2, R-Inv & D-Rdg	Mean	88.87	89.34	89.59	89.80	89.93	90.00	90.07	90.13	90.18
			Std	0.413	0.353	0.281	0.279	0.257	0.239	0.242	0.225	0.210
Testing Accuracy (%) for $\lambda = 10^{-1}$	Gen.	Orig. & Exg-E	Mean	86.73	88.05	88.56	88.86	89.01	89.09	89.11	89.01	88.86
			Std	0.819	0.469	0.313	0.288	0.313	0.461	0.706	1.095	1.657
	Rdg.	Chol-1, Chol-2, R-Inv & D-Rdg	Mean	86.73	87.94	88.48	88.79	89.00	89.15	89.26	89.34	89.41
			Std	0.819	0.476	0.320	0.279	0.250	0.247	0.221	0.197	0.190

TABLE VI: Snapshot Results of Training Time on MNIST Dataset and the Corresponding Speedups

No. of Feature Nodes	No. of Enhancement Nodes	Additional Training Time (seconds)					Accumulative Training Time (seconds)						
		Time for Each Update					Time for Each Update						
		Orig.	R-Inv	Exg-E	Chol-2	Chol-1	Speedups of Chol-1		Orig.	R-Inv	Exg-E	Chol-2	Chol-1
60	3000	9.56	9.58	4.93	4.93	4.92	1.94		9.56	9.58	4.93	4.93	4.92
→ 70	→ 5000	15.33	15.47	8.77	8.89	5.53	2.77	1.59	24.89	25.05	13.70	13.81	10.45
→ 80	→ 7000	22.62	22.72	13.85	13.97	8.52	2.65	1.63	47.51	47.77	27.55	27.79	18.97
→ 90	→ 9000	29.69	29.80	19.39	19.57	11.71	2.54	1.66	77.20	77.57	46.94	47.36	30.68
→ 100	→ 11000	36.91	37.09	25.43	25.59	15.50	2.38	1.64	114.12	114.66	72.37	72.95	46.18
→ 110	→ 13000	43.81	44.19	31.47	31.65	19.54	2.24	1.61	157.93	158.85	103.84	104.60	65.72
→ 120	→ 15000	51.04	51.49	37.99	38.25	24.03	2.12	1.58	208.97	210.34	141.82	142.85	89.75
→ 130	→ 17000	57.73	58.24	44.53	44.75	28.49	2.03	1.56	266.70	268.58	186.36	187.59	118.24
→ 140	→ 19000	65.27	65.75	51.87	52.26	33.81	1.93	1.53	331.96	334.34	238.23	239.86	152.05
→ 150	→ 21000	71.70	72.51	59.03	59.39	38.85	1.85	1.52	403.66	406.84	297.25	299.24	190.90
→ 160	→ 23000	79.13	80.00	67.12	67.33	44.83	1.77	1.50	482.79	486.84	364.37	366.57	235.74
→ 170	→ 25000	85.82	87.00	74.83	75.07	50.44	1.70	1.48	568.61	573.84	439.21	441.64	286.17

#### D. Implementation Aspects of the Efficient Inverse Cholesky Factorization: Parallelization in Distributed Systems, Memory Saving, Square-Root Free and Division Free

The efficient inverse Cholesky factorization [21] updates the inverse Cholesky factor of an  $(i-1) \times (i-1)$  Hermitian matrix  $\mathbf{R}_{i-1}$  into that of the  $i \times i$  Hermitian matrix  $\mathbf{R}_i$ , which includes  $\mathbf{R}_{i-1}$  as the  $(i-1) \times (i-1)$  leading principal submatrix. Then to develop an efficient solution for the incremental Broad Learning System (BLS) on added nodes [16], the efficient inverse Cholesky factorization is extended in this paper to update the inverse Cholesky factor of an  $i \times i$  Hermitian matrix  $\mathbf{R}_i$  into that of the  $k \times k$  Hermitian matrix  $\mathbf{R}_k$  through

only 1 iteration, where  $k > i$ , and  $\mathbf{R}_k$  includes  $\mathbf{R}_i$  as the  $i \times i$  leading principal submatrix. In this subsection, we introduce the implementation aspects of the above-described efficient inverse Cholesky factorization. In Appendix D, we develop the memory-saving parallel implementation of the inverse Cholesky factorization for MIMD (Multiple Instruction and Multiple Data Stream) computers [29] with multiple processors.

In the inverse Cholesky factorization, there are square-root and division operations which are time-consuming for conventional multiply-add digital computers [30], and require high bit precision and quite a few clock cycles in fixed-

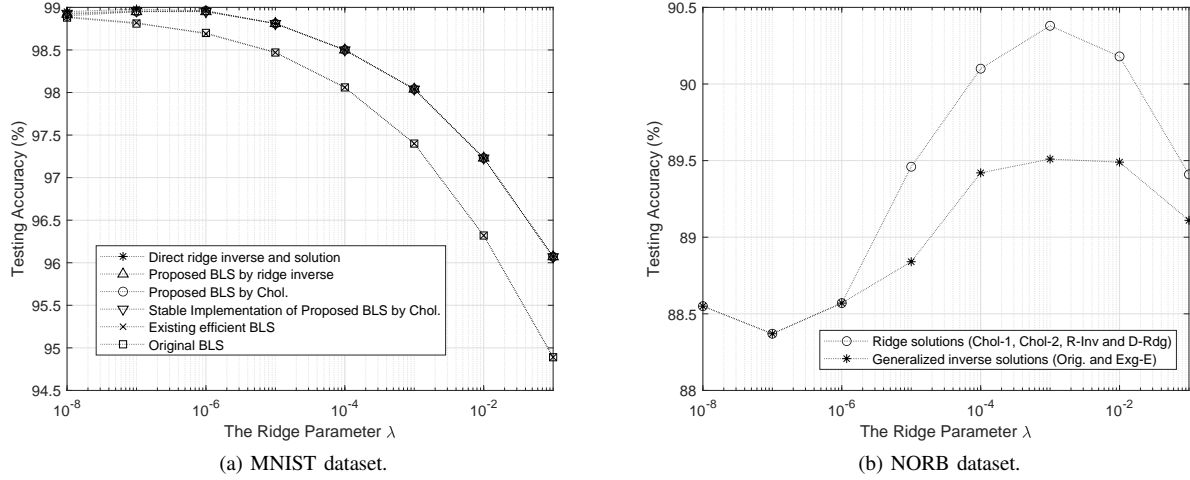


Fig. 1: The maximum testing accuracies achieved under different ridge parameters on MNIST and NORB datasets.

point implementations [31], [32]. Accordingly, we develop the memory-saving parallel implementation of the inverse  $LDL^T$  factorization in Appendix E, which can avoid the square-root operations. Furthermore, we also develop the memory-saving parallel implementation of the division free inverse  $LDL^T$  factorization in Appendix F.

In Appendix E, we give some analysis about the parallel performance on MIMD computers [29] of the proposed parallel implementation of the inverse  $LDL^T$  factorization, and we describe the application of the inverse  $LDL^T$  factorization to the distributed BLS. Notice that only for the inverse  $LDL^T$  factorization, we give the analysis of the parallel performance and describe the application to the distributed BLS.

The above-described memory-saving parallel implementations of the inverse Cholesky factorization, the inverse  $LDL^T$  factorization and the division free inverse  $LDL^T$  factorization compute the inverse Cholesky factor, the inverse  $LDL^T$  factors and the division free inverse  $LDL^T$  factors of a Hermitian matrix  $\mathbf{R}_k \in \mathbb{R}^{k \times k}$  by  $k$  iterations. In the theoretical situation where the parallel algorithm runs on  $1 + 2 + \dots + k = \frac{(k+1)k}{2}$  processors, i.e., each entry in the upper-triangular part of  $\mathbf{R}_k$  is stored in an exclusive processor, the proposed parallel implementations update all entries in columns  $i + 1$  to  $k$  of the upper-triangular part of  $\mathbf{R}_k$  except row  $i$  simultaneously in the  $i^{th}$  ( $i = 1, 2, \dots, k$ ) iteration, and each entry is updated with a multiplication and an addition executed serially. In the situation where the parallel algorithm runs on  $k$  processors, and each column of the upper-triangular part of  $\mathbf{R}_k$  is stored in an exclusive processor,  $\mathbf{R}(1 : i, i), \mathbf{R}(i, i + 1), \mathbf{R}(i, i + 2), \dots, \mathbf{R}(i, j - 1)$  need to be transmitted in the  $i^{th}$  ( $i = 1, 2, \dots, k$ ) iteration to the processor storing the  $j^{th}$  column of  $\mathbf{R}$  from the processors storing the  $i^{th}, (i + 1)^{th}, (i + 2)^{th}, \dots, (j - 1)^{th}$  columns of  $\mathbf{R}$ , respectively, where  $j > i$ . In the general case where the columns of  $\mathbf{R}$  are stored in  $\tau \leq k$  processors, and processors  $1, 2, \dots, \tau$  store  $v_1, v_2, \dots, v_\tau$  columns of  $\mathbf{R}$ , respectively,  $\mathbf{R}(1 : i, i)$  and  $\mathbf{R}(i, i + 1 : \tilde{v}_\mu)$  in processor  $\mu$  need to be transmitted to processors  $\mu + 1, \mu + 2, \dots, \tau$ , while

$\mathbf{R}(i, \tilde{v}_{\zeta-1} + 1 : \tilde{v}_\zeta)$  in processor  $\zeta$  needs to be transmitted to processors  $\zeta + 1, \zeta + 2, \dots, \tau$ , where  $\zeta = \mu + 1, \mu + 2, \dots, \tau - 1$ . The above-mentioned general case of the proposed parallel implementations can be applied in the distributed BLS with model-parallelism.

## VI. CONCLUSION

In the original BLS algorithm [16], the generalized inverse solution for the output weights is computed from the generalized inverse, which is updated efficiently by the Greville's method [19], and approximated by ridge regression, i.e., the ridge inverse with the ridge parameter  $\lambda \rightarrow 0$  assumed. Then an efficient implementation of the original BLS on added nodes was proposed in [20], where  $\lambda \rightarrow 0$  is still assumed. In this paper, we propose two ridge solutions for the BLS on added nodes, where the assumption of  $\lambda \rightarrow 0$  is no longer required, and  $\lambda$  can be any positive real number.

In the proposed ridge solution based on the ridge inverse, a sub-matrix in the ridge inverse is utilized to update the output weights, and the ridge inverse is updated by extending the Greville's method that computes the generalized inverse of a partitioned matrix. The proposed algorithm to update the ridge inverse and the Greville's method are equivalent when  $\lambda \rightarrow 0$ , but are usually different when  $\lambda \rightarrow 0$  is not satisfied. So the proposed algorithm to update the ridge inverse includes the Greville's method as a special case, and expands the application range of the Greville's method from the generalized inverse to the ridge inverse. On the other hand, the proposed efficient ridge solution based on the inverse Cholesky factor utilizes the sub-matrices in the inverse Cholesky factor to update the output weights, and updates the inverse Cholesky factor by an efficient inverse Cholesky factorization for a Hermitian matrix partitioned into  $2 \times 2$  blocks, which extends the corresponding algorithm in [21]. Moreover, we also develop another implementation of the proposed efficient ridge solution, which is numerically more stable when the ridge parameter  $\lambda$  is very small.

The proposed ridge solution based on the ridge inverse and the numerically more stable implementation of the proposed efficient ridge solution require the same dominant flops as the original BLS algorithm and the existing efficient generalized inverse solution, respectively. Compared to the proposed efficient ridge solution based on the inverse Cholesky factor, in each update the original BLS algorithm requires about 3 times of flops, and the existing efficient generalized inverse solution usually requires more than  $\frac{5}{3}$  times of flops. In the numerical experiments, the speedups of the proposed efficient ridge solution to the original BLS and the existing efficient generalized inverse solution are  $1.99 \sim 2.52$  and  $1.31 \sim 1.58$ , respectively, when the total training time is considered.

The numerical experiments on MNIST and NORB datasets show that both the proposed ridge solutions for BLS achieve better testing accuracies than the original BLS and the existing efficient generalized inverse solution for BLS. The proposed ridge solution based on the ridge inverse, the proposed efficient ridge solution and its numerically more stable implementation all achieve the maximum testing accuracy of  $98.95\% \sim 98.96\%$  on the MNIST dataset when  $\lambda = 10^{-7}, 10^{-6}$ , and achieve the maximum testing accuracy of  $90.38\%$  on the NORB dataset when  $\lambda = 10^{-3}$ . As a comparison, the original BLS and the existing efficient generalized inverse solution both achieve the maximum testing accuracy of  $98.88\% \sim 98.89\%$  on the MNIST dataset when  $\lambda = 10^{-8}$ , and achieve the maximum testing accuracy of  $89.51\%$  on the NORB dataset when  $\lambda = 10^{-3}$ .

#### APPENDIX A THE DERIVATION OF (99)

From (98) we obtain

$$\mathbf{F}_{k+q}^{-1} = \begin{bmatrix} \mathbf{F}_k^{-1} & -\mathbf{F}_k^{-1}\mathbf{T}\mathbf{G}^{-1} \\ \mathbf{0} & \mathbf{G}^{-1} \end{bmatrix}, \quad (73)$$

which is substituted into (90) to obtain

$$\mathbf{R}_{k+q} = \begin{bmatrix} \mathbf{F}_k^{-1} & -\mathbf{F}_k^{-1}\mathbf{T}\mathbf{G}^{-1} \\ \mathbf{0} & \mathbf{G}^{-1} \end{bmatrix}^T \begin{bmatrix} \mathbf{F}_k^{-1} & -\mathbf{F}_k^{-1}\mathbf{T}\mathbf{G}^{-1} \\ \mathbf{0} & \mathbf{G}^{-1} \end{bmatrix} \begin{bmatrix} \mathbf{F}_k^{-T}\mathbf{F}_k^{-1} & -\mathbf{F}_k^{-T}\mathbf{F}_k^{-1}\mathbf{T}\mathbf{G}^{-1} \\ \left( \begin{array}{c} -\mathbf{G}^{-T}\mathbf{T}^T \\ \times \mathbf{F}_k^{-T}\mathbf{F}_k^{-1} \end{array} \right) & \left( \begin{array}{c} \mathbf{G}^{-T}\mathbf{T}^T\mathbf{F}_k^{-T}\mathbf{F}_k^{-1} \times \\ \mathbf{T}\mathbf{G}^{-1} + \mathbf{G}^{-T}\mathbf{G}^{-1} \end{array} \right) \end{bmatrix}. \quad (74)$$

Then (74) can be compared with (96) to deduce

$$\begin{cases} -\mathbf{F}_k^{-T}\mathbf{F}_k^{-1}\mathbf{T}\mathbf{G}^{-1} = \mathbf{A}_k^T\mathbf{H} \\ \mathbf{G}^{-T}\mathbf{T}^T\mathbf{F}_k^{-T}\mathbf{F}_k^{-1}\mathbf{T}\mathbf{G}^{-1} + \mathbf{G}^{-T}\mathbf{G}^{-1} = \mathbf{H}^T\mathbf{H} + \lambda\mathbf{I}. \end{cases} \quad (75a) \quad (75b)$$

We can deduce (99b) from (75a). On the other hand, let us substitute (99b) into (75b) to obtain

$$\begin{aligned} \mathbf{G}^{-T}\mathbf{G}^{-1} &= \mathbf{H}^T\mathbf{H} + \lambda\mathbf{I} - \mathbf{G}^{-T}(\mathbf{F}_k\mathbf{F}_k^T\mathbf{A}_k^T\mathbf{H}\mathbf{G})^T\mathbf{F}_k^{-T}\mathbf{F}_k^{-1} \times \\ &\quad \mathbf{F}_k\mathbf{F}_k^T\mathbf{A}_k^T\mathbf{H}\mathbf{G}\mathbf{G}^{-1} = \mathbf{H}^T\mathbf{H} + \lambda\mathbf{I} - \mathbf{H}^T\mathbf{A}_k\mathbf{F}_k\mathbf{F}_k^T\mathbf{A}_k^T\mathbf{H}, \end{aligned}$$

from which we can deduce (99a).

#### APPENDIX B THE DERIVATION OF (52)

Substitute (49) and (64) into the left side of (52) successively to obtain

$$\begin{aligned} \mathbf{D}^T\mathbf{A}_k^T\mathbf{C} &= \mathbf{D}^T\mathbf{A}_k^T(\mathbf{H} - \mathbf{A}_k\mathbf{D}) \\ &= \mathbf{D}^T\mathbf{A}_k^T(\mathbf{H} - \mathbf{A}_k\mathbf{A}_k^\dagger\mathbf{H}). \end{aligned} \quad (76)$$

Also substitute [26][Eqn. (20)]

$$(\mathbf{A}^T\mathbf{A} + \lambda\mathbf{I})^{-1}\mathbf{A}^T = \mathbf{A}^T(\mathbf{A}\mathbf{A}^T + \lambda\mathbf{I})^{-1} \quad (77)$$

into (7) to get another form of (7), i.e.,

$$\mathbf{A}^\dagger = \mathbf{A}^T(\mathbf{A}\mathbf{A}^T + \lambda\mathbf{I})^{-1}, \quad (78)$$

which is then substituted into (76) to obtain

$$\begin{aligned} \mathbf{D}^T\mathbf{A}_k^T\mathbf{C} &= \mathbf{D}^T\mathbf{A}_k^T\left(\mathbf{H} - \mathbf{A}_k\mathbf{A}_k^T(\mathbf{A}_k\mathbf{A}_k^T + \lambda\mathbf{I})^{-1}\mathbf{H}\right) \\ &= \mathbf{D}^T\mathbf{A}_k^T\left(\mathbf{H} - \left(\mathbf{I} - \lambda(\mathbf{A}_k\mathbf{A}_k^T + \lambda\mathbf{I})^{-1}\right)\mathbf{H}\right) \\ &= \lambda\mathbf{D}^T\mathbf{A}_k^T(\mathbf{A}_k\mathbf{A}_k^T + \lambda\mathbf{I})^{-1}\mathbf{H}. \end{aligned} \quad (79)$$

To deduce (52) finally, we substitute (78) and (64) into (79) successively to obtain  $\mathbf{D}^T\mathbf{A}_k^T\mathbf{C} = \lambda\mathbf{D}^T\mathbf{A}_k^\dagger\mathbf{H} = \lambda\mathbf{D}^T\mathbf{D}$ .

#### APPENDIX C

TO VERIFY THAT (65) IS EQUAL TO (21) WHEN  $\lambda \rightarrow 0$

When  $\bar{\mathbf{C}} \neq \mathbf{0}$ , we need to verify that  $\mathbf{B}^T$  in (65) is equal to  $\bar{\mathbf{B}}^T$  in (21a) if  $\lambda \rightarrow 0$ . We can let  $\lambda \rightarrow 0$  in (65) to write

$$\begin{aligned} \lim_{\lambda \rightarrow 0} \mathbf{B}^T &= \lim_{\lambda \rightarrow 0} (\mathbf{C}^T\mathbf{C} + \lambda\mathbf{D}^T\mathbf{D} + \lambda\mathbf{I})^{-1}\mathbf{C}^T \\ &= (\bar{\mathbf{C}}^T\bar{\mathbf{C}})^{-1}\bar{\mathbf{C}}^T = \bar{\mathbf{B}}^T, \end{aligned} \quad (80)$$

where  $\lim_{\lambda \rightarrow 0} \mathbf{C} = \bar{\mathbf{C}}$  and (21a) are utilized successively.

When  $\bar{\mathbf{C}} = \mathbf{0}$ , we need to verify that  $\mathbf{B}^T$  in (65) is equal to  $\bar{\mathbf{B}}^T$  in (21b) if  $\lambda \rightarrow 0$ . Firstly, we use  $\bar{\mathbf{C}} = \mathbf{0}$  to write  $\mathbf{C}$  defined by (49) in another form. Let  $\bar{\mathbf{C}} = \mathbf{0}$  in (22) to obtain  $\mathbf{H} = \mathbf{A}_k\bar{\mathbf{D}}$ , which is substituted into (49) to obtain

$$\begin{aligned} \mathbf{C} &= \mathbf{A}_k\bar{\mathbf{D}} - \mathbf{A}_k\mathbf{D} = \mathbf{A}_k\mathbf{A}_k^\dagger\mathbf{H} - \mathbf{A}_k\mathbf{A}_k^\dagger\mathbf{H} \\ &= \mathbf{A}_k(\mathbf{A}_k^T\mathbf{A}_k)^{-1}\mathbf{A}_k^T\mathbf{H} - \mathbf{A}_k(\mathbf{A}_k^T\mathbf{A}_k + \lambda\mathbf{I})^{-1}\mathbf{A}_k^T\mathbf{H} \\ &= \mathbf{A}_k\left((\mathbf{A}_k^T\mathbf{A}_k)^{-1} - (\mathbf{A}_k^T\mathbf{A}_k + \lambda\mathbf{I})^{-1}\right)\mathbf{A}_k^T\mathbf{H}, \end{aligned} \quad (81)$$

where (23), (64), (3) and (7) are utilized. To simplify (81), we utilize a special case of the Woodbury matrix identity [27, equation (68)], i.e.,

$$(\Psi + \Lambda)^{-1} = \Psi^{-1} - \Psi^{-1}(\Psi^{-1} + \Lambda^{-1})^{-1}\Psi^{-1}, \quad (82)$$

to write  $(\mathbf{A}^T\mathbf{A} + \lambda\mathbf{I})^{-1}$  in (81) as

$$\begin{aligned} &(\mathbf{A}^T\mathbf{A} + \lambda\mathbf{I})^{-1} \\ &= (\mathbf{A}^T\mathbf{A})^{-1} - (\mathbf{A}^T\mathbf{A})^{-1}((\mathbf{A}^T\mathbf{A})^{-1} + \lambda^{-1}\mathbf{I})^{-1}(\mathbf{A}^T\mathbf{A})^{-1} \\ &= (\mathbf{A}^T\mathbf{A})^{-1} - \lambda(\mathbf{A}^T\mathbf{A})^{-1}(\mathbf{I} + \lambda(\mathbf{A}^T\mathbf{A})^{-1})^{-1}(\mathbf{A}^T\mathbf{A})^{-1} \\ &= (\mathbf{A}^T\mathbf{A})^{-1} - \lambda(\mathbf{A}^T\mathbf{A})^{-1}\Phi(\mathbf{A}^T\mathbf{A})^{-1}, \end{aligned} \quad (83)$$

where for simplicity, we define

$$\Phi = (\mathbf{I} + \lambda(\mathbf{A}^T\mathbf{A})^{-1})^{-1} \quad (84)$$

satisfying

$$\lim_{\lambda \rightarrow 0} \Phi = \lim_{\lambda \rightarrow 0} (\mathbf{I} + \lambda(\mathbf{A}^T \mathbf{A})^{-1})^{-1} = \mathbf{I}. \quad (85)$$

Then we substitute (83) into (81) to simplify (81) into

$$\begin{aligned} \mathbf{C} &= \mathbf{A}_k \left( (\mathbf{A}_k^T \mathbf{A}_k)^{-1} - (\mathbf{A}_k^T \mathbf{A}_k)^{-1} + \lambda (\mathbf{A}_k^T \mathbf{A}_k)^{-1} \Phi (\mathbf{A}_k^T \mathbf{A}_k)^{-1} \right)^{-1} \mathbf{A}_k^T \mathbf{H} \\ &= \lambda \mathbf{A}_k (\mathbf{A}_k^T \mathbf{A}_k)^{-1} \Phi (\mathbf{A}_k^T \mathbf{A}_k)^{-1} \mathbf{A}_k^T \mathbf{H} \\ &= \lambda (\mathbf{A}_k^+)^T \Phi \mathbf{A}_k^+ \mathbf{H} \\ &= \lambda (\mathbf{A}_k^+)^T \Phi \bar{\mathbf{D}}, \end{aligned} \quad (86)$$

where (3) and (23) are utilized successively.

Finally, let us utilize (86) to verify that (65) is equal to (21b) when  $\lambda \rightarrow 0$ . We substitute (86) into (65) to obtain

$$\begin{aligned} \mathbf{B}^T &= (\lambda \bar{\mathbf{D}}^T \Phi \mathbf{A}_k^+ \lambda (\mathbf{A}_k^+)^T \Phi \bar{\mathbf{D}} + \lambda \bar{\mathbf{D}}^T \bar{\mathbf{D}} + \lambda \mathbf{I})^{-1} \lambda \bar{\mathbf{D}}^T \Phi \mathbf{A}_k^+ \\ &= \frac{1}{\lambda} (\bar{\mathbf{D}}^T \bar{\mathbf{D}} + \mathbf{I} + \lambda \bar{\mathbf{D}}^T \Phi \mathbf{A}_k^+ (\mathbf{A}_k^+)^T \Phi \bar{\mathbf{D}})^{-1} \lambda \bar{\mathbf{D}}^T \Phi \mathbf{A}_k^+ \\ &= (\bar{\mathbf{D}}^T \bar{\mathbf{D}} + \mathbf{I} + \lambda \bar{\mathbf{D}}^T \Phi \mathbf{A}_k^+ (\mathbf{A}_k^+)^T \Phi \bar{\mathbf{D}})^{-1} \bar{\mathbf{D}}^T \Phi \mathbf{A}_k^+, \end{aligned} \quad (87)$$

and then let  $\lambda \rightarrow 0$  in (87) to obtain

$$\begin{aligned} \lim_{\lambda \rightarrow 0} \mathbf{B}^T &= \lim_{\lambda \rightarrow 0} (\bar{\mathbf{D}}^T \bar{\mathbf{D}} + \mathbf{I} + \lambda \bar{\mathbf{D}}^T \Phi \mathbf{A}_k^+ (\mathbf{A}_k^+)^T \Phi \bar{\mathbf{D}})^{-1} \bar{\mathbf{D}}^T \Phi \mathbf{A}_k^+ \\ &= (\bar{\mathbf{D}}^T \bar{\mathbf{D}} + \mathbf{I})^{-1} \bar{\mathbf{D}}^T \mathbf{I} \mathbf{A}_k^+ = (\bar{\mathbf{D}}^T \bar{\mathbf{D}} + \mathbf{I})^{-1} \bar{\mathbf{D}}^T \mathbf{A}_k^+ = \bar{\mathbf{B}}^T, \end{aligned}$$

where (85) and (21b) are applied in turn.

## APPENDIX D

### THE EFFICIENT INVERSE CHOLESKY FACTORIZATION AND THE CORRESPONDING PARALLELIZATION

In this section, we will summarize the efficient inverse Cholesky factorization firstly, and then develop the memory-saving parallel implementation of the inverse Cholesky factorization.

#### A. The Existing Efficient Inverse Cholesky Factorization

In [21], the inverse Cholesky factor of a Hermitian matrix  $\mathbf{R}_i \in \mathbb{R}^{i \times i}$  is the upper-triangular  $\mathbf{F}_i$  satisfying

$$\mathbf{F}_i \mathbf{F}_i^T = \mathbf{R}_i^{-1} = (\mathbf{A}_i^T \mathbf{A}_i + \lambda \mathbf{I})^{-1}, \quad (88)$$

where  $\mathbf{A}_i$  is with  $i$  columns, the ridge parameter  $\lambda$  is a positive real number, and  $\mathbf{R}_i$  is defined by

$$\mathbf{R}_i = \mathbf{A}_i^T \mathbf{A}_i + \lambda \mathbf{I}. \quad (89)$$

From (88), we can deduce

$$\mathbf{F}_i^{-T} \mathbf{F}_i^{-1} = \mathbf{R}_i, \quad (90)$$

which shows that the lower-triangular  $\mathbf{F}_i^{-T}$  is the conventional Cholesky factor [23, Theorem 4.2.5] of  $\mathbf{R}_i$ .

$\mathbf{A}_i$  can be partitioned into

$$\mathbf{A}_i = [\mathbf{A}_{i-1} \quad \mathbf{a}_i], \quad (91)$$

where  $\mathbf{A}_{i-1}$  and  $\mathbf{a}_i$  denotes the first  $i-1$  columns and the  $i^{th}$  column of  $\mathbf{A}_i$ , respectively. Then (91) can be substituted into (89) to partition  $\mathbf{R}_i$  into

$$\mathbf{R}_i = \begin{bmatrix} \mathbf{A}_{i-1}^T \mathbf{A}_{i-1} + \lambda \mathbf{I} & \mathbf{A}_{i-1}^T \mathbf{a}_i \\ \mathbf{a}_i^T \mathbf{A}_{i-1} & \mathbf{a}_i^T \mathbf{a}_i + \lambda \end{bmatrix} = \begin{bmatrix} \mathbf{R}_{i-1} & \mathbf{p} \\ \mathbf{p}^T & u \end{bmatrix}, \quad (92)$$

where  $\mathbf{p}$  and  $u$  are a column vector and a scalar, respectively, and  $\mathbf{R}_{i-1}$ , the  $(i-1) \times (i-1)$  leading principal submatrix of  $\mathbf{R}_i$ , is also defined from  $\mathbf{A}_{i-1}$  by (89). The efficient inverse Cholesky factorization [21] updates the inverse Cholesky factor of  $\mathbf{R}_{i-1}$  into that of  $\mathbf{R}_i$  by

$$\mathbf{F}_i = \begin{bmatrix} \mathbf{F}_{i-1} & \bar{\mathbf{f}}_i \\ \mathbf{0}_{i-1}^T & f_{ii} \end{bmatrix} = \begin{bmatrix} \left( \begin{matrix} \mathbf{F}_{i-1} \\ \mathbf{0}_{i-1}^T \end{matrix} \right) & \mathbf{f}_i \end{bmatrix}, \quad (93)$$

where  $\bar{\mathbf{f}}_i$  and  $f_{ii}$  are computed by

$$\begin{cases} \bar{\mathbf{f}}_i = 1 / \sqrt{u - \mathbf{p}^T \mathbf{F}_i \mathbf{F}_i^T \mathbf{p}} \\ f_{ii} = -g \mathbf{F}_i \mathbf{F}_i^T \mathbf{p}. \end{cases} \quad (94a)$$

$$(94b)$$

In (93) and (94),  $\mathbf{f}_i$  and  $f_{ii}$  denote the  $i^{th}$  column and diagonal entry of  $\mathbf{F}_i$ , respectively, while  $\bar{\mathbf{f}}_i$  denotes  $\mathbf{f}_i$  with the last entry  $f_{ii}$  removed.

In this paper, (91) is extended into a column-partitioned matrix

$$\mathbf{A}_k = [\mathbf{A}_i \quad \underline{\mathbf{A}}_{k-i}], \quad (95)$$

where  $\mathbf{A}_i$  and  $\underline{\mathbf{A}}_{k-i}$  are the first  $i$  and last  $k-i$  columns of  $\mathbf{A}_k$  with  $k$  columns, respectively. Then (95) can be substituted into (89) to partition  $\mathbf{R}_k$  into the  $2 \times 2$  block matrix, i.e.,

$$\mathbf{R}_k = \begin{bmatrix} \mathbf{R}_i & \mathbf{A}_i^T \underline{\mathbf{A}}_{k-i} \\ \underline{\mathbf{A}}_{k-i}^T \mathbf{A}_i & \underline{\mathbf{A}}_{k-i}^T \underline{\mathbf{A}}_{k-i} + \lambda \mathbf{I} \end{bmatrix} = \begin{bmatrix} \mathbf{R}_i & \mathbf{P} \\ \mathbf{P}^T & \mathbf{U} \end{bmatrix}, \quad (96)$$

where

$$\begin{cases} \mathbf{U} = \underline{\mathbf{A}}_{k-i}^T \underline{\mathbf{A}}_{k-i} + \lambda \mathbf{I} \in \mathbb{R}^{(k-i) \times (k-i)} \\ \mathbf{P} = \mathbf{A}_i^T \underline{\mathbf{A}}_{k-i} \in \mathbb{R}^{i \times (k-i)}. \end{cases} \quad (97a)$$

$$(97b)$$

The inverse Cholesky factor of  $\mathbf{R}_i$  is updated into that of  $\mathbf{R}_k$  by

$$\mathbf{F}_k = \begin{bmatrix} \mathbf{F}_i & \mathbf{T} \\ \mathbf{0} & \mathbf{G} \end{bmatrix} \quad (98)$$

where  $\mathbf{T} \in \mathbb{R}^{i \times (k-i)}$  and  $\mathbf{G} \in \mathbb{R}^{(k-i) \times (k-i)}$  are computed by

$$\begin{cases} \mathbf{G} \mathbf{G}^T = (\underline{\mathbf{A}}_{k-i}^T \underline{\mathbf{A}}_{k-i} + \lambda \mathbf{I} - \underline{\mathbf{A}}_{k-i}^T \mathbf{A}_i \mathbf{F}_i \mathbf{F}_i^T \mathbf{A}_i^T \underline{\mathbf{A}}_{k-i})^{-1} \\ \mathbf{T} = -\mathbf{F}_i \mathbf{F}_i^T \mathbf{A}_i^T \underline{\mathbf{A}}_{k-i} \mathbf{G}. \end{cases} \quad (99a)$$

$$(99b)$$

In this paper, the inverse Cholesky factor of  $\mathbf{R}_i$  is updated into that of  $\mathbf{R}_k$  by the above-described block inverse Cholesky factorization, where  $\mathbf{F}_i$  is updated into  $\mathbf{F}_k$  by (99) and (98), and the initial  $\mathbf{F}_i$  is computed by (88).  $\mathbf{G}$  in (99a) is also the upper-triangular inverse Cholesky factor, which can be computed by the efficient inverse Cholesky factorization in [21] or by inverting and transposing the lower-triangular Cholesky factor.

#### B. The Memory-Saving Parallel Implementation of the Inverse Cholesky Factorization

In (99) for the block inverse Cholesky factorization,  $-\mathbf{F}_i \mathbf{F}_i^T \mathbf{A}_i^T \underline{\mathbf{A}}_{k-i}$  and  $\underline{\mathbf{A}}_{k-i}^T \underline{\mathbf{A}}_{k-i} + \lambda \mathbf{I} -$



$\underline{\mathbf{A}}_{k-i}^T \mathbf{A}_i \mathbf{F}_i \mathbf{F}_i^T \mathbf{A}_i^T \underline{\mathbf{A}}_{k-i}$  can be written as

$$\begin{cases} \mathbf{\Pi}_i = -\mathbf{F}_i \mathbf{F}_i^T \mathbf{A}_i^T \underline{\mathbf{A}}_{k-i} & (100a) \\ \mathbf{\Xi}_{k-i} = \underline{\mathbf{A}}_{k-i}^T \underline{\mathbf{A}}_{k-i} + \lambda \mathbf{I} - \underline{\mathbf{A}}_{k-i}^T \mathbf{A}_i \mathbf{F}_i \mathbf{F}_i^T \mathbf{A}_i^T \underline{\mathbf{A}}_{k-i}, & (100b) \end{cases}$$

where  $i = 1, 2, \dots, k-1$ ,  $\mathbf{\Pi}_i \in \mathbb{R}^{i \times (k-i)}$ , and  $\mathbf{\Xi}_{k-i} \in \mathbb{R}^{(k-i) \times (k-i)}$ . On the other hand, it can be seen from (94) and (93) for the efficient inverse Cholesky factorization [21] that in the  $i^{th}$  iteration, the  $i^{th}$  column of  $\mathbf{F}_i$  is computed by (94), and then merged with  $\mathbf{F}_{i-1}$  to obtain  $\mathbf{F}_i$  by (93). Then in the  $i^{th}$  ( $i = 1, 2, \dots, k-1$ ) iteration of the efficient inverse Cholesky factorization [21], we can use  $\mathbf{F}_i$  to compute  $\mathbf{\Pi}_i$  and  $\mathbf{\Xi}_{k-i}$  by (100a) and (100b), respectively, in order to improve the parallelization.

To reduce the computational complexity, we utilize  $\mathbf{\Xi}_{k-i+1}$  and  $\mathbf{\Pi}_{i-1}$  to compute  $\mathbf{\Xi}_{k-i}$  and  $\mathbf{\Pi}_i$  by

$$\mathbf{\Xi}_{k-i} = \mathbf{\Xi}_{k-i+1}^{[-1,-1]} - f_{ii}^2 \mathbf{\Xi}_{k-i+1}(1, 2 : \text{end})^T \mathbf{\Xi}_{k-i+1}(1, 2 : \text{end}) \quad (101)$$

and

$$\mathbf{\Pi}_i = \begin{bmatrix} \mathbf{\Pi}_{i-1}(:, 2 : \text{end}) - \mathbf{\Pi}_{i-1}(:, 1) \cdot f_{ii}^2 \mathbf{\Xi}_{k-i+1}(1, 2 : \text{end}) \\ -f_{ii}^2 \mathbf{\Xi}_{k-i+1}(1, 2 : \text{end}) \end{bmatrix}, \quad (102)$$

respectively, instead of (100a) and (100b), and compute the  $i^{th}$  column of  $\mathbf{F}_i$  (i.e.,  $\bar{\mathbf{f}}_i$  and  $f_{ii}$  in (93)) by

$$\begin{cases} f_{ii} = 1/\sqrt{\mathbf{\Xi}_{k-i+1}(1, 1)} & (103a) \\ \bar{\mathbf{f}}_i = f_{ii} \mathbf{\Pi}_{i-1}(:, 1). & (103b) \end{cases}$$

In the next subsection, we will derive the above (101), (102) and (103), where  $\mathbf{\Xi}_{k-i+1}^{[-1,-1]}$  is  $\mathbf{\Xi}_{k-i+1}$  with the first row and column removed, and the notations  $\mathbf{\Xi}_{k-i+1}(1, 2 : \text{end})$ ,  $\mathbf{\Pi}_{i-1}(:, 2 : \text{end})$ ,  $\mathbf{\Pi}_{i-1}(:, 1)$  and  $\mathbf{\Xi}_{k-i+1}(1, 1)$  follow the MATLAB standard. Notice that in the remainder of this paper, the notations will also follow the MATLAB standard.

To save memories, we will give an implementation that cover the upper-triangular part of the Hermitian matrix  $\mathbf{R}_k$  with  $\mathbf{F}_k$ , the inverse Cholesky factor of  $\mathbf{R}_k$ . It can be seen from (96) that

$$\begin{cases} \mathbf{R}(1 : i, i+1 : k) = \mathbf{P} = \mathbf{A}_i^T \underline{\mathbf{A}}_{k-i} & (104a) \\ \mathbf{R}(i+1 : k, i+1 : k) = \mathbf{U} = \underline{\mathbf{A}}_{k-i}^T \underline{\mathbf{A}}_{k-i} + \lambda \mathbf{I}, & (104b) \end{cases}$$

which are substituted into (100a) and (100b) to obtain

$$\begin{cases} \mathbf{\Pi}_i = -\mathbf{F}_i \mathbf{F}_i^T \mathbf{R}(1 : i, i+1 : k) & (105a) \\ \mathbf{\Xi}_{k-i} = \mathbf{R}(i+1 : k, i+1 : k) - & (105b) \\ \mathbf{R}(1 : i, i+1 : k)^T \mathbf{F}_i \mathbf{F}_i^T \mathbf{R}(1 : i, i+1 : k). \end{cases}$$

Let  $k = 1$  in (88) to obtain

$$\mathbf{F}_1 \mathbf{F}_1^T = 1/\mathbf{R}(1, 1), \quad (106)$$

which is substituted into (105) with  $i = 1$ , i.e.,

$$\begin{cases} \mathbf{\Pi}_1 = -\mathbf{F}_1 \mathbf{F}_1^T \mathbf{R}(1, 2 : k) & (107a) \\ \mathbf{\Xi}_{k-1} = \mathbf{R}(2 : k, 2 : k) - \mathbf{R}(1, 2 : k)^T \mathbf{F}_1 \mathbf{F}_1^T \mathbf{R}(1, 2 : k), & (107b) \end{cases}$$

to compute the initial  $\mathbf{\Pi}_1$  and  $\mathbf{\Xi}_{k-1}$  by

$$\begin{cases} \mathbf{\Pi}_1 = -\frac{\mathbf{R}(1, 2 : k)}{\mathbf{R}(1, 1)} & (108a) \\ \mathbf{\Xi}_{k-1} = \mathbf{R}(2 : k, 2 : k) - \frac{\mathbf{R}(1, 2 : k)^T \mathbf{R}(1, 2 : k)}{\mathbf{R}(1, 1)}. & (108b) \end{cases}$$

Moreover, we compute the initial  $\mathbf{F}_1$  by writing (106) as

$$\mathbf{F}_1 = \sqrt{1/\mathbf{R}(1, 1)}. \quad (109)$$

When  $i \geq 2$ , none of the entries of  $\mathbf{R}$  are required in (101), (102), (103a) and (103b), which are utilized to compute  $\mathbf{\Xi}_{k-i}$ ,  $\mathbf{\Pi}_i$ ,  $f_{ii}$  and  $\bar{\mathbf{f}}_i$ , respectively. Then to save memories, we store  $\mathbf{\Xi}_{k-1}$ ,  $\mathbf{\Pi}_1$  and  $\mathbf{F}_1$  in  $\mathbf{R}(2 : k, 2 : k)$ ,  $\mathbf{R}(1, 2 : k)$  and  $\mathbf{R}(1, 1)$ , respectively, to write (108b), (108a) and (109) as

$$\begin{cases} \mathbf{R}(2 : k, 2 : k) = \mathbf{R}(2 : k, 2 : k) \\ -\frac{\mathbf{R}(1, 2 : k)^T \mathbf{R}(1, 2 : k)}{\mathbf{R}(1, 1)} & (110a) \end{cases}$$

$$\begin{cases} \mathbf{R}(1, 2 : k) = -\frac{\mathbf{R}(1, 2 : k)}{\mathbf{R}(1, 1)} & (110b) \end{cases}$$

$$\begin{cases} \mathbf{R}(1, 1) = \sqrt{1/\mathbf{R}(1, 1)}. & (110c) \end{cases}$$

In the  $i^{th}$  ( $i \geq 2$ ) iteration, we can also save memories by storing  $\mathbf{\Xi}_{k-i}$ ,  $\mathbf{\Pi}_i$ ,  $f_{ii}$  and  $\bar{\mathbf{f}}_i$  in  $\mathbf{R}(i+1 : k, i+1 : k)$ ,  $\mathbf{R}(1 : i, i+1 : k)$ ,  $\mathbf{R}(i, i)$  and  $\mathbf{R}(1 : i-1, i)$ , respectively, to write (101), (102), (103a) and (103b) as

$$\begin{cases} \mathbf{R}(i+1 : k, i+1 : k) = \mathbf{R}(i+1 : k, i+1 : k) \\ -\frac{\mathbf{R}(i, i+1 : k)^T \mathbf{R}(i, i+1 : k)}{\mathbf{R}(i, i)} & (111a) \end{cases}$$

$$\begin{cases} \mathbf{R}(1 : i, i+1 : k) = \begin{bmatrix} \mathbf{R}(1 : i-1, i+1 : k) - \frac{\mathbf{R}(1 : i-1, i) \mathbf{R}(i, i+1 : k)}{\mathbf{R}(i, i)} \\ -\frac{\mathbf{R}(i, i+1 : k)}{\mathbf{R}(i, i)} \end{bmatrix} & (111b) \end{cases}$$

$$\begin{cases} \mathbf{R}(i, i) = \sqrt{1/\mathbf{R}(i, i)} & (111c) \end{cases}$$

$$\begin{cases} \mathbf{R}(1 : i-1, i) = \mathbf{R}(i, i) \mathbf{R}(1 : i-1, i). & (111d) \end{cases}$$

Notice that to deduce (111), we utilize the fact that  $\mathbf{\Xi}_{k-(i-1)} = \mathbf{\Xi}_{k-i+1}$  and  $\mathbf{\Pi}_{i-1}$  have been stored in  $\mathbf{R}((i-1)+1 : k, (i-1)+1 : k) = \mathbf{R}(i : k, i : k)$  and  $\mathbf{R}(1 : i-1, (i-1)+1 : k) = \mathbf{R}(1 : i-1, i : k)$ , respectively, where  $i \geq 2$ .

It can be seen that (110) is equivalent to (111) with  $i = 1$ . Then we can compute (111) iteratively for  $i = 1, 2, \dots, k$ , to cover the upper-triangular part of  $\mathbf{R}_k$  with the inverse Cholesky factor  $\mathbf{F}_k$  satisfying  $\mathbf{F}_k \mathbf{F}_k^T = \mathbf{R}_k^{-1}$ . The corresponding implementation is summarized in **Algorithm 11**.

---

**Algorithm 11 : The parallel implementation of the inverse Cholesky factorization**

---

**Input:** The upper-triangular part of a Hermitian matrix  $\mathbf{R}$

**Output:** The inverse Cholesky factor of  $\mathbf{R}$  in the upper-triangular part of  $\mathbf{R}$

- 1: **for**  $i = 1 : k$  ( $k$  is the size of  $\mathbf{R}$ ) **do**
  - 2:  $\mathbf{R}(i+1 : k, i+1 : k) = \mathbf{R}(i+1 : k, i+1 : k) - \frac{\mathbf{R}(i, i+1 : k)^T \mathbf{R}(i, i+1 : k)}{\mathbf{R}(i, i)};$
  - 3:  $\mathbf{R}(1 : i, i+1 : k) = \begin{bmatrix} \mathbf{R}(1 : i-1, i+1 : k) - \frac{\mathbf{R}(1 : i-1, i) \mathbf{R}(i, i+1 : k)}{\mathbf{R}(i, i)} \\ -\frac{\mathbf{R}(i, i+1 : k)}{\mathbf{R}(i, i)} \end{bmatrix};$
  - 4:  $\mathbf{R}(i, i) = \sqrt{1/\mathbf{R}(i, i)};$
  - 5:  $\mathbf{R}(1 : i-1, i) = \mathbf{R}(i, i) \mathbf{R}(1 : i-1, i);$
  - 6: **end for**
  - 7: Now the upper-triangular part of  $\mathbf{R}$  becomes the inverse Cholesky factor  $\mathbf{F}$  satisfying  $\mathbf{F} \mathbf{F}^T = \mathbf{R}^{-1};$
-

### C. The Derivation of (101), (102) and (103)

In this subsection, let us deduce (101), (102) and (103) utilized in the last subsection.

Obviously,  $\underline{\mathbf{A}}_{k-i}$  in (95) satisfies

$$\underline{\mathbf{A}}_{k-(i-1)} = \underline{\mathbf{A}}_{k-i+1} = \begin{bmatrix} \mathbf{a}_i & \underline{\mathbf{A}}_{k-i} \end{bmatrix}, \quad (112)$$

where  $\mathbf{a}_i$  is the  $i^{th}$  column of  $\mathbf{A}_k$ . Then use (112) to write

$$\begin{aligned} \mathbf{F}_{i-1}^T \mathbf{A}_{i-1}^T \underline{\mathbf{A}}_{k-(i-1)} &= \mathbf{F}_{i-1}^T \mathbf{A}_{i-1}^T \begin{bmatrix} \mathbf{a}_i & \underline{\mathbf{A}}_{k-i} \end{bmatrix} \\ &= \begin{bmatrix} \mathbf{F}_{i-1}^T \mathbf{A}_{i-1}^T \mathbf{a}_i & \mathbf{F}_{i-1}^T \mathbf{A}_{i-1}^T \underline{\mathbf{A}}_{k-i} \end{bmatrix}. \end{aligned} \quad (113)$$

From (92), we can write  $\begin{bmatrix} \mathbf{p} \\ u \end{bmatrix} = \begin{bmatrix} \mathbf{A}_{i-1}^T \mathbf{a}_i \\ \mathbf{a}_i^T \mathbf{a}_i + \lambda \end{bmatrix}$ , which is substituted into (94) to obtain

$$\begin{cases} f_{ii} = 1/\sqrt{\mathbf{a}_i^T \mathbf{a}_i + \lambda - \mathbf{a}_i^T \mathbf{A}_{i-1} \mathbf{F}_{i-1} \mathbf{F}_{i-1}^T \mathbf{A}_{i-1}^T \mathbf{a}_i} & (114a) \\ \bar{\mathbf{f}}_i = -f_{ii} \mathbf{F}_{i-1} \mathbf{F}_{i-1}^T \mathbf{A}_{i-1}^T \mathbf{a}_i. & (114b) \end{cases}$$

To update  $\Pi_{i-1}$  into  $\Pi_i$  efficiently, substitute (113) into (100a) with  $i = i - 1$  to obtain

$$\begin{aligned} \Pi_{i-1} &= -\mathbf{F}_{i-1} \begin{bmatrix} \mathbf{F}_{i-1}^T \mathbf{A}_{i-1}^T \mathbf{a}_i & \mathbf{F}_{i-1}^T \mathbf{A}_{i-1}^T \underline{\mathbf{A}}_{k-i} \end{bmatrix} \\ &= -\begin{bmatrix} \mathbf{F}_{i-1} \mathbf{F}_{i-1}^T \mathbf{A}_{i-1}^T \mathbf{a}_i & \mathbf{F}_{i-1} \mathbf{F}_{i-1}^T \mathbf{A}_{i-1}^T \underline{\mathbf{A}}_{k-i} \end{bmatrix}, \end{aligned} \quad (115)$$

which can be written as

$$\begin{cases} \Pi_{i-1}(:, 1) = -\mathbf{F}_{i-1} \mathbf{F}_{i-1}^T \mathbf{A}_{i-1}^T \mathbf{a}_i & (116a) \\ \Pi_{i-1}(:, 2 : \text{end}) = -\mathbf{F}_{i-1} \mathbf{F}_{i-1}^T \mathbf{A}_{i-1}^T \underline{\mathbf{A}}_{k-i}. & (116b) \end{cases}$$

Also substitute (93) and (91) into  $\mathbf{F}_i^T \mathbf{A}_i^T \underline{\mathbf{A}}_{k-i}$  to obtain

$$\begin{aligned} \mathbf{F}_i^T \mathbf{A}_i^T \underline{\mathbf{A}}_{k-i} &= \begin{bmatrix} \mathbf{F}_{i-1}^T & \mathbf{0}_{i-1} \\ \mathbf{f}_i^T & \end{bmatrix} \begin{bmatrix} \mathbf{A}_{i-1}^T \\ \mathbf{a}_i^T \end{bmatrix} \underline{\mathbf{A}}_{k-i} \\ &= \begin{bmatrix} \mathbf{F}_{i-1}^T \mathbf{A}_{i-1}^T \underline{\mathbf{A}}_{k-i} \\ \mathbf{f}_i^T \begin{bmatrix} \mathbf{A}_{i-1} & \mathbf{a}_i \end{bmatrix}^T \underline{\mathbf{A}}_{k-i} \end{bmatrix} \\ &= \begin{bmatrix} \mathbf{F}_{i-1}^T \mathbf{A}_{i-1}^T \underline{\mathbf{A}}_{k-i} \\ \mathbf{f}_i^T \mathbf{A}_i^T \underline{\mathbf{A}}_{k-i} \end{bmatrix}, \end{aligned} \quad (117)$$

and then substitute (117) and (93) into (100a) to obtain

$$\begin{aligned} \Pi_i &= -\begin{bmatrix} \mathbf{F}_{i-1} \\ \mathbf{0}_{i-1}^T \end{bmatrix} \mathbf{f}_i \begin{bmatrix} \mathbf{F}_{i-1}^T \mathbf{A}_{i-1}^T \underline{\mathbf{A}}_{k-i} \\ \mathbf{f}_i^T \mathbf{A}_i^T \underline{\mathbf{A}}_{k-i} \end{bmatrix} \\ &= \begin{pmatrix} -\mathbf{F}_{i-1} \mathbf{F}_{i-1}^T \mathbf{A}_{i-1}^T \underline{\mathbf{A}}_{k-i} \\ \mathbf{0}_{k-i}^T \end{pmatrix} - \mathbf{f}_i \mathbf{f}_i^T \mathbf{A}_i^T \underline{\mathbf{A}}_{k-i}. \end{aligned} \quad (118)$$

Finally, substitute (116b) into (118) to obtain

$$\Pi_i = \begin{pmatrix} \Pi_{i-1}(:, 2 : \text{end}) \\ \mathbf{0}_{k-i}^T \end{pmatrix} - \mathbf{f}_i \mathbf{f}_i^T \mathbf{A}_i^T \underline{\mathbf{A}}_{k-i}. \quad (119)$$

To update  $\Xi_{k-(i-1)}$  into  $\Xi_{k-i}$  efficiently, substitute (117) into (100b) to obtain

$$\begin{aligned} \Xi_{k-i} &= \underline{\mathbf{A}}_{k-i}^T \underline{\mathbf{A}}_{k-i} + \lambda \mathbf{I} - \underline{\mathbf{A}}_{k-i}^T \mathbf{A}_i \mathbf{F}_i \mathbf{F}_i^T \mathbf{A}_i^T \underline{\mathbf{A}}_{k-i} \\ &= \underline{\mathbf{A}}_{k-i}^T \underline{\mathbf{A}}_{k-i} + \lambda \mathbf{I} - \begin{bmatrix} \mathbf{F}_{i-1}^T \mathbf{A}_{i-1}^T \underline{\mathbf{A}}_{k-i} \\ \mathbf{f}_i^T \mathbf{A}_i^T \underline{\mathbf{A}}_{k-i} \end{bmatrix}^T \begin{bmatrix} \mathbf{F}_{i-1}^T \mathbf{A}_{i-1}^T \underline{\mathbf{A}}_{k-i} \\ \mathbf{f}_i^T \mathbf{A}_i^T \underline{\mathbf{A}}_{k-i} \end{bmatrix} \\ &= \underline{\mathbf{A}}_{k-i}^T \underline{\mathbf{A}}_{k-i} + \lambda \mathbf{I} - \underline{\mathbf{A}}_{k-i}^T \mathbf{A}_{i-1} \mathbf{F}_{i-1} \mathbf{F}_{i-1}^T \mathbf{A}_{i-1}^T \underline{\mathbf{A}}_{k-i} \\ &\quad - \underline{\mathbf{A}}_{k-i}^T \mathbf{A}_i \mathbf{f}_i \mathbf{f}_i^T \mathbf{A}_i^T \underline{\mathbf{A}}_{k-i}, \end{aligned} \quad (120)$$

and substitute (112) and (113) into (100b) with  $i = i - 1$  to

obtain

$$\begin{aligned} \Xi_{k-i+1} &= \underline{\mathbf{A}}_{k-i+1}^T \underline{\mathbf{A}}_{k-i+1} + \lambda \mathbf{I} \\ &\quad - \underline{\mathbf{A}}_{k-i+1}^T \mathbf{A}_{i-1} \mathbf{F}_{i-1} \mathbf{F}_{i-1}^T \mathbf{A}_{i-1}^T \underline{\mathbf{A}}_{k-i+1} \\ &= \begin{bmatrix} \mathbf{a}_i & \underline{\mathbf{A}}_{k-i} \end{bmatrix}^T \begin{bmatrix} \mathbf{a}_i & \underline{\mathbf{A}}_{k-i} \end{bmatrix} + \lambda \mathbf{I} \\ &\quad - \begin{bmatrix} \mathbf{F}_{i-1}^T \mathbf{A}_{i-1}^T \mathbf{a}_i & \mathbf{F}_{i-1}^T \mathbf{A}_{i-1}^T \underline{\mathbf{A}}_{k-i} \end{bmatrix}^T \\ &\quad \times \begin{bmatrix} \mathbf{F}_{i-1}^T \mathbf{A}_{i-1}^T \mathbf{a}_i & \mathbf{F}_{i-1}^T \mathbf{A}_{i-1}^T \underline{\mathbf{A}}_{k-i} \end{bmatrix} \\ &= \begin{bmatrix} \mathbf{a}_i^T \mathbf{a}_i + \lambda & \mathbf{a}_i^T \underline{\mathbf{A}}_{k-i} \\ \underline{\mathbf{A}}_{k-i}^T \mathbf{a}_i & \underline{\mathbf{A}}_{k-i}^T \underline{\mathbf{A}}_{k-i} + \lambda \mathbf{I} \end{bmatrix} - \\ &\quad \begin{bmatrix} \begin{pmatrix} \mathbf{a}_i^T \mathbf{A}_{i-1} \mathbf{F}_{i-1} \times \\ \mathbf{F}_{i-1}^T \mathbf{A}_{i-1}^T \mathbf{a}_i \end{pmatrix} & \begin{pmatrix} \mathbf{a}_i^T \mathbf{A}_{i-1} \mathbf{F}_{i-1} \times \\ \mathbf{F}_{i-1}^T \mathbf{A}_{i-1}^T \underline{\mathbf{A}}_{k-i} \end{pmatrix} \\ \begin{pmatrix} \underline{\mathbf{A}}_{k-i}^T \mathbf{A}_{i-1} \mathbf{F}_{i-1} \times \\ \mathbf{F}_{i-1}^T \mathbf{A}_{i-1}^T \mathbf{a}_i \end{pmatrix} & \begin{pmatrix} \underline{\mathbf{A}}_{k-i}^T \mathbf{A}_{i-1} \mathbf{F}_{i-1} \times \\ \mathbf{F}_{i-1}^T \mathbf{A}_{i-1}^T \underline{\mathbf{A}}_{k-i} \end{pmatrix} \end{bmatrix} \\ &= \begin{bmatrix} \begin{pmatrix} \mathbf{a}_i^T \mathbf{a}_i + \lambda - \\ \mathbf{a}_i^T \mathbf{A}_{i-1} \mathbf{F}_{i-1} \times \\ \mathbf{F}_{i-1}^T \mathbf{A}_{i-1}^T \mathbf{a}_i \end{pmatrix} & \begin{pmatrix} \mathbf{a}_i^T \underline{\mathbf{A}}_{k-i} - \\ \mathbf{a}_i^T \mathbf{A}_{i-1} \mathbf{F}_{i-1} \times \\ \mathbf{F}_{i-1}^T \mathbf{A}_{i-1}^T \underline{\mathbf{A}}_{k-i} \end{pmatrix} \\ \begin{pmatrix} \underline{\mathbf{A}}_{k-i}^T \mathbf{a}_i - \\ \underline{\mathbf{A}}_{k-i}^T \mathbf{A}_{i-1} \mathbf{F}_{i-1} \times \\ \mathbf{F}_{i-1}^T \mathbf{A}_{i-1}^T \mathbf{a}_i \end{pmatrix} & \begin{pmatrix} \underline{\mathbf{A}}_{k-i}^T \underline{\mathbf{A}}_{k-i} + \lambda \mathbf{I} \\ -\underline{\mathbf{A}}_{k-i}^T \mathbf{A}_{i-1} \mathbf{F}_{i-1} \times \\ \mathbf{F}_{i-1}^T \mathbf{A}_{i-1}^T \underline{\mathbf{A}}_{k-i} \end{pmatrix} \end{bmatrix}. \end{aligned} \quad (121)$$

It can be seen from (121) that  $\Xi_{k-i+1}$  with the first row and column removed is

$$\Xi_{k-i+1}^{[-1,-1]} = \underline{\mathbf{A}}_{k-i}^T \underline{\mathbf{A}}_{k-i} + \lambda \mathbf{I} - \underline{\mathbf{A}}_{k-i}^T \mathbf{A}_{i-1} \mathbf{F}_{i-1} \mathbf{F}_{i-1}^T \mathbf{A}_{i-1}^T \underline{\mathbf{A}}_{k-i},$$

which is substituted into (120) to compute  $\Xi_{k-i}$  efficiently by

$$\Xi_{k-i} = \Xi_{k-i+1}^{[-1,-1]} - \underline{\mathbf{A}}_{k-i}^T \mathbf{A}_i \mathbf{f}_i \mathbf{f}_i^T \mathbf{A}_i^T \underline{\mathbf{A}}_{k-i}. \quad (122)$$

Firstly, let us deduce (103). We can obtain (103b) by substituting (116a) into (114b). On the other hand, we deduce

$$\Xi_{k-i+1}(1, 1) = \mathbf{a}_i^T \mathbf{a}_i + \lambda - \mathbf{a}_i^T \mathbf{A}_{i-1} \mathbf{F}_{i-1} \mathbf{F}_{i-1}^T \mathbf{A}_{i-1}^T \mathbf{a}_i \quad (123)$$

from (121), and then substitute (123) into (114a) to obtain (103a).

Lastly, let us deduce (101) and (102). From (93), we write

$$\mathbf{f}_i = \begin{bmatrix} \bar{\mathbf{f}}_i^T & f_{ii} \end{bmatrix}^T, \quad (124)$$

into which substitute (114b) to obtain

$$\mathbf{f}_i = \begin{bmatrix} -f_{ii}(\mathbf{F}_{i-1} \mathbf{F}_{i-1}^T \mathbf{A}_{i-1}^T \mathbf{a}_i)^T & f_{ii} \end{bmatrix}^T. \quad (125)$$

Then substitute (125) and (91) into  $\mathbf{f}_i^T \mathbf{A}_i^T \underline{\mathbf{A}}_{k-i}$  in (122) and (119), to obtain

$$\begin{aligned} \mathbf{f}_i^T \mathbf{A}_i^T \underline{\mathbf{A}}_{k-i} &= \begin{bmatrix} -f_{ii} \mathbf{F}_{i-1} \mathbf{F}_{i-1}^T \mathbf{A}_{i-1}^T \mathbf{a}_i \\ f_{ii} \end{bmatrix}^T \begin{bmatrix} \mathbf{A}_{i-1} & \mathbf{a}_i \end{bmatrix}^T \underline{\mathbf{A}}_{k-i} \\ &= f_{ii} (\mathbf{a}_i^T \underline{\mathbf{A}}_{k-i} - \mathbf{a}_i^T \mathbf{A}_{i-1} \mathbf{F}_{i-1} \mathbf{F}_{i-1}^T \mathbf{A}_{i-1}^T \underline{\mathbf{A}}_{k-i}). \end{aligned} \quad (126)$$

Moreover, let us deduce

$$\begin{aligned} \Xi_{k-i+1}(1, 2 : \text{end}) &= \\ &\quad \mathbf{a}_i^T \underline{\mathbf{A}}_{k-i} - \mathbf{a}_i^T \mathbf{A}_{i-1} \mathbf{F}_{i-1} \mathbf{F}_{i-1}^T \mathbf{A}_{i-1}^T \underline{\mathbf{A}}_{k-i} \end{aligned} \quad (127)$$

from (121), and substitute (127) into (126) to obtain

$$\mathbf{f}_i^T \mathbf{A}_i^T \underline{\mathbf{A}}_{k-i} = f_{ii} \Xi_{k-i+1}(1, 2 : \text{end}). \quad (128)$$

Finally, we substitute (128) into (122) to further simplify it into (101). On the other hand, we substitute (103b) into (124)

to obtain

$$\mathbf{f}_i = \begin{bmatrix} f_{ii}\mathbf{\Pi}_{i-1}(:,1)^T & f_{ii} \end{bmatrix}^T, \quad (129)$$

and then substitute (129) and (128) into (119) to further simplify it into  $\mathbf{\Pi}_i = \begin{pmatrix} \mathbf{\Pi}_{i-1}(:,2:end) \\ \mathbf{0}_{k-i}^T \end{pmatrix} - \begin{bmatrix} f_{ii}\mathbf{\Pi}_{i-1}(:,1) \\ f_{ii} \end{bmatrix} f_{ii}\mathbf{\Xi}_{k-i+1}(1,2:end)$ , i.e., (102).

## APPENDIX E

### THE INVERSE $\text{LDL}^T$ FACTORIZATION AND THE CORRESPONDING PARALLELIZATION

To avoid the square-root operation in (111c), we can use the inverse  $\text{LDL}^T$  factorization instead of the inverse Cholesky factorization. The inverse  $\text{LDL}^T$  factors of  $\mathbf{R}_i$  are the unit upper-triangular  $\mathbf{L}_i$  and the diagonal  $\mathbf{D}_i$  satisfying

$$\mathbf{L}_i \mathbf{D}_i \mathbf{L}_i^T = \mathbf{R}_i^{-1}, \quad (130)$$

from which we can deduce

$$\mathbf{L}_i^{-T} \mathbf{D}_i^{-1} \mathbf{L}_i^{-1} = \mathbf{R}_i. \quad (131)$$

Notice that in (131), the unit lower-triangular  $\mathbf{L}_i^{-T}$  and the diagonal  $\mathbf{D}_i^{-1}$  are the conventional  $\text{LDL}^T$  factors [23] of  $\mathbf{R}_i$ .

#### A. The Block Inverse $\text{LDL}^T$ Factorization

Obviously, the upper-triangular  $\mathbf{L}_k$  and the diagonal  $\mathbf{D}_k$  can be written as

$$\begin{cases} \mathbf{L}_k = \begin{bmatrix} \mathbf{L}_i & \mathbf{\Gamma} \\ \mathbf{0} & \mathbf{\Delta} \end{bmatrix} \\ \mathbf{D}_k = \begin{bmatrix} \mathbf{D}_i & \mathbf{0} \\ \mathbf{0} & \mathbf{\Phi} \end{bmatrix}. \end{cases} \quad (132a) \quad (132b)$$

In this subsection, we will deduce an efficient algorithm to compute  $\mathbf{\Gamma}$ ,  $\mathbf{\Delta}$  and  $\mathbf{\Phi}$  in (132) by

$$\begin{cases} \mathbf{\Gamma} = -\mathbf{L}_i \mathbf{D}_i \mathbf{L}_i^T \mathbf{P} \mathbf{\Delta} \\ \mathbf{\Delta} \mathbf{\Phi} \mathbf{\Delta}^T = (\mathbf{U} - \mathbf{P}^T \mathbf{L}_i \mathbf{D}_i \mathbf{L}_i^T \mathbf{P})^{-1}, \end{cases} \quad (133a) \quad (133b)$$

which can be regarded as a special case of the inverse  $\text{LDM}^T$  factorization introduced in [33]. Notice that in (133b), the unit upper-triangular  $\mathbf{\Delta}$  and the diagonal  $\mathbf{\Phi}$  are the inverse  $\text{LDL}^T$  factors of  $\mathbf{U} - \mathbf{P}^T \mathbf{L}_i \mathbf{D}_i \mathbf{L}_i^T \mathbf{P}$ . The derivation of (133) is in the next paragraph.

From (132) we can deduce  $\mathbf{L}_k^{-1} = \begin{bmatrix} \mathbf{L}_i^{-1} & -\mathbf{L}_i^{-1} \mathbf{\Gamma} \mathbf{\Delta}^{-1} \\ \mathbf{0} & \mathbf{\Delta}^{-1} \end{bmatrix}$  and  $\mathbf{D}_k^{-1} = \begin{bmatrix} \mathbf{D}_i^{-1} & \mathbf{0} \\ \mathbf{0} & \mathbf{\Phi}^{-1} \end{bmatrix}$ , which are substituted into (131) to obtain

$$\begin{bmatrix} \mathbf{L}_i^{-T} & \mathbf{0} \\ -\mathbf{\Delta}^{-T} \mathbf{\Gamma}^T \mathbf{L}_i^{-T} & \mathbf{\Delta}^{-T} \end{bmatrix} \begin{bmatrix} \mathbf{D}_i^{-1} & \mathbf{0} \\ \mathbf{0} & \mathbf{\Phi}^{-1} \end{bmatrix} \times \begin{bmatrix} \mathbf{L}_i^{-1} & -\mathbf{L}_i^{-1} \mathbf{\Gamma} \mathbf{\Delta}^{-1} \\ \mathbf{0} & \mathbf{\Delta}^{-1} \end{bmatrix} = \mathbf{R}_k. \quad (134)$$

Then let us substitute (96) into (134) to deduce

$$\begin{bmatrix} \mathbf{L}_i^{-T} \mathbf{D}_i^{-1} \mathbf{L}_i^{-1} & -\mathbf{L}_i^{-T} \mathbf{D}_i^{-1} \mathbf{L}_i^{-1} \mathbf{\Gamma} \mathbf{\Delta}^{-1} \\ \begin{pmatrix} -\mathbf{\Delta}^{-T} \times \\ \mathbf{\Gamma}^T \mathbf{L}_i^{-T} \times \\ \mathbf{D}_i^{-1} \mathbf{L}_i^{-1} \end{pmatrix} & \begin{pmatrix} \mathbf{\Delta}^{-T} \mathbf{\Gamma}^T \mathbf{L}_i^{-T} \times \\ \mathbf{D}_i^{-1} \mathbf{L}_i^{-1} \mathbf{\Gamma} \mathbf{\Delta}^{-1} + \\ \mathbf{\Delta}^{-T} \mathbf{\Phi}^{-1} \mathbf{\Delta}^{-1} \end{pmatrix} \end{bmatrix} = \begin{bmatrix} \mathbf{R}_i & \mathbf{P} \\ \mathbf{P}^T & \mathbf{U} \end{bmatrix}, \quad (135)$$

from which we can obtain

$$\begin{cases} -\mathbf{L}_i^{-T} \mathbf{D}_i^{-1} \mathbf{L}_i^{-1} \mathbf{\Gamma} \mathbf{\Delta}^{-1} = \mathbf{P} \\ \mathbf{\Delta}^{-T} \mathbf{\Gamma}^T \mathbf{L}_i^{-T} \mathbf{D}_i^{-1} \mathbf{L}_i^{-1} \mathbf{\Gamma} \mathbf{\Delta}^{-1} + \mathbf{\Delta}^{-T} \mathbf{\Phi}^{-1} \mathbf{\Delta}^{-1} = \mathbf{U}. \end{cases} \quad (136a) \quad (136b)$$

Finally, write (136a) as (133a), which is then substituted into (136b) to get  $\mathbf{P}^T \mathbf{L}_i \mathbf{D}_i \mathbf{L}_i^T \mathbf{P} + \mathbf{\Delta}^{-T} \mathbf{\Phi}^{-1} \mathbf{\Delta}^{-1} = \mathbf{U}$ , i.e., (133b).

#### B. The Memory-Saving Parallel Implementation of the Inverse $\text{LDL}^T$ Factorization

Let us substitute (130) into (88) to obtain

$$\mathbf{F}_i \mathbf{F}_i^T = \mathbf{L}_i \mathbf{D}_i \mathbf{L}_i^T. \quad (137)$$

On the other hand, we can write the unit upper-triangular  $\mathbf{L}_i$  and the diagonal  $\mathbf{D}_i$  as<sup>12</sup>

$$\mathbf{L}_i = \begin{bmatrix} \mathbf{L}_{i-1} & \bar{\mathbf{L}}_i \\ \mathbf{0}_{i-1}^T & 1 \end{bmatrix} \quad (138a)$$

$$\mathbf{D}_i = \begin{bmatrix} \mathbf{D}_{i-1} & \mathbf{0}_{i-1} \\ \mathbf{0}_{i-1}^T & d_i \end{bmatrix}, \quad (138b)$$

where  $\bar{\mathbf{L}}_i$  denotes the  $i^{\text{th}}$  column of  $\mathbf{L}_i$  with the last entry removed, and  $d_i$  denotes the  $i^{\text{th}}$  diagonal entry of the diagonal  $\mathbf{D}_i$ . Then substitute (138) and (93) into (137)

to obtain  $\begin{bmatrix} \mathbf{L}_{i-1} & \bar{\mathbf{L}}_i \\ \mathbf{0}_{i-1}^T & 1 \end{bmatrix} \begin{bmatrix} \mathbf{D}_{i-1} & \mathbf{0}_{i-1} \\ \mathbf{0}_{i-1}^T & d_i \end{bmatrix} \begin{bmatrix} \mathbf{L}_{i-1} & \bar{\mathbf{L}}_i \\ \mathbf{0}_{i-1}^T & 1 \end{bmatrix}^T = \begin{bmatrix} \mathbf{F}_{i-1} & \bar{\mathbf{f}}_i \\ \mathbf{0}_{i-1}^T & f_{ii} \end{bmatrix} \begin{bmatrix} \mathbf{F}_{i-1} & \bar{\mathbf{f}}_i \\ \mathbf{0}_{i-1}^T & f_{ii} \end{bmatrix}^T$ , from which we can deduce

$$\begin{cases} d_i = f_{ii}^2 \\ \bar{\mathbf{L}}_i = \bar{\mathbf{f}}_i / f_{ii}. \end{cases} \quad (139a) \quad (139b)$$

We can substitute (103b) into (139b) to obtain

$$\bar{\mathbf{L}}_i = \mathbf{\Pi}_{i-1}(:,1). \quad (140)$$

Moreover, substitute (103a) into (139a), (101) and (102) to obtain

$$d_i = 1/\mathbf{\Xi}_{k-i+1}(1,1), \quad (141)$$

$$\mathbf{\Xi}_{k-i} = \mathbf{\Xi}_{k-i+1}^{[-1,-1]} - \frac{\mathbf{\Xi}_{k-i+1}(1,2:end)^T \mathbf{\Xi}_{k-i+1}(1,2:end)}{\mathbf{\Xi}_{k-i+1}(1,1)} \quad (142)$$

and

$$\mathbf{\Pi}_i = \begin{bmatrix} \mathbf{\Pi}_{i-1}(:,2:end) - \frac{\mathbf{\Pi}_{i-1}(:,1) \mathbf{\Xi}_{k-i+1}(1,2:end)}{\mathbf{\Xi}_{k-i+1}(1,1)} \\ -\frac{\mathbf{\Xi}_{k-i+1}(1,2:end)}{\mathbf{\Xi}_{k-i+1}(1,1)} \end{bmatrix}, \quad (143)$$

respectively.

<sup>12</sup>The following equation (138) has been presented in [34].

Since the unit upper-triangular  $\mathbf{L}_1 = \mathbf{I}$ , it can be seen from (130) with  $k = 1$  that the diagonal

$$\mathbf{D}_1 = d_{11} = 1/\mathbf{R}(1, 1). \quad (144)$$

To save memories, we store  $\mathbf{D}_1 = d_{11}$ ,  $\Xi_{k-1}$  and  $\Pi_1$  in  $\mathbf{R}(1, 1)$ ,  $\mathbf{R}(2 : k, 2 : k)$  and  $\mathbf{R}(1, 2 : k)$ , respectively, by computing

$$\begin{cases} \mathbf{R}(1, 1) = 1/\mathbf{R}(1, 1) \\ \mathbf{R}(2 : k, 2 : k) = \mathbf{R}(2 : k, 2 : k) - \\ \quad \mathbf{R}(1, 2 : k)^T \mathbf{R}(1, 1) \mathbf{R}(1, 2 : k) \\ \mathbf{R}(1, 2 : k) = -\mathbf{R}(1, 1) \mathbf{R}(1, 2 : k), \end{cases} \quad (145a)$$

which are deduced in the rest part of this paragraph. We use the  $i^{th}$  ( $i = 1, 2, \dots, k$ ) diagonal entry of  $\mathbf{R}$  to store the  $i^{th}$  diagonal entry of the diagonal  $\mathbf{D}$ . Accordingly, we compute and store  $\mathbf{D}_1 = d_{11}$  in  $\mathbf{R}(1, 1)$  by (145a), which is then substituted into (110a) and (110b) to obtain (145b) and (145c), respectively.

In the  $i^{th}$  ( $i \geq 2$ ) iteration, we also save memories by storing  $\bar{\mathbf{I}}_i$  in  $\mathbf{R}(1 : i - 1, i)$ , i.e.,

$$\mathbf{R}(1 : i - 1, i) = \bar{\mathbf{I}}_i, \quad (146)$$

and storing  $d_i$ ,  $\Xi_{k-i}$  and  $\Pi_i$  in  $\mathbf{R}(i, i)$ ,  $\mathbf{R}(i + 1 : k, i + 1 : k)$  and  $\mathbf{R}(1 : i, i + 1 : k)$ , respectively, by

$$\begin{cases} \mathbf{R}(i, i) = 1/\mathbf{R}(i, i) \\ \mathbf{R}(i + 1 : k, i + 1 : k) = \mathbf{R}(i + 1 : k, i + 1 : k) - \\ \quad \mathbf{R}(i, i + 1 : k)^T \mathbf{R}(i, i) \mathbf{R}(i, i + 1 : k) \\ \mathbf{R}(1 : i, i + 1 : k) = \\ \quad \left[ \begin{pmatrix} \mathbf{R}(1 : i - 1, i + 1 : k) - \mathbf{R}(i, i) \\ \times \mathbf{R}(1 : i - 1, i) \mathbf{R}(i, i + 1 : k) \\ -\mathbf{R}(i, i) \mathbf{R}(i, i + 1 : k) \end{pmatrix} \right]. \end{cases} \quad (147a)$$

The above (146) and (147) are deduced in the next paragraph.

When  $i = 2$ , we can deduce (146) and (147a) from (140) and (141), respectively, and then substitute (147a) into (111a) and (111b) to obtain (147b) and (147c), respectively, since  $\Xi_{k-1}$  and  $\Pi_1$  have been stored in  $\mathbf{R}(2 : k, 2 : k)$  and  $\mathbf{R}(1, 2 : k)$ , respectively. When  $i \geq 3$ , we can also deduce (146) and (147a) from (140) and (141), respectively, and then substitute (147a) into (111a) and (111b) to obtain (147b) and (147c), respectively, since  $\Xi_{k-(i-1)} = \Xi_{k-i+1}$  and  $\Pi_{i-1}$  have been stored in  $\mathbf{R}((i-1)+1 : k, (i-1)+1 : k) = \mathbf{R}(i : k, i : k)$  and  $\mathbf{R}(1 : i - 1, (i-1)+1 : k) = \mathbf{R}(1 : i - 1, i : k)$ , respectively. Thus we have verified (146) and (147) for any  $i = 2, 3, \dots, k$ .

Obviously, (145) is equivalent to (147) with  $i = 1$ . Then we can compute (147) iteratively for  $i = 1, 2, \dots, k$ , to cover the upper-triangular part of  $\mathbf{R}_k$  with the unit upper-triangular  $\mathbf{L}_k$  and the diagonal  $\mathbf{D}_k$  satisfying  $\mathbf{L}_k \mathbf{D}_k \mathbf{L}_k^T = \mathbf{R}_k^{-1}$ . **Algorithm 12** summarizes the corresponding implementation.

### C. Parallel Performance of the Proposed Inverse $LDL^T$ Factorization

The inverse  $LDL^T$  factorization summarized in **Algorithm 12** computes (147) iteratively for  $i = 1, 2, \dots, k$ , which can

### Algorithm 12 : The parallel implementation of the inverse $LDL^T$ factorization

**Input:** The upper-triangular part of a Hermitian matrix  $\mathbf{R}$   
**Output:** The inverse  $LDL^T$  factors of  $\mathbf{R}$  in the upper-triangular part of  $\mathbf{R}$

- 1: **for**  $i = 1 : k$  ( $k$  is the size of  $\mathbf{R}$ ) **do**
- 2:    $\mathbf{R}(i, i) = 1/\mathbf{R}(i, i)$ ;
- 3:    $\mathbf{R}(i + 1 : k, i + 1 : k) = \mathbf{R}(i + 1 : k, i + 1 : k) -$   
 $\mathbf{R}(i, i + 1 : k)^T \mathbf{R}(i, i) \mathbf{R}(i, i + 1 : k)$ ;
- 4:    $\mathbf{R}(1 : i, i + 1 : k) =$   
 $\left[ \begin{matrix} \mathbf{R}(1 : i - 1, i + 1 : k) - \mathbf{R}(1 : i - 1, i) \mathbf{R}(i, i) \mathbf{R}(i, i + 1 : k) \\ -\mathbf{R}(i, i) \mathbf{R}(i, i + 1 : k) \end{matrix} \right]$ ;
- 5: **end for**
- 6:  $\mathbf{D} = \text{diag}(\text{diag}(\mathbf{R}))$ , i.e., the diagonal entries of  $\mathbf{R}$  form the diagonal matrix  $\mathbf{D}$ ;
- 7:  $\mathbf{L} = \text{triu}(\mathbf{R} - \mathbf{D} + \mathbf{I}_k)$ , i.e., the upper-triangular part of  $\mathbf{R}$  except the diagonal entries forms the unit upper-triangular matrix  $\mathbf{L}$ ;

be written as

$$\mathbf{R}(i, i) = 1/\mathbf{R}(i, i) \quad (148a)$$

$$\xi_{k-i}^T = \mathbf{R}(i, i + 1 : k) \quad (148b)$$

$$\mathbf{R}(i, i + 1 : k) = -\mathbf{R}(i, i) \xi_{k-i}^T \quad (148c)$$

$$\begin{cases} \mathbf{R}([1 : i - 1, i + 1 : k], i + 1 : k) = \\ \quad \mathbf{R}([1 : i - 1, i + 1 : k], i + 1 : k) + \\ \quad \left[ \mathbf{R}(1 : i - 1, i)^T \quad \xi_{k-i}^T \right]^T (-\mathbf{R}(i, i) \xi_{k-i}^T). \end{cases} \quad (148d)$$

It can be seen that the dominant computational complexity of (148) comes from (148d), where all entries in columns  $i + 1$  to  $k$  of the upper-triangular  $\mathbf{R}$  except row  $i$  are updated with a multiplication and an addition<sup>13</sup>. Then the dominant complexity of (148) is  $(i + 1 - 1) + (i + 2 - 1) + \dots + (k - 1) = (i + k - 1)(k - i)/2$  multiplication and addition in the  $i^{th}$  iteration, and is  $\sum_{i=1}^k \frac{(i+k-1)(k-i)}{2} \approx \frac{k^3}{3}$  in total. Accordingly, it can be seen that the proposed parallel implementation does not change the dominant computational complexity.

Let us assume a theoretical situation where the parallel algorithm runs on  $1 + 2 + \dots + k = \frac{(k+1)k}{2}$  processors, i.e., each entry in the upper-triangular  $\mathbf{R}_k$  is stored in an exclusive processor. Then in (148d), all entries in columns  $i + 1$  to  $k$  of the upper-triangular  $\mathbf{R}$  except row  $i$  can be updated simultaneously, and each entry is updated with a multiplication and an addition executed serially.

We can also assume a situation where the parallel algorithm runs on  $k$  processors, and each column of the upper-triangular  $\mathbf{R}_k$  is stored in an exclusive processor. The corresponding parallel implementation is described in **Algorithm 13**. As can be seen from **Algorithm 13**,  $\mathbf{R}(1 : i, i)$  and  $\xi_{k-i}(1 : j - i)$  are required for the processor storing the  $j^{th}$  ( $j = i + 1, i + 2, \dots, k$ ) column of the upper-triangular  $\mathbf{R}$  to update that column. The column vector  $\mathbf{R}(1 : i, i)$  is in the processor storing the  $i^{th}$  column of  $\mathbf{R}$ , while the  $(j - i)$  entries in  $\xi_{k-i}^T(1 : j - i) = \mathbf{R}(i, i + 1 : j)$  are in the processors storing columns  $i + 1, i + 2, \dots, j$  of  $\mathbf{R}$ . Accordingly,

<sup>13</sup>We do not need to compute  $-\mathbf{R}(i, i) \xi_{k-i}^T$  in (148d), since it has been computed in (148c)

$\mathbf{R}(1:i, i), \mathbf{R}(i, i+1), \mathbf{R}(i, i+2), \dots, \mathbf{R}(i, j-1)$  need to be transmitted to the processor storing the  $j^{th}$  column of  $\mathbf{R}$  from the processors storing the  $i^{th}, (i+1)^{th}, (i+2)^{th}, \dots, (j-1)^{th}$  columns of  $\mathbf{R}$ , respectively.

---

**Algorithm 13 : The parallel implementation of the inverse  $LDL^T$  factorization when each column of the upper-triangular  $\mathbf{R}_k$  is stored in an exclusive processor**

---

**Input:** The upper-triangular part of a Hermitian matrix  $\mathbf{R}$

**Output:** The inverse  $LDL^T$  factors of  $\mathbf{R}$  in the upper-triangular part of  $\mathbf{R}$

- 1: **for**  $i = 1 : k$  ( $k$  is the size of  $\mathbf{R}$ ) **do**
  - 2:    $\mathbf{R}(i, i) = 1/\mathbf{R}(i, i)$ ;
  - 3:    $\xi_{k-i}^T = \mathbf{R}(i, i+1 : k)$ ;
  - 4:   **for**  $j = i+1 : k$  **do**
  - 5:      $\mathbf{R}(i, j) = -\mathbf{R}(i, i)\xi_{k-i}(j-i)$ ;
  - 6:      $\mathbf{R}([1:i-1, i+1:j], j) = \mathbf{R}([1:i-1, i+1:j], j) +$   
 $\quad [ \mathbf{R}(1:i-1, i)^T \quad \xi_{k-i}(1:j-i)^T ]^T \mathbf{R}(i, j)$ ;
  - 7:   **end for**
  - 8: **end for**
  - 9:  $\mathbf{D} = \text{diag}(\text{diag}(\mathbf{R}))$ , i.e., the diagonal entries of  $\mathbf{R}$  form the diagonal matrix  $\mathbf{D}$ ;
  - 10:  $\mathbf{L} = \text{triu}(\mathbf{R} - \mathbf{D} + \mathbf{I}_k)$ , i.e., the upper-triangular part of  $\mathbf{R}$  except the diagonal entries forms the unit upper-triangular matrix  $\mathbf{L}$ ;
- 

Let us consider a general case where the columns of  $\mathbf{R}$  are stored in  $\tau \leq k$  processors, and processors  $1, 2, \dots, \tau$  store  $v_1, v_2, \dots, v_\tau$  columns of  $\mathbf{R}$ , respectively. Assume that the columns stored in processors  $1, 2, \dots, \tau$  are columns  $1 : \tilde{v}_1, (\tilde{v}_1 + 1) : \tilde{v}_2, \dots, (\tilde{v}_{\tau-1} + 1) : \tilde{v}_\tau$  of  $\mathbf{R}$  with

$$1 \leq \tilde{v}_1 < \tilde{v}_2 < \dots < \tilde{v}_{\tau-1} < \tilde{v}_\tau = k. \quad (149)$$

Then it can be seen that

$$v_1 + v_2 + \dots + v_\tau = k, \quad (150)$$

and columns  $(\tilde{v}_{\mu-1} + 1) : \tilde{v}_\mu$  of  $\mathbf{R}$  are stored in processor  $\mu$  ( $\mu = 1, 2, \dots, \tau$ ), where  $\tilde{v}_0 = 0$  and

$$v_1 + v_2 + \dots + v_\mu = \tilde{v}_\mu. \quad (151)$$

Now let us consider communication cost in the  $i^{th}$  ( $i = 1, 2, \dots, k$ ) iteration of **Algorithm 13**. When  $\tilde{v}_{\mu-1} + 1 \leq i \leq \tilde{v}_\mu$ , it can be seen that  $\mathbf{R}(1:i, i)$  and  $\mathbf{R}(i, i+1 : \tilde{v}_\mu)$  in processor  $\mu$  need to be transmitted to processors  $\mu+1, \mu+2, \dots, \tau$ . Moreover,  $\mathbf{R}(i, \tilde{v}_{\varsigma-1} + 1 : \tilde{v}_\varsigma)$  in processor  $\varsigma$  needs to be transmitted to processors  $\varsigma+1, \varsigma+2, \dots, \tau$ , where  $\varsigma = \mu+1, \mu+2, \dots, \tau-1$ .

#### D. Application of the Proposed Inverse $LDL^T$ Factorization to the Distributed BLS

In this subsection, we introduce the distributed BLS that adopts the inverse  $LDL^T$  factorization summarized in **Algorithm 12**. To implement the distributed BLS with model-parallelism, we can partition all  $\tilde{k}_p$  feature and enhancement nodes into  $p$  workers. Then we have

$$\mathbf{A}_k = [ \mathbf{A}_{v_1} \quad \mathbf{A}_{v_2} \quad \dots \quad \mathbf{A}_{v_\tau} ], \quad (152)$$

where  $\mathbf{A}_{v_\mu}$  ( $\mu = 1, 2, \dots, \tau$ ) denotes the  $v_\mu$  nodes partitioned into the  $\mu^{th}$  worker. Then substitute (152) into (89) to write the upper-triangular blocks of  $\mathbf{R}_k$  as

$$\begin{aligned} \mathbf{R}_k &= \mathbf{A}_k^T \mathbf{A}_k + \lambda \mathbf{I} \\ &= \begin{bmatrix} \mathbf{A}_{v_1}^T \mathbf{A}_{v_1} & \mathbf{A}_{v_1}^T \mathbf{A}_{v_2} & \dots & \mathbf{A}_{v_1}^T \mathbf{A}_{v_\tau} \\ \times & \mathbf{A}_{v_2}^T \mathbf{A}_{v_2} & \dots & \mathbf{A}_{v_2}^T \mathbf{A}_{v_\tau} \\ \vdots & \vdots & \ddots & \vdots \\ \times & \times & \dots & \mathbf{A}_{v_\tau}^T \mathbf{A}_{v_\tau} \end{bmatrix} + \lambda \mathbf{I}. \end{aligned} \quad (153)$$

It can be seen from (153) that  $\mathbf{A}_{v_\mu}$  in worker  $\mu$  need to be transmitted to workers  $\mu+1, \mu+2, \dots, \tau$ , where  $\mu = 1, 2, \dots, \tau$ , and then  $v_\mu$  columns of the upper-triangular  $\mathbf{R}_k$ , i.e., columns  $(\tilde{v}_{\mu-1} + 1) : \tilde{v}_\mu$ , can be computed from  $\mathbf{A}_{v_1}, \mathbf{A}_{v_2}, \dots, \mathbf{A}_{v_{\mu-1}}, \mathbf{A}_{v_\mu}$  in worker  $\mu$ .

Now workers  $1, 2, \dots, \tau$  store  $v_1, v_2, \dots, v_\tau$  columns of  $\mathbf{R}_k$ , respectively, and the columns stored in workers  $1, 2, \dots, \tau$  are columns  $1 : \tilde{v}_1, (\tilde{v}_1 + 1) : \tilde{v}_2, \dots, (\tilde{v}_{\tau-1} + 1) : \tilde{v}_\tau$  that satisfy (149). Accordingly, the parallel implementation described in **Algorithm 13** can be applied to compute the inverse  $LDL^T$  factors of the upper-triangular  $\mathbf{R}_k$  for the distributed BLS with model-parallelism.

#### APPENDIX F

##### THE DIVISION FREE INVERSE $LDL^T$ FACTORIZATION AND THE CORRESPONDING PARALLELIZATION

There is still a division operation in (147a). To avoid that division operation, we can use the alternative  $LDL^T$  factors of  $\mathbf{R}_i^{-1}$ , i.e.,  $\tilde{\mathbf{L}}_i, \tilde{\mathbf{D}}_i$  and  $\sigma_i$  satisfying

$$\tilde{\mathbf{L}}_i (\tilde{\mathbf{D}}_i / \sigma_i) \tilde{\mathbf{L}}_i^T = \mathbf{L}_i \mathbf{D}_i \mathbf{L}_i^T = \mathbf{R}_i^{-1}. \quad (154)$$

The corresponding division free block inverse  $LDL^T$  factorization and its parallelization will be introduced in this section.

##### A. Division Free Block Inverse $LDL^T$ Factorization

The division free block inverse  $LDL^T$  factorization update  $\tilde{\mathbf{L}}_i, \tilde{\mathbf{D}}_i$  and  $\sigma_i$  into  $\tilde{\mathbf{L}}_k, \tilde{\mathbf{D}}_k$  and  $\sigma_k$  (with  $k > i$ ) by

$$\begin{cases} \tilde{\Delta}(\tilde{\Phi}/\eta) \tilde{\Delta}^T = (\sigma_i \mathbf{U} - \mathbf{P}^T \tilde{\mathbf{L}}_i \tilde{\mathbf{D}}_i \tilde{\mathbf{L}}_i^T \mathbf{P})^{-1} \end{cases} \quad (155a)$$

$$\begin{cases} \text{Scaling of } \eta \text{ and } \tilde{\Delta} \end{cases} \quad (155b)$$

$$\begin{cases} \tilde{\mathbf{L}}_k = \begin{bmatrix} \tilde{\mathbf{L}}_i & -\tilde{\mathbf{L}}_i \tilde{\mathbf{D}}_i \tilde{\mathbf{L}}_i^T \mathbf{P} \tilde{\Delta} \\ \mathbf{0} & \sigma_i \tilde{\Delta} \end{bmatrix} \end{cases} \quad (155c)$$

$$\begin{cases} \tilde{\mathbf{D}}_k = \begin{bmatrix} \eta \tilde{\mathbf{D}}_i & \mathbf{0} \\ \mathbf{0} & \tilde{\Phi} \end{bmatrix} \end{cases} \quad (155d)$$

$$\begin{cases} \sigma_k = \sigma_i \eta, \end{cases} \quad (155e)$$

where  $\tilde{\Delta}, \tilde{\Phi}$  and  $\eta$ , which satisfy (155a), are also the alternative  $LDL^T$  factors defined by (154). The above division free block inverse  $LDL^T$  factorization by (155) can be regarded as a special case of the division free block inverse  $LDM^T$  factorization introduced in [33]. We will give the derivation of (155) in what follows.

Firstly, substitute (154) into (133b) to obtain

$$\begin{aligned} \Delta \Phi \Delta^T &= (\mathbf{U} - \mathbf{P}^T \tilde{\mathbf{L}}_i (\tilde{\mathbf{D}}_i / \sigma_i) \tilde{\mathbf{L}}_i^T \mathbf{P})^{-1} \\ \Delta (\Phi / \sigma_i) \Delta^T &= (\sigma_i \mathbf{U} - \mathbf{P}^T \tilde{\mathbf{L}}_i \tilde{\mathbf{D}}_i \tilde{\mathbf{L}}_i^T \mathbf{P})^{-1}. \end{aligned} \quad (156)$$

For the right side of (156), we can write the alternative LDL<sup>T</sup> factors defined by (154), i.e.,  $\tilde{\Delta}$ ,  $\tilde{\Phi}$  and  $\eta$  satisfying (155a). Then (155a) is substituted into (156) to obtain

$$\tilde{\Delta}(\sigma_i \tilde{\Phi}/\eta) \tilde{\Delta}^T = \Delta \Phi \Delta^T. \quad (157)$$

Now we only need to deduce (155c), (155d) and (155e). Substitute (133) into (132), and substitute (132) into (130) to obtain

$$\begin{aligned} \mathbf{R}_k^{-1} &= \begin{bmatrix} \mathbf{L}_i & -\mathbf{L}_i \mathbf{D}_i \mathbf{L}_i^T \mathbf{P} \Delta \\ \mathbf{0} & \tilde{\Delta} \end{bmatrix} \begin{bmatrix} \mathbf{D}_i & \mathbf{0} \\ \mathbf{0} & \tilde{\Phi} \end{bmatrix} \begin{bmatrix} \mathbf{L}_i^T & \mathbf{0} \\ -\Delta^T \mathbf{P}^T \mathbf{L}_i \mathbf{D}_i \mathbf{L}_i^T & \Delta^T \end{bmatrix} \\ &= \begin{bmatrix} \mathbf{L}_i \mathbf{D}_i \mathbf{L}_i^T + \mathbf{L}_i \mathbf{D}_i \mathbf{L}_i^T \mathbf{P} \times \Delta \Phi \Delta^T \mathbf{P}^T \mathbf{L}_i \mathbf{D}_i \mathbf{L}_i^T & -\mathbf{L}_i \mathbf{D}_i \mathbf{L}_i^T \times \mathbf{P} \Delta \Phi \Delta^T \\ -\Delta \Phi \Delta^T \mathbf{P}^T \mathbf{L}_i \mathbf{D}_i \mathbf{L}_i^T & \Delta \Phi \Delta^T \end{bmatrix}, \end{aligned}$$

into which substitute (154) and (157) to obtain

$$\begin{aligned} \mathbf{R}_k^{-1} &= \begin{bmatrix} \left( \frac{\tilde{\mathbf{L}}_i \tilde{\mathbf{D}}_i \tilde{\mathbf{L}}_i^T}{\sigma_i} + \frac{\tilde{\mathbf{L}}_i \tilde{\mathbf{D}}_i \tilde{\mathbf{L}}_i^T \mathbf{P} \times}{\sigma_i} \right) & \left( \frac{-\tilde{\mathbf{L}}_i \tilde{\mathbf{D}}_i \tilde{\mathbf{L}}_i^T \times}{\mathbf{P} \Delta \sigma_i \tilde{\Phi} \Delta^T} \right) \\ \frac{-\tilde{\Delta} \sigma_i \tilde{\Phi} \Delta^T}{\eta} \mathbf{P}^T \tilde{\mathbf{L}}_i \tilde{\mathbf{D}}_i \tilde{\mathbf{L}}_i^T & \frac{\tilde{\Delta} \sigma_i \tilde{\Phi} \Delta^T}{\eta} \end{bmatrix} \\ &= \begin{bmatrix} \left( \frac{\tilde{\mathbf{L}}_i \tilde{\mathbf{D}}_i \tilde{\mathbf{L}}_i^T}{\sigma_i} + \frac{\tilde{\mathbf{L}}_i \tilde{\mathbf{D}}_i \tilde{\mathbf{L}}_i^T \times}{\mathbf{P} \Delta \sigma_i \tilde{\Phi} \Delta^T} \right) & \left( \frac{-\tilde{\mathbf{L}}_i \tilde{\mathbf{D}}_i \tilde{\mathbf{L}}_i^T}{\times \mathbf{P} \Delta \sigma_i \tilde{\Phi} \Delta^T} \right) \\ \frac{-\tilde{\Delta} \sigma_i \tilde{\Phi} \Delta^T}{\eta} \mathbf{P}^T \tilde{\mathbf{L}}_i \tilde{\mathbf{D}}_i \tilde{\mathbf{L}}_i^T & \frac{\tilde{\Delta} \sigma_i \tilde{\Phi} \Delta^T}{\eta} \end{bmatrix}, \quad (158) \\ &= \begin{bmatrix} \tilde{\mathbf{L}}_i & -\tilde{\mathbf{L}}_i \tilde{\mathbf{D}}_i \tilde{\mathbf{L}}_i^T \mathbf{P} \tilde{\Delta} \\ \mathbf{0} & \sigma_i \tilde{\Delta} \end{bmatrix} \frac{1}{\sigma_i \eta} \begin{bmatrix} \eta \tilde{\mathbf{D}}_i & \mathbf{0} \\ \mathbf{0} & \tilde{\Phi} \end{bmatrix} \\ &\quad \times \begin{bmatrix} \tilde{\mathbf{L}}_i^T & \mathbf{0} \\ -\mathbf{P}^T \tilde{\mathbf{L}}_i \tilde{\mathbf{D}}_i \tilde{\mathbf{L}}_i^T & \sigma_i \tilde{\Delta}^T \end{bmatrix}. \quad (159) \end{aligned}$$

From (159), we can deduce (155c), (155d) and (155e) finally, which compute  $\tilde{\mathbf{L}}_k$ ,  $\tilde{\mathbf{D}}_k$  and  $\sigma_k$  satisfying (154).

The iterations in (155) will lead to numerically unlimited results, which may cause a problem in fixed-point implementations [31]. We alleviate this problem by scaling in (155b), as in [31]. Scaling is achieved by dividing (or multiplying) only by powers of 2 [31], which is a shift operation in binary fixed-point implementation. We can multiply  $\eta$  by  $c_i^2$  and multiply  $\tilde{\Delta}$  by  $c_i$  accordingly, which will not change  $\mathbf{R}_k^{-1}$  computed by (158). Then we end up with  $\eta c_i^2$  and  $\tilde{\Delta} c_i$ , where  $\eta c_i^2$  is always between 0.5 and 2, and  $c_i$  is powers of 2.

In the special case with  $k - i = 1$ ,  $\mathbf{P}$  and  $\mathbf{U}$  in (155) becomes the column vector  $\mathbf{p}$  and the scalar  $u$ , respectively, and (155) with  $i = i - 1$  becomes<sup>14</sup>

$$\begin{cases} \eta = \sigma_{i-1} u - \mathbf{p}^T \tilde{\mathbf{L}}_{i-1} \tilde{\mathbf{D}}_{i-1} \tilde{\mathbf{L}}_{i-1}^T \mathbf{p} & (160a) \\ \tilde{\mathbf{L}}_i = -\tilde{\mathbf{L}}_{i-1} \tilde{\mathbf{D}}_{i-1} \tilde{\mathbf{L}}_{i-1}^T \mathbf{p} & (160b) \\ l_{ii} = \sigma_{i-1} & (160c) \\ \text{Scaling of } \eta, \tilde{\mathbf{L}}_i \text{ and } l_{ii} & (160d) \end{cases}$$

$$\begin{cases} \tilde{\mathbf{L}}_i = \begin{bmatrix} \tilde{\mathbf{L}}_{i-1} & \tilde{\mathbf{L}}_i \\ \mathbf{0} & l_{ii} \end{bmatrix} & (160e) \end{cases}$$

$$\begin{cases} \tilde{\mathbf{D}}_i = \begin{bmatrix} \eta \tilde{\mathbf{D}}_{i-1} & \mathbf{0} \\ \mathbf{0} & 1 \end{bmatrix} & (160f) \end{cases}$$

$$\begin{cases} \sigma_i = \sigma_{i-1} \eta. & (160g) \end{cases}$$

Notice that  $\tilde{\Delta} = \tilde{\Phi} = 1$  and  $\eta$  computed by (160a), which

satisfy (155a), are substituted into (155c) and (155d) to obtain (160b) and (160f), respectively. Moreover, it can be seen from (154) with  $i = 1$  that we can let the initial

$$\begin{cases} \tilde{\mathbf{L}}_1 = 1, & (161a) \end{cases}$$

$$\begin{cases} \tilde{\mathbf{D}}_1 = 1, & (161b) \end{cases}$$

$$\begin{cases} \sigma_1 = \mathbf{R}_1 = \mathbf{R}(1, 1), & (161c) \end{cases}$$

$$\begin{cases} \text{Scaling of } \sigma_1 \text{ and } \tilde{\mathbf{L}}_1. & (161d) \end{cases}$$

From the initial  $\tilde{\mathbf{L}}_1$ ,  $\tilde{\mathbf{D}}_1$  and  $\sigma_1$  computed by (161), we can use (160) to compute  $\tilde{\mathbf{L}}_i$ ,  $\tilde{\mathbf{D}}_i$  and  $\sigma_i$  from  $\tilde{\mathbf{L}}_{i-1}$ ,  $\tilde{\mathbf{D}}_{i-1}$  and  $\sigma_{i-1}$  iteratively, till we obtain  $\tilde{\mathbf{L}}_k$ ,  $\tilde{\mathbf{D}}_k$  and  $\sigma_k$  finally.

The iterations in (160) will lead to numerically unlimited results, and then we alleviate this problem by scaling in (160d) and the initial (161d). To implement the scaling in (161d), we can multiply  $\sigma_1$  by  $c_1^2$  and multiply  $\tilde{\mathbf{L}}_1$  by  $c_1$  accordingly, which will not change  $\mathbf{R}_1^{-1}$  computed by (154) with  $i = 1$ . Then we end up with  $\sigma_1 c_1^2$  and  $\tilde{\mathbf{L}}_1 c_1$ , where  $\sigma_1 c_1^2$  is always between 0.5 and 2, and  $c_1$  is powers of 2. Moreover, substitute (160e), (160f) and (160g) into (154) to get

$$\begin{aligned} \mathbf{R}_i^{-1} &= \begin{bmatrix} \tilde{\mathbf{L}}_{i-1} & \tilde{\mathbf{L}}_i \\ \mathbf{0} & l_{ii} \end{bmatrix} \frac{\begin{bmatrix} \eta \tilde{\mathbf{D}}_{i-1} & \mathbf{0} \\ \mathbf{0} & 1 \end{bmatrix}}{\sigma_{i-1} \eta} \begin{bmatrix} \tilde{\mathbf{L}}_{i-1} & \tilde{\mathbf{L}}_i \\ \mathbf{0} & l_{ii} \end{bmatrix}^T \\ &= \frac{1}{\sigma_{i-1}} \begin{bmatrix} \tilde{\mathbf{L}}_{i-1} \tilde{\mathbf{D}}_{i-1} \tilde{\mathbf{L}}_{i-1}^T + \frac{1}{\eta} \tilde{\mathbf{L}}_i \tilde{\mathbf{L}}_i^T & \frac{1}{\eta} l_{ii} \tilde{\mathbf{L}}_i \\ \frac{1}{\eta} l_{ii} \tilde{\mathbf{L}}_i^T & \frac{1}{\eta} l_{ii}^2 \end{bmatrix}. \quad (162) \end{aligned}$$

It can be seen that  $\mathbf{R}_i^{-1}$  computed by (162) will not change, if we implement the scaling in (160d) by multiplying  $\eta$  with  $c_i^2$  and multiply  $\tilde{\mathbf{L}}_i$  and  $l_{ii}$  with  $c_i$  accordingly. Then we end up with  $\eta c_i^2$ ,  $\tilde{\mathbf{L}}_i c_i$  and  $l_{ii} c_i$ , where  $\eta c_i^2$  is always between 0.5 and 2, and  $c_i$  is powers of 2.

### B. The Memory-Saving Parallel Implementation of the Division Free Inverse LDL<sup>T</sup> Factorization

Let us define  $-\tilde{\mathbf{L}}_k \tilde{\mathbf{D}}_k \tilde{\mathbf{L}}_k^T \mathbf{P}$  in (155c) and  $\sigma_k \mathbf{U} - \mathbf{P}^T \tilde{\mathbf{L}}_k \tilde{\mathbf{D}}_k \tilde{\mathbf{L}}_k^T \mathbf{P}$  in (155a) as

$$\begin{cases} \tilde{\Pi}_i = -\tilde{\mathbf{L}}_i \tilde{\mathbf{D}}_i \tilde{\mathbf{L}}_i^T \mathbf{P} & (163a) \end{cases}$$

$$\begin{cases} \tilde{\Xi}_{k-i} = \sigma_i \mathbf{U} - \mathbf{P}^T \tilde{\mathbf{L}}_i \tilde{\mathbf{D}}_i \tilde{\mathbf{L}}_i^T. & (163b) \end{cases}$$

The above  $\tilde{\Pi}_i$  and  $\tilde{\Xi}_{k-i}$  satisfy

$$\begin{cases} \Pi_i = \tilde{\Pi}_i / \sigma_i & (164a) \end{cases}$$

$$\begin{cases} \Xi_{k-i} = \tilde{\Xi}_{k-i} / \sigma_i. & (164b) \end{cases}$$

To deduce (164a) and (164b), substitute (154) into (88) to obtain

$$\tilde{\mathbf{L}}_i \tilde{\mathbf{D}}_i \tilde{\mathbf{L}}_i^T = \sigma_i \mathbf{F}_i \mathbf{F}_i^T, \quad (165)$$

which is substituted into (163) to obtain

$$\begin{cases} \tilde{\Pi}_i = -\sigma_i \mathbf{F}_i \mathbf{F}_i^T \mathbf{P} & (166a) \end{cases}$$

$$\begin{cases} \tilde{\Xi}_{k-i} = \sigma_i \mathbf{U} - \mathbf{P}^T \sigma_i \mathbf{F}_i \mathbf{F}_i^T \mathbf{P}. & (166b) \end{cases}$$

Then we substitute (97b) into (100a) to write  $\Pi_i = -\mathbf{F}_i \mathbf{F}_i^T \mathbf{P}$ , which is substituted into (166a) to obtain (164a). We also substitute (97b) and (97a) into (100b) to write  $\Xi_{k-i} = \mathbf{U} - \mathbf{P}^T \mathbf{F}_i \mathbf{F}_i^T \mathbf{P}$ , which is substituted into (166b) to obtain (164b).

<sup>14</sup>The following equation (160) has been presented in [34], while the scaling scheme presented in [34] is different from the scaling scheme proposed in this paper.

Let us substitute (161c) into (164a) and (164b) with  $i = 1$  to obtain  $\tilde{\Pi}_1 = \mathbf{R}(1,1)\Pi_1$  and  $\tilde{\Xi}_{k-1} = \mathbf{R}(1,1)\Xi_{k-1}$ , respectively, into which substitute (108) to obtain

$$\begin{cases} \tilde{\Pi}_1 = -\mathbf{R}(1,2:k) \\ \tilde{\Xi}_{k-1} = \mathbf{R}(1,1)\mathbf{R}(2:k,2:k) - \mathbf{R}(1,2:k)^T\mathbf{R}(1,2:k). \end{cases} \quad (167a) \quad (167b)$$

In order to save memories, we store  $\tilde{\Xi}_{k-1}$ ,  $\tilde{\Pi}_1$  and  $\tilde{\mathbf{L}}_1$  in  $\mathbf{R}(2:k,2:k)$ ,  $\mathbf{R}(1,2:k)$  and  $\mathbf{R}(1,1)$ , respectively, by computing

$$\begin{cases} \sigma = \mathbf{R}(1,1) & (168a) \\ \mathbf{R}(1,1) = 1 & (168b) \\ \text{Scaling of } \sigma \text{ and } \mathbf{R}(1,:) & (168c) \\ \mathbf{R}(2:k,2:k) = \sigma\mathbf{R}(2:k,2:k) - \mathbf{R}(1,2:k)^T\mathbf{R}(1,2:k) & (168d) \\ \mathbf{R}(1,2:k) = -\mathbf{R}(1,1)\mathbf{R}(1,2:k) & (168e) \\ \mathbf{D}(1,1) = 1, & (168f) \end{cases}$$

where (168a), (168b), (168d), (168e) and (168f) are deduced from (161c), (161a), (167b), (167a) and (161b), respectively. In (168c), the scaling of  $\sigma$  and  $\mathbf{R}(1,:)$  is achieved by multiplying  $\sigma$  and  $\mathbf{R}(1,:)$  by  $c_k^2$  and  $c_k$ , respectively, to end up with  $\sigma c_k^2$  and  $\mathbf{R}(1,:)c_k$ , where  $\sigma c_k^2$  is always between 0.5 and 2, and  $c_k$  is powers of 2.

In the  $i^{th}$  ( $i \geq 2$ ) iteration,  $\tilde{\Xi}_{k-i}$  and  $\tilde{\Pi}_i$  can be computed efficiently by

$$\begin{aligned} \tilde{\Xi}_{k-i} = \\ \eta \tilde{\Xi}_{k-i+1}^{[-1,-1]} - \tilde{\Xi}_{k-i+1}(1,2:end)^T \tilde{\Xi}_{k-i+1}(1,2:end) \end{aligned} \quad (169)$$

and

$$\begin{aligned} \tilde{\Pi}_i = \\ \left[ \begin{array}{c} \eta \tilde{\Pi}_{i-1}(:,2:end) - \tilde{\Pi}_{i-1}(:,1) \tilde{\Xi}_{k-i+1}(1,2:end) \\ -\sigma_{i-1} \tilde{\Xi}_{k-i+1}(1,2:end) \end{array} \right], \end{aligned} \quad (170)$$

respectively. To deduce (169) and (170), substitute (160g), (160e), (160f), (138a) and (138b), (i.e.,  $\sigma_i = \sigma_{i-1}\eta$ , the partitioned  $\tilde{\mathbf{L}}_i$ ,  $\tilde{\mathbf{D}}_i$ ,  $\mathbf{L}_i$  and  $\mathbf{D}_i$ ) into (154) (i.e.,  $\tilde{\mathbf{L}}_i(\tilde{\mathbf{D}}_i/\sigma_i)\tilde{\mathbf{L}}_i^T = \mathbf{L}_i\mathbf{D}_i\mathbf{L}_i^T$ ) to obtain  $d_i = \tilde{\mathbf{L}}_i^2/(\eta\sigma_{i-1})$ , into which substitute (160c) (i.e.,  $l_{ii} = \sigma_{i-1}$ ) to obtain

$$d_i = \sigma_{i-1}/\eta. \quad (171)$$

Then substitute (141) and (164b) into (142) to obtain  $\frac{\tilde{\Xi}_{k-i}}{\sigma_i} = \frac{\tilde{\Xi}_{k-i+1}^{[-1,-1]}}{\sigma_{i-1}} - d_i \frac{\tilde{\Xi}_{k-i+1}(1,2:end)^T \tilde{\Xi}_{k-i+1}(1,2:end)}{\sigma_{i-1}}$ , into which substitute (160g) and (171) to obtain  $\frac{\tilde{\Xi}_{k-i}}{\sigma_{i-1}\eta} = \frac{\tilde{\Xi}_{k-i+1}^{[-1,-1]}}{\sigma_{i-1}} - \frac{\sigma_{i-1}}{\eta} \frac{\tilde{\Xi}_{k-i+1}(1,2:end)^T \tilde{\Xi}_{k-i+1}(1,2:end)}{\sigma_{i-1}}$ , i.e., (169). On the other hand, let us substitute (141) and (164) into (143) to obtain  $\frac{\tilde{\Pi}_i}{\sigma_i} = \left[ \begin{array}{c} \frac{\tilde{\Pi}_{i-1}(:,2:end)}{\sigma_{i-1}} - \frac{\tilde{\Pi}_{i-1}(:,1)}{\sigma_{i-1}} d_i \frac{\tilde{\Xi}_{k-i+1}(1,2:end)}{\sigma_{i-1}} \\ -d_i \frac{\tilde{\Xi}_{k-i+1}(1,2:end)}{\sigma_{i-1}} \end{array} \right]$ , into which substitute (160g) and (171) to obtain  $\frac{\tilde{\Pi}_i}{\sigma_{i-1}\eta} = \left[ \begin{array}{c} \frac{\tilde{\Pi}_{i-1}(:,2:end)}{\sigma_{i-1}} - \frac{\tilde{\Pi}_{i-1}(:,1)}{\sigma_{i-1}} \frac{\sigma_{i-1}}{\eta} \frac{\tilde{\Xi}_{k-i+1}(1,2:end)}{\sigma_{i-1}} \\ -\frac{\sigma_{i-1}}{\eta} \frac{\tilde{\Xi}_{k-i+1}(1,2:end)}{\sigma_{i-1}} \end{array} \right]$ , i.e., (170).

To save memories in the  $i^{th}$  ( $i \geq 2$ ) iteration, we also store  $\Xi_{k-i}$  and  $\Pi_i$  in  $\mathbf{R}(i+1:k,i+1:k)$  and  $\mathbf{R}(1:i,i+1:k)$ ,

respectively, by computing

$$\begin{cases} \eta = \mathbf{R}(i,i) & (172a) \\ \mathbf{R}(i,i) = \sigma & (172b) \\ \text{Scaling of } \eta, \mathbf{R}(1:i,i) \text{ and } \mathbf{R}(i,i+1:k) & (172c) \\ \tilde{\mathbf{D}}(1:i-1,1:i-1) = \eta\tilde{\mathbf{D}}(1:i-1,1:i-1) & (172d) \\ \sigma = \sigma \times \eta & (172e) \\ \mathbf{R}(i+1:k,i+1:k) = \eta\mathbf{R}(i+1:k,i+1:k) & (172f) \\ \quad -\mathbf{R}(i,i+1:k)^T\mathbf{R}(i,i+1:k) \\ \mathbf{R}(1:i,i+1:k) = & \\ \left[ \begin{array}{c} \eta\mathbf{R}(1:i-1,i+1:k) - \mathbf{R}(1:i-1,i)\mathbf{R}(i,i+1:k) \\ -\mathbf{R}(i,i)\mathbf{R}(i,i+1:k) \end{array} \right] & (172g) \\ \mathbf{D}(i,i) = 1, & (172h) \end{cases}$$

which will be deduced in what follows. Firstly, we compare (163b) (with  $i = i-1$ ) and (160a) to obtain  $\eta = \tilde{\Xi}_{k-i+1}(1,1)$ , from which we deduce (172a) since  $\Xi_{k-i+1}$  has been stored in  $\mathbf{R}(i:k,i:k)$ . Then (172b) is deduced from (160c) since  $l_{ii}$  is stored in  $\mathbf{R}(i,i)$ , while (172d) and (172h) are deduced from (160f). Lastly, (172e), (172f) and (172g) are deduced from (160g), (169) and (170), respectively. Moreover, we can compare (163a) (with  $i = i-1$ ) and (160b) to deduce that  $\tilde{\mathbf{L}}_i$  is the first column of  $\tilde{\Pi}_{i-1}$ , while  $\tilde{\Pi}_{i-1}$  is stored in  $\mathbf{R}(1:i-1,i:k)$ . Thus we can conclude that  $\tilde{\mathbf{L}}_i$  is stored in  $\mathbf{R}(1:i-1,i)$ .

In (172c), the scaling of  $\mathbf{R}(1:i,i)$ ,  $\mathbf{R}(i,i+1:k)$  and  $\eta$  is achieved by multiplying  $\mathbf{R}(1:i,i)$  and  $\mathbf{R}(i,i+1:k)$  by  $c_k$ , and multiplying  $\eta$  by  $c_k^2$ . Then we end up with  $\mathbf{R}(1:i,i)c_k$ ,  $\mathbf{R}(i,i+1:k)c_k$  and  $\eta c_k^2$ , where  $\eta c_k^2$  is always between 0.5 and 2, and  $c_k$  is powers of 2.

When we set the initial  $\sigma = 1$ , (168) is equivalent to (172) with  $i = 1$ . Then we can compute (172) iteratively for  $i = 1, 2, \dots, k$ , to obtain  $\tilde{\mathbf{D}}_k$  and  $\sigma_k$ , and cover the upper-triangular part of  $\mathbf{R}_k$  with the upper-triangular  $\tilde{\mathbf{L}}_k$ , where  $\tilde{\mathbf{L}}_k$ ,  $\tilde{\mathbf{D}}_k$  and  $\sigma_k$  satisfy  $\tilde{\mathbf{L}}_k(\tilde{\mathbf{D}}_k/\sigma_k)\tilde{\mathbf{L}}_k^T = \mathbf{R}_k^{-1}$ . The corresponding implementation is summarized in **Algorithm 14**, where we set the initial  $\tilde{\mathbf{D}} = \mathbf{I}_k$  to avoid the execution of (172h) in each iteration.

---

**Algorithm 14 : The parallel implementation of the division-free inverse  $LDL^T$  factorization**

---

**Input:** The upper-triangular part of a Hermitian matrix  $\mathbf{R}$

**Output:** The division-free inverse  $LDL^T$  factors of  $\mathbf{R}$ , i.e.,

$\tilde{\mathbf{L}}$ ,  $\tilde{\mathbf{D}}$  and  $\sigma$  satisfying  $\tilde{\mathbf{L}}\tilde{\mathbf{D}}\tilde{\mathbf{L}}^T/\sigma = \mathbf{R}^{-1}$ ;

- 1: The initial  $\tilde{\mathbf{D}} = \mathbf{I}_k$  and  $\sigma = 1$ ;
  - 2: **for**  $i = 1 : k$  ( $k$  is the size of  $\mathbf{R}$ ) **do**
  - 3:    $\eta = \mathbf{R}(i,i)$ ;
  - 4:    $\mathbf{R}(i,i) = \sigma$ ;
  - 5:   Scaling of  $\eta$ ,  $\mathbf{R}(1:i,i)$  and  $\mathbf{R}(i,i+1:k)$ ;
  - 6:    $\tilde{\mathbf{D}}(1:i-1,1:i-1) = \eta\tilde{\mathbf{D}}(1:i-1,1:i-1)$ ;
  - 7:    $\sigma = \sigma \times \eta$ ;
  - 8:    $\mathbf{R}(i+1:k,i+1:k) = \eta\mathbf{R}(i+1:k,i+1:k)$   
 $\quad -\mathbf{R}(i,i+1:k)^T\mathbf{R}(i,i+1:k)$ ;
  - 9:    $\mathbf{R}(1:i,i+1:k) =$   
 $\quad \left[ \begin{array}{c} \eta\mathbf{R}(1:i-1,i+1:k) - \mathbf{R}(1:i-1,i)\mathbf{R}(i,i+1:k) \\ -\mathbf{R}(i,i)\mathbf{R}(i,i+1:k) \end{array} \right]$ ;
  - 10: **end for**
  - 11: The diagonal  $\tilde{\mathbf{D}}$ , the scalar  $\sigma$  and the upper-triangular  $\tilde{\mathbf{L}}$  = triu( $\mathbf{R}$ ) (i.e., the upper-triangular part of  $\mathbf{R}$  forms  $\mathbf{L}$ );
-

## REFERENCES

- [1] G. E. Hinton, S. Osindero, and Y.-W. Teh, "A fast learning algorithm for deep belief nets," *Neural Computation*, vol. 18, pp. 0899–7667, 2006.
- [2] G. E. Hinton and R. R. Salakhutdinov, "Reducing the dimensionality of data with neural networks," *Science*, vol. 313, no. 5786, pp. 504–507, 2006.
- [3] R. Salakhutdinov and G. E. Hinton, "Deep boltzmann machines," in *AISTATS*, vol. 1, 2009, p. 3.
- [4] Y. Lecun, L. Bottou, Y. Bengio, and P. Haffner, "Gradient-based learning applied to document recognition," *Proceedings of the IEEE*, vol. 86, no. 11, pp. 2278–2324, Nov 1998.
- [5] K. Simonyan and A. Zisserman, "Very deep convolutional networks for large-scale image recognition," *CoRR*, vol. abs/1409.1556, 2014.
- [6] M. Gong, J. Zhao, J. Liu, Q. Miao, and L. Jiao, "Change detection in synthetic aperture radar images based on deep neural networks," *IEEE Transactions on Neural Networks and Learning Systems*, vol. 27, no. 1, pp. 125–138, Jan 2016.
- [7] W. Hou, X. Gao, D. Tao, and X. Li, "Blind image quality assessment via deep learning," *IEEE Transactions on Neural Networks and Learning Systems*, vol. 26, no. 6, pp. 1275–1286, June 2015.
- [8] S. Li, M.-C. Lee, and C.-M. Pun, "Complex Zernike moments features for shape-based image retrieval," *IEEE Trans. Syst., Man, Cybern. A, Syst., Humans*, vol. 39, no. 1, pp. 227–237, Jan. 2009.
- [9] G. E. Hinton et al., "Deep neural networks for acoustic modeling in speech recognition: The shared views of four research groups," *IEEE Signal Process. Mag.*, vol. 29, no. 6, pp. 82–97, Nov. 2012.
- [10] Y. LeCun et al., "Handwritten digit recognition with a back-propagation network," *Proc. Neural Inf. Process. Syst. (NIPS)*, 1990, pp. 396–404.
- [11] Y.-H. Pao and Y. Takefuji, "Functional-link net computing: Theory, system architecture, and functionalities," *Computer*, vol. 25, no. 5, pp. 76–79, May 1992.
- [12] M. Leshno, V. Y. Lin, A. Pinkus, and S. Schocken, "Multilayer feedforward networks with a nonpolynomial activation function can approximate any function," *Neural Netw.*, vol. 6, no. 6, pp. 861–867.
- [13] Y.-H. Pao, G.-H. Park, and D. J. Sobajic, "Learning and generalization characteristics of the random vector functional-link net," *Neurocomputing*, vol. 6, no. 2, pp. 163–180, 1994.
- [14] J. S. Denker et al., "Neural network recognizer for hand-written zip code digits," *Advances in Neural Information Processing Systems*, D. S. Touretzky, Ed. San Francisco, CA, USA: Morgan Kaufmann, 1989, pp. 323–331.
- [15] C. L. Philip Chen and J. Z. Wan, "A rapid learning and dynamic stepwise updating algorithm for flat neural networks and the application to timeseries prediction," *IEEE Trans. Syst., Man, Cybern. B, Cybern.*, vol. 29, no. 1, pp. 62–72, Feb. 1999.
- [16] C. L. Philip Chen and Z. Liu, "Broad Learning System: An Effective and Efficient Incremental Learning System Without the Need for Deep Architecture," *IEEE Transactions on Neural Networks and Learning Systems*, vol. 29, no. 1, Jan. 2018.
- [17] C. L. Philip Chen, Z. Liu, and S. Feng, "Universal Approximation Capability of Broad Learning System and Its Structural Variations," *IEEE Transactions on Neural Networks and Learning Systems*, vol. 30, no. 4, April 2019.
- [18] Donald W. Marquardt, "Generalized Inverses, Ridge Regression, Biased Linear Estimation, and Nonlinear Estimation," *Technometrics*, vol. 12, no. 3, Aug. 1970.
- [19] A. Ben-Israel and T. Greville, *Generalized Inverses: Theory and Applications*, New York, USA, Wiley, 1974.
- [20] H. Zhu, Z. Liu, C. L. P. Chen and Y. Liang, "An Efficient Algorithm for the Incremental Broad Learning System by Inverse Cholesky Factorization of a Partitioned Matrix," *IEEE Access*, vol. 9, pp. 19294–19303, 2021, doi: 10.1109/ACCESS.2021.3052102.
- [21] H. Zhu, W. Chen, B. Li, and F. Gao, "An Improved Square-Root Algorithm for V-BLAST Based on Efficient Inverse Cholesky Factorization," *IEEE Trans. Wireless Commun.*, vol. 10, no. 1, Jan. 2011.
- [22] C. Leonides, "Control and dynamic systems V18", *Advances in Theory and Applications (Control and dynamic systems)*, Amsterdam, The Netherlands: Elsevier, 2012.
- [23] G. H. Golub and C. F. Van Loan, *Matrix Computations*, third ed. Baltimore, MD: Johns Hopkins Univ. Press, 1996.
- [24] Y. LeCun, L. Bottou, Y. Bengio, and P. Haffner, "Gradient-based learning applied to document recognition," *Proc. IEEE*, vol. 86, no. 11, pp. 2278–2324, Nov. 1998.
- [25] Y. LeCun, F. J. Huang, and L. Bottou, "Learning methods for generic object recognition with invariance to pose and lighting," *Proc. IEEE Comput. Soc. Conf. Comput. Vis. Pattern Recognit. (CVPR)*, vol. 2, Jun. 2004, pp. II-94–II-104.
- [26] H. V. Henderson and S. R. Searle, "On Deriving the Inverse of a Sum of Matrices", *SIAM Review*, vol. 23, no. 1, January 1981.
- [27] R. Wang, "Review of Linear Algebra", *Lecture Notes for the Machine Learning Course*, available online at <https://fourier.eng.hmc.edu/e176/lectures/algebra/node6.html>.
- [28] Joost Verbraeken, Matthijs Wolting, Jonathan Katzy, Jeroen Kloppenburg, Tim Verbelen, and Jan S. Rellermeyer, "A Survey on Distributed Machine Learning", *ACM Computing Surveys*, <https://doi.org/10.1145/3377454>.
- [29] Wahid Nasri, Zaher Mahjoub, "Optimal parallelization of a recursive algorithm for triangular matrix inversion on MIMD computers", *Parallel Computing*, Volume 27, Issue 13, 2001, Pages 1767–1782, ISSN 0167-8191, [https://doi.org/10.1016/S0167-8191\(01\)00111-9](https://doi.org/10.1016/S0167-8191(01)00111-9).
- [30] J. G. Proakis, C. M. Rader, F. Ling, C. L. Nikias, M. Moonen and I. K. Prouder, *Algorithms for Statistical Signal Processing*, Prentice Hall 2002.
- [31] L. M. Davis, "Scaled and decoupled Cholesky and QR decompositions with application to spherical MIMO detection", *IEEE WCNC*, 2003.
- [32] E. N. Frantzeskakis and K. J. R. Liu, "A class of square root and division free algorithms and architectures for QRD-based adaptive signal processing", *IEEE Trans. on Signal Processing*, Sep 1994.
- [33] H. Zhu, "Inverse LDM and LU Factorizations of a Partitioned Matrix with the Square-root and Division Free Version for V-BLAST", <https://doi.org/10.48550/arXiv.1912.04475>.
- [34] H. Zhu, W. Chen, and B. Li, "Efficient Square-Root and Division Free Algorithms for Inverse  $LDL^T$  Factorization and the Wide-Sense Givens Rotation with Application to V-BLAST", *IEEE Vehicular Technology Conference (VTC)*, 2010 Fall, 6–9 Sept., 2010.